Virtual surgical planning in DIEP flap breast reconstructions: How to plan DIEP flap volume?

E. Karstanje

Master Thesis
Technical Medicine
June 2024

Graduation committee:
Technical supervisor UT and chairman: prof. dr. ir. R.M. Verdaasdonk
Medical supervisor MST/ ZGT: dr. H.A. Rakhorst
Additional supervisor MST: J.B. Waldner-Troost MSc.
Additional supervisor Radboudumc: dr. S. Hummelink
External member UT: dr. J.K. van Zandwijk
Process supervisor: E.M. Walter MSc.

Abstract

Background: One in three women with breast cancer is treated with a mastectomy. A mastectomy can lead to a lowered quality of life, mostly related to a lower body image, for which asymmetry is an important factor. After a mastectomy multiple reconstruction options are possible. The most used option with autologous tissue is the deep inferior epigastric perforator (DIEP) flap. Reducing asymmetry after DIEP flap breast reconstruction can lead to a reduction of revisions, an improved body image and quality of life. Using pre-operative planning to determine the volume of the DIEP flap, could aid in improving the symmetry. This study focusses on a virtual planning for DIEP flap volume using CTA scans and a desired volume.

Methods: A semi-automatic algorithm has been developed that determines the delineation of the abdominal incision based on manually chosen landmarks. The algorithm automatically attempts to reach the desired volume by iteratively changing the delineation and thus the corresponding DIEP flap volume. The predicted volume was validated using a retrospective and prospective feasibility study, with the aim of a maximum deviation of 10% compared to actual weight. The retrospective study (n=13) compared the surgically obtained weight of the flap to a virtual flap weight acquired using the delineation of the plastic surgeon which was transferred using a 3D scan. The prospective study (n=4) transferred the virtual planning to the patient using a 3D printed patient-specific mould.

Results and discussion: The retrospective study resulted in a mean difference in weight between the virtual and actual flap of 11.9%. A significant correlation was found between the CTA age (days between acquiring the CTA and surgery) and the difference in weight, where a low CTA age resulted in an underestimation of weight. Furthermore, large error margins were observed in the dataset. The prospective study showed a difference in weight of less than 10% for all patients. The delineation of the planning was correct for two patients and was adjusted for the other two patients.

Conclusion: A virtual planning for DIEP flap volume transferred using a 3D printed mould could predict the volume within a 10% deviation according to the feasibility study. However, more research is needed due to the small population.

List of abbreviations

2D	Two dimensional
3D	Three dimensional
AR	Augmented reality
BMI	Body mass index
CTA	Computed tomography angiography
DIEP	Deep inferior epigastric perforator
HU	Hounsfield units
PLA	Polylactic acid
SIAS	Spina iliaca anterior superior

Table of contents

Chapter 1 Introduction

1.1 Clinical background

Annually, approximately 17.000 women in the Netherlands are diagnosed with breast cancer.[1,2] Various treatments are possible, such as radiotherapy, chemotherapy, hormone therapy and surgery.[3] Surgical options are a breast-conserving surgery, also called a lumpectomy, or a breast-removing surgery, called a mastectomy. One in three women with breast cancer is treated with a mastectomy.[3,4] Research has shown that the quality of life of mastectomy patients without breast reconstruction is lower than patients who have had breast-conserving surgery or a mastectomy with breast reconstruction.[5–7] The reduced quality of life is primarily associated to a lower body image, for which asymmetry is an important factor.[7,8] After a mastectomy, the breast can be reconstructed, which can be done immediately or delayed. Immediate reconstruction is conducted during the same surgical session as the mastectomy, whereas delayed reconstruction is performed in a subsequent surgery. During the mastectomy before a delayed reconstruction, there is a choice to keep the chest flat or to insert a tissue expander. The breast can be reconstructed with an implant or with autologous material. Both have their advantages and disadvantages regarding e.g. complication risk, secondary surgeries and patient satisfaction. Implants should be replaced after ten years, leading to additional surgeries. In contrast, autologous reconstructions do not require periodic replacement but have a higher complication risk during the initial surgery.[9] An additional benefit of autologous reconstruction is the better patient-reported outcome in the long term compared to implant-based reconstruction.[10]

1.2 Deep inferior epigastric perforator flap breast reconstruction

Various locations of the body can provide an autologous tissue flap for breast reconstruction, like the abdomen, thighs and back. Furthermore, most flaps consist of skin and fat, but some flaps can include muscle as well. The deep inferior epigastric perforator (DIEP) flap breast reconstruction, shown in Figure 1, is the preferred autologous breast reconstruction method in most hospitals.[4,11] During a DIEP flap breast reconstruction, a flap of subcutaneous fat and skin is removed from the lower abdomen, while keeping vascularization by the deep inferior epigastric artery and vena intact. During dissection, the perforators are identified and followed through the m. rectus abdominis to near the origin of the deep inferior epigastric artery and deep inferior epigastric vein.[12,13] The flap is transferred and reshaped to reconstruct the breast.[13]

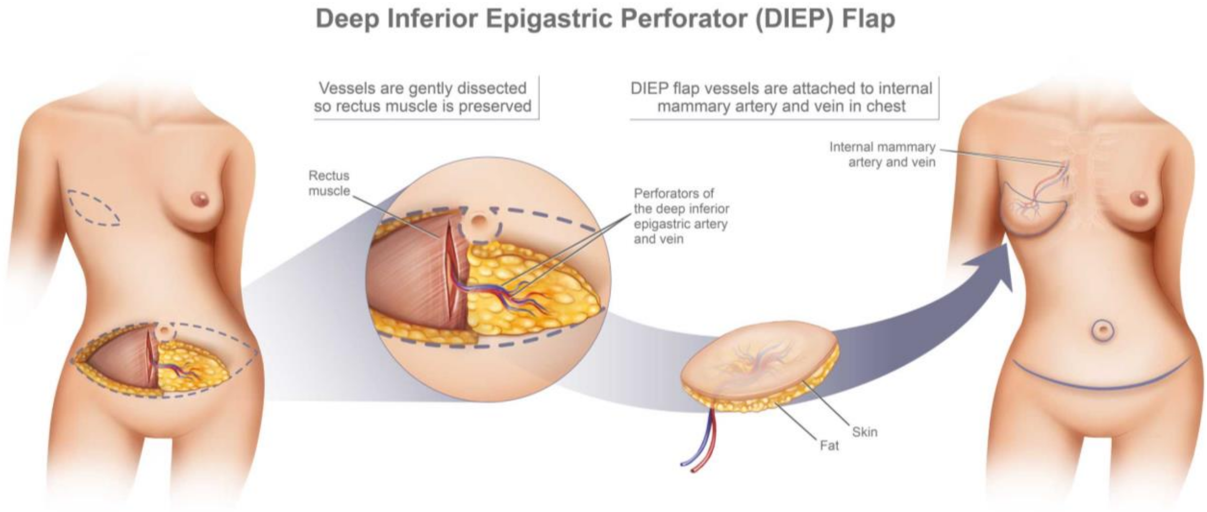

Figure 1. Schematic overview of DIEP flap breast reconstruction. The flap is harvested from the abdomen while maintaining vascularization by the deep inferior epigastric artery and vena perforators. The flap is transferred to the chest and the vessels are reattached to the mammary artery and vein.[14]

At the start of a DIEP flap surgery, the delineation of the flap that will be removed is drawn on the patient's skin. There are some rough guidelines for a DIEP flap delineation that must be followed. The primary consideration during DIEP flap delineation is the location of the perforators to ensure good vascularization. For this, the guideline was given that the perforator should be at least 2 to 3 centimetres below the cranial incision. Additionally, for unilateral reconstruction, the flap can extend 3 to 4 centimetres beyond the midline.[15] Furthermore, the caudal incision is transversely placed above the pubic bone, similar to the typical transverse Caesarean section incision. The incision extends laterally and superior to the inguinal ligament finishing near the spina iliaca anterior superior (SIAS). The cranial incision is made above the umbilicus and curves laterally to meet the caudal incision.[12] This is illustrated in Figure 2. However, even though this is a guideline, it cannot always be followed. For instance, patients with tight skin need less distance between the caudal and cranial incision to ensure that the skin can be closed. In such cases, it is preferable to move the caudal incision superiorly, as this results in a smaller reduction in flap volume compared to moving the cranial incision inferiorly. Moreover, different hospitals, as well as different plastic surgeons within the same institution have different approaches for the DIEP plan delineation. Various DIEP flap designs can be identified by looking at studies that involve DIEP flaps, as well as Appendix A.[16–21] For instance, some surgeons opt to make an indentation towards the umbilicus in the cranial delineation to reduce the tension on the closure. Since the medial part of the abdomen is the most stretched, this part of the wound is the most under tension, so increasing the amount of skin that is available to close the wound at that part, reduces the tension on the wound to prevent dehiscence.

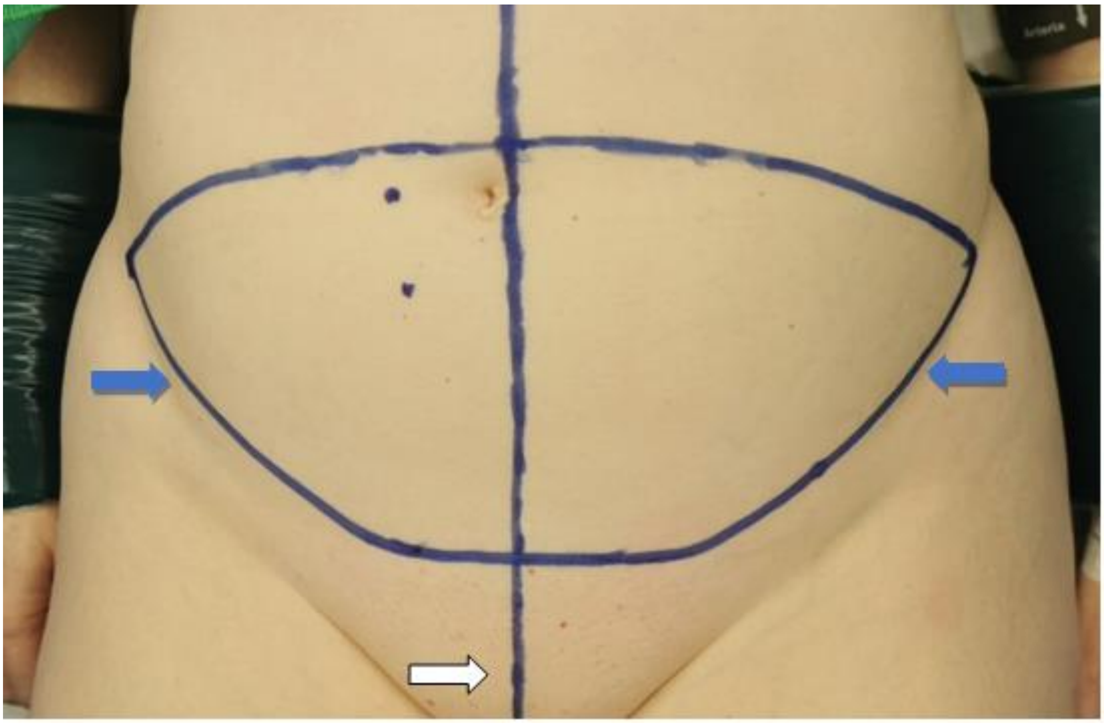

Figure 2. Example of DIEP flap delineation, the drawn midline and identified perforators (dots). The white arrow indicates the approximate location of the pubic bone, and the blue arrows indicate the approximate location of the SIAS.

After determining and drawing the delineation with a marker, the surgery commences, and the cranial skin incision is made. The incision continues approximately perpendicular to the skin until the fascia is encountered. Dissection over the fascia cranial to the incision facilitates closure of the abdomen after the DIEP flap is extracted. Furthermore, by pulling the skin and fat down towards the caudal incision, the maximal length of the DIEP flap is per-operatively determined. If the planned caudal incision cannot be reached, the incision will be moved cranially to ensure wound closure. The extracted DIEP flap will be weighed and compared to the breast, with any excessive volume removed to achieve a breast with the appropriate volume.

1.3 Clinical challenge

As stated, the different reconstructions have advantages and disadvantages. A challenge of DIEP flap breast reconstruction is to achieve aesthetically pleasing and symmetric breasts, due to the difficult transformation of a two-dimensional (2D) flap into a three-dimensional (3D) breast. Thus, a revision surgery can be required to reshape the breast to improve patient satisfaction regarding size or symmetry. Nelson et al. found that 59.6% of DIEP flap breast reconstruction needed revision surgery.[22] Such revision is a burden for the patient and a costly procedure. Although costs can be reduced with quicker procedures, expenses can be cut down even further if the first surgery achieves a higher patient satisfaction and no revision is required.[23,24]

Moreover, an autologous breast reconstruction is a lengthy surgery. Prolonged operative durations should be prevented due to a higher risk of complications and infections.[25,26] The duration of a DIEP flap breast reconstruction depends on various factors like immediate or delayed and uni- or bilateral reconstruction. However, duration is often estimated at 6-8 hours, with studies aimed at reducing durations reporting times as low as 4 hours.[27–31] Pre-operative planning may lead to surgical benefits including a reduced learning curve, a decrease in surgery time, improved patient satisfaction, improved flap viability and thus patient safety, and decrease in operative stress.[11,16,30,32–38]

1.4 Literature

Various research has been done to improve the patient satisfaction and efficiency of DIEP flap breast reconstruction. This includes process mapping, 3D printed anatomical models or breast moulds, pre-operative computed tomography angiography (CTA) assessment and augmented reality (AR).[16–18,39–44] The 3D printed models and AR show the perforators and their intramuscular course.[16,17,40,43] This helps to reduce the harvest time of the flap. Chae et al. used a 3D template which reduced intra-operative perforator identification by 7.29 minutes.[16] Most visualizations show the perforators in a 2D plane, while a body is 3D. Showing the perforators in 3D would make their course clearer. This has been done with holographic AR done by Wesselius et al.[43] Furthermore, pre-operative delineation of the DIEP flap based on the required volume, could help to achieve more symmetrical breasts, and thus higher patient satisfaction, especially in case of a unilateral breast reconstruction. Hummelink et al. planned the volume within a global outline of the DIEP flap made by the operating plastic surgeon with a planned versus harvested flap mean difference of 5 ± 27 g.[17] Moreover, various calculators have been designed to estimate the DIEP flap volume based on factors like flap width and length.[19,21]

DIEP flap breast reconstruction offers an increase in quality of life for mastectomy patients, but improvements can be made in efficiency and patient satisfaction. Operation times can be decreased by improving the speed of locating and dissecting the perforators. Furthermore, patient satisfaction can be increased by improving the symmetry of the breast and abdominal scar location with pre-operative volume planning. Moreover, pre-operative volume planning can limit the amount of harvested tissue to just the volume needed for a symmetrical breast, and thus decrease the amount of tissue that is discarded, which minimizes the surgical area to reduce complication risk.[15] While previous studies have focused on visualizing the perforators to reduce the harvesting time, further improvement of breast symmetry and reduction of the complication risk can be achieved by also taking the volume and delineation of the DIEP flap into account.

1.5 Thesis outline

This led to the following research question:
How to virtually plan a DIEP flap volume pre-operatively using CTA and a desired volume?

- *How to pre-operatively compute the DIEP flap delineation for the abdominal incision?*
- *How to compute the corresponding volume of the generated delineation?*
- *How can the virtual planning be transferred to the patient?*

- *To what extend does the planned flap volume correlate with the surgically obtained flap volume?*

To answer these questions, data was collected to gain more knowledge about the problems and to be able to develop and validate the planning. This will be discussed in Chapter 2. The development of the planning will be elaborated on in Chapter 3. This chapter also includes a validation based on patient data. Chapter 4 shows the first step towards the implementation of such a planning as developed in Chapter 3. Finally, the discussion and conclusion are addressed in Chapter 5.

Chapter 2 Data acquisition and processing for surgical planning

To be able virtually plan a DIEP flap volume using CTA, various data is needed, of which most is already acquired during the regular workflow of a DIEP flap breast reconstruction. Achieving symmetrical breasts necessitates knowing the desired size of the breast, which can be determined through 3D photographs and patient anamnesis. This desired volume must be matched with the abdominal subcutaneous fat, which can be visualized using a computed tomography angiography (CTA) scan. These values can be validated by comparing the determined volume on the CTA scan, with the weight of the flap as measured during surgery. To also compare the virtual and actual abdominal delineations, 2D and 3D images of the DIEP flap delineation are obtained. This is summarized in Figure 3.

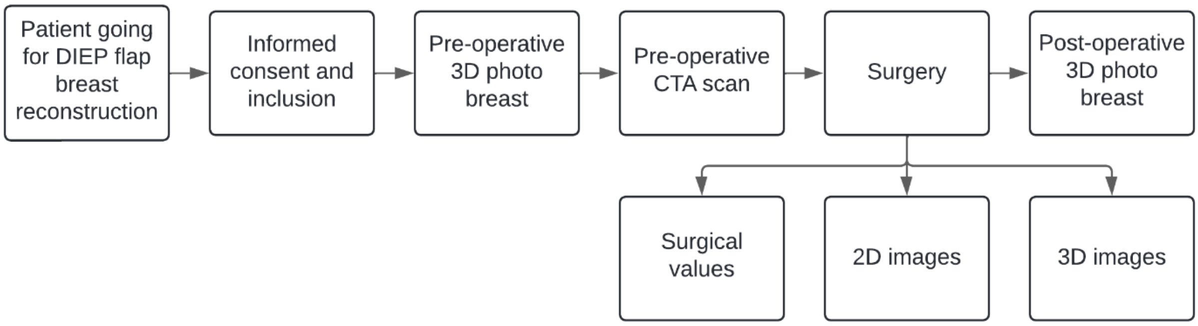

Figure 3. Flowchart of the data collected for each patient.

2.1 Collected data

2.1.1 Participants

Patients going for a DIEP breast reconstruction, both unilateral or bilateral and both immediate and delayed, were included in Ziekenhuisgroep Twente (ZGT) hospital from July 2023 till May 2024. Further inclusion criteria were that the patient is ≥18 years old and able to give informed consent. Exclusion criteria are contraindications for a CTA, such as renal impairment. nWMO consent was given for this study and written informed consent was obtained for all participants.

2.1.2 CTA

As part of the standard protocol for a DIEP flap breast reconstruction, a CTA scan is made of the abdomen.[45] The CTA scans were acquired using a Siemens Somatom X.cite (Siemens Healthcare GmbH, Forchheim, Germany). This CTA scan provides information about the subcutaneous abdominal fat layer, the vascularization and the skin, which can be used to define the DIEP flap delineation and volume. The CTA scan is performed following a specific DIEP flap protocol. This protocol has a larger delay from injecting the bolus to acquiring the images compared to a regular CTA of the aorta and its major branches. This extended delay allows the contrast to move from the aorta to the perforators in the abdomen, optimizing their visualization. With this protocol, surgeons can determine the quality and location of the perforators. This can determine whether a patient is suitable for a DIEP flap breast reconstruction, and it reduces the time needed to identify the perforators with Doppler during surgery. Identifying the perforators with Doppler in turn aids the surgeon with identifying the perforators during dissection of the flap.

The protocol described above was further optimized during the inclusion phase, leading to some differences in the acquired data. The plastic surgery department is a collaboration of Medisch Spectrum Twente (MST) and ZGT. Different hospitals can have variations in protocols. This also applied to the protocol used for the CTA DIEP. During this study, efforts were made to minimize these differences. Adjustments included the slice thickness and bolus timing, as well as modifying the field of view to reduce the radiation dose for the patient. Furthermore, the protocol was made more appropriate for future research. This included the removal of underwear that was compressing the abdomen and interfering with volume measurements, as well as trying to mimic the operative position of the patient to reduce the effect of the malleable soft tissues. These changes are summarized in Table 1. During multiple meetings with radiologists of both hospitals and a plastic surgeon, the differences between the protocols of both hospitals were discussed, and the best options were selected to make a uniform protocol, facilitating more consistent assessment of the CTA scans by plastic surgeons.

Table 1. Changes made to the CTA DIEP protocol to ensure uniformity within the hospitals and more appropriate data for (future) research.

Variable	Old ZGT protocol	Old MST protocol	New protocol
Slice thickness	0.75mm	1mm	0.75mm
Slice thickness coronal/sagittal	1mm	3mm	1mm
Field of view	Breasts till thighs	4cm above iliac crest till thighs	4cm above iliac crest till os pubis
Bolus	Test bolus, triggered on a. iliaca	Bolus tracking, triggered on aorta descendens at height of diaphragm, with delay of 18 seconds	Test bolus, triggered on a. iliaca
Positioning	Knees raised or down, trousers down, underwear on	Knees raised or down, trousers down, underwear on	Raised knees, no underwear

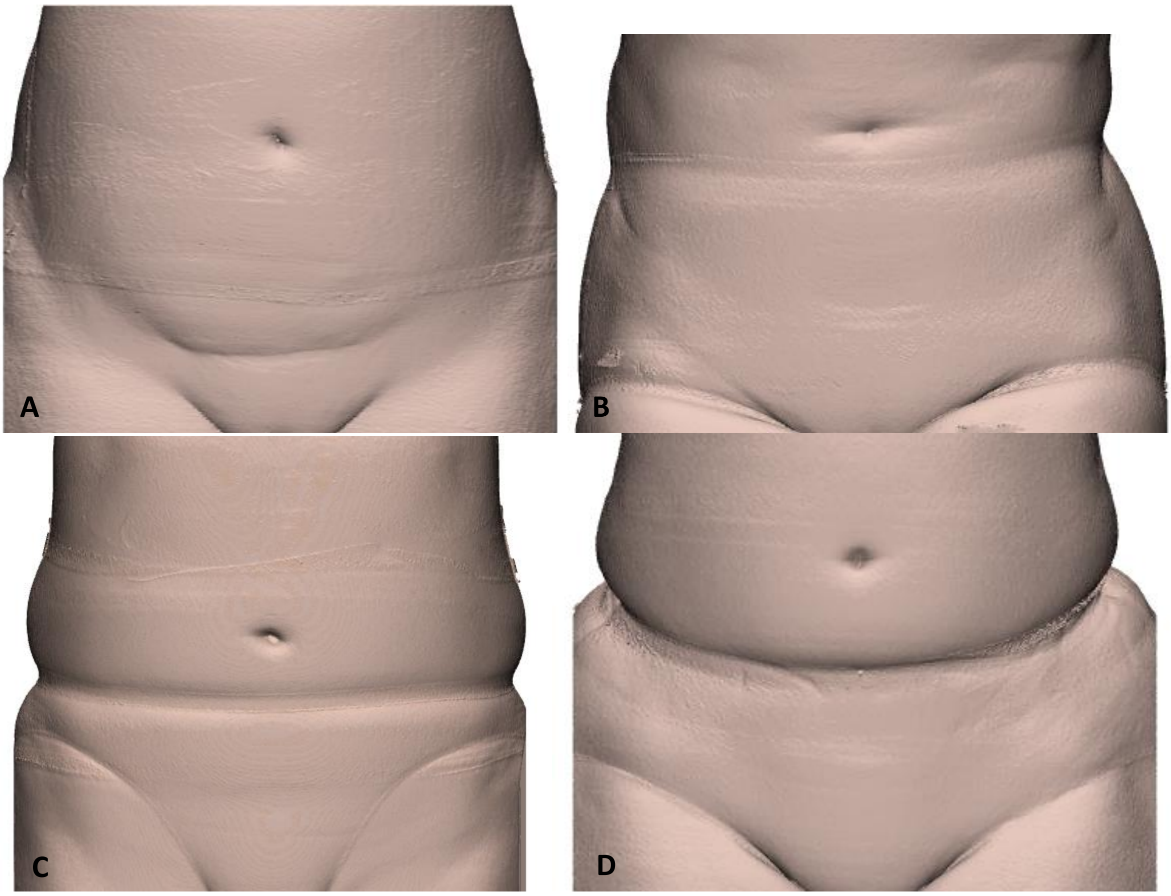

Figure 4. Examples of underwear grades. A. No underwear (-). B. Underwear, but insignificant effect (+/-). C. Underwear, with effect (+). D. Underwear, severe effect (++).

Because the protocol was improved during the study, the dataset has CTA scans with and without underwear. The effects of the underwear were visualized on the 3D models of the CTA scans and graded as follows: No underwear (-). Underwear, but insignificant effect (+/-). Underwear, with effect (+). Underwear, severe effect (++). Figure 4 shows a visualisation of those grades.

2.1.3 3D photos

Various research has been done to estimate breast volume with 3D photos. A commonly used appliance is the Vectra XT (Canfield Sci, New Jersey, USA) with the specialized Breast Sculptor (Canfield Sci, New Jersey, USA) software. The results are considered sufficiently accurate for clinical use, although minor errors did occur. Additionally, the accuracy varies for cup sizes and is reduced for pseudoptotic breasts.[46–50] 3D photos of the breasts were acquired using the Vectra XT at three moments, namely pre-operative, 2 weeks post-operative during routine wound control and 3 months post-operative during routine control with the surgeon. These photos were further processed using Breast Sculptor to get an estimate of the breast volume, as illustrated in Figure 5. Breast Sculptor incorporates an automatic landmark detection system, which was utilized whenever feasible. Placed landmarks were verified for accuracy and manual adjustments were made if necessary. For certain situations like breasts without nipples or a high grade of asymmetry, automatic landmark detection does not work. In those cases, landmarks were placed completely manually. The landmarks used by Breast Sculptor are the sternal notch and on both the left and right side the medial mammary fold, clavicle, nipple, areola, inframammary and lateral mammary fold. A schematic of the landmarks is shown in Appendix B. The determined breast volume, complemented with the information obtained during anamnesis, is used as the desired volume that has to be extracted from the abdomen during DIEP flap breast reconstruction.

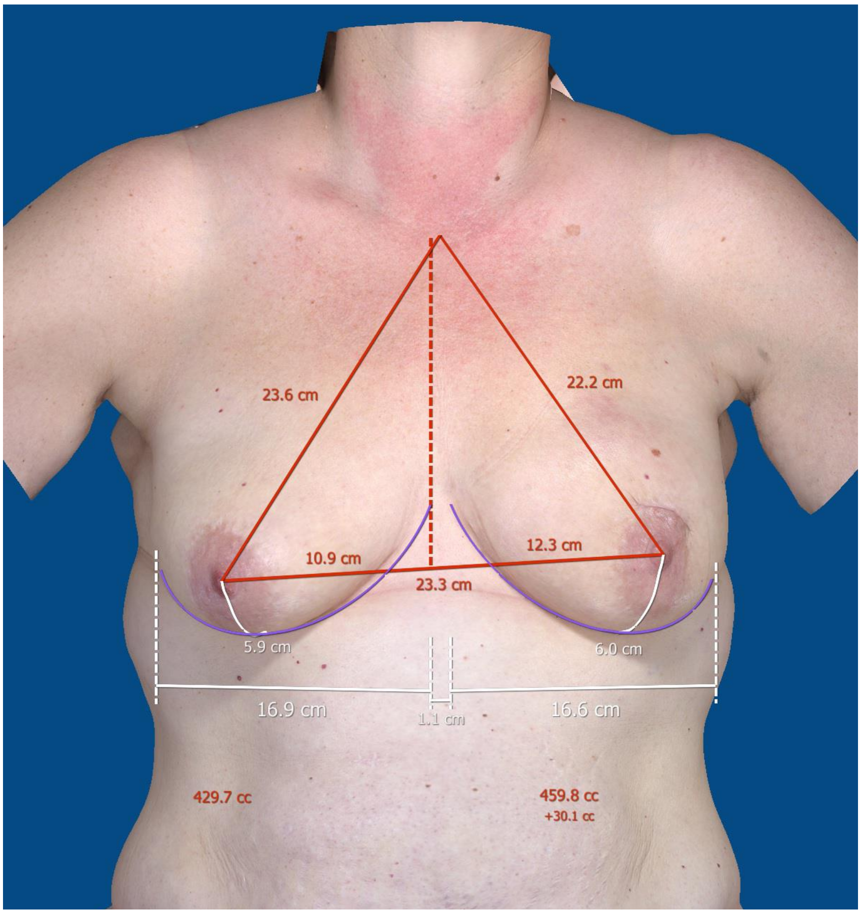

Figure 5. Example of volume calculation by Vectra XT. The numbers by the lines give the distances in centimetres. The numbers on the abdomen give the volume of the breast in cc. Below the largest breast, the difference in volume (cc) is also shown.

2.1.4 Surgical values

To determine the volume of a flap obtained with a certain delineation the per-operative weight of the harvested DIEP flap is collected. Furthermore, the discarded tissue and the final weight of the implanted flap were collected for future research.

An important factor in this process is the fact that the breast and other data in this study is measured in volume, while the DIEP flap is measured in weight. To compare the two measurements, one of those should be corrected with the right density. Studies done to determine the density of abdominal fat tissue have shown a high range. Van der Pot et al. determined the density of the abdominoplasty specimens of thirty-two women. The mean specific density was 1.12 mL/g (range, 1.02 to 1.32 mL/g; standard deviation 0.04).[51] Razzano et al. found a similar density of 1.19 mL/g (range: 1.10 - 1.32 mL/g) assessing the contralateral side of DIEP flaps used for unilateral reconstructions.[21] An independent experiment described in Appendix C yielded comparable results, which were closer to the density of 1.12 mL/g than 1.19 mL/g. The choice was made to use the 1.12 mL/g reported by Van der Pot et al. due to the more reliable method of calculating water displacement and the more comparable results of the experiment in Appendix C.

2.1.5 Per-operative images

During surgery, 2D photos of the delineation of the DIEP flap are made with a mobile phone, seen in Figure 6, as well as 3D scans using a Revopoint POP 2 (Revopoint 3D Technologies), shown in Figure 7. These images were made on the operating table after the plastic surgeons made the delineation for the DIEP flap, but before the surgical area was made sterile. Initially, only 2D images were obtained to simplify the data collection, aiming to include more patients and gather larger datasets for validation purposes. However, 2D images turned out to be insufficient (see Appendix D), necessitating the additional acquirement of 3D scans.

For all images, it was also noted if this was the final delineation used for the incision or not. Plastic surgeons prioritize getting the right volume. After delineating the DIEP flap, the cranial incision is made, followed by dissection over the fascia cranially to mobilize the remaining fat layer towards the caudal delineation. If the layer does not reach the delineation, the caudal incision is moved to align with the mobilized layer. In these cases, an estimate had to be made about the exact caudal incision, because the tissue is already manipulated and thus distorted. This uncertainty would compromise the reliability of additional 3D scans taken at that stage. Furthermore, it did not fit the current workflow, as it would have led to additional precautions that would have to be taken to ensure sterility.

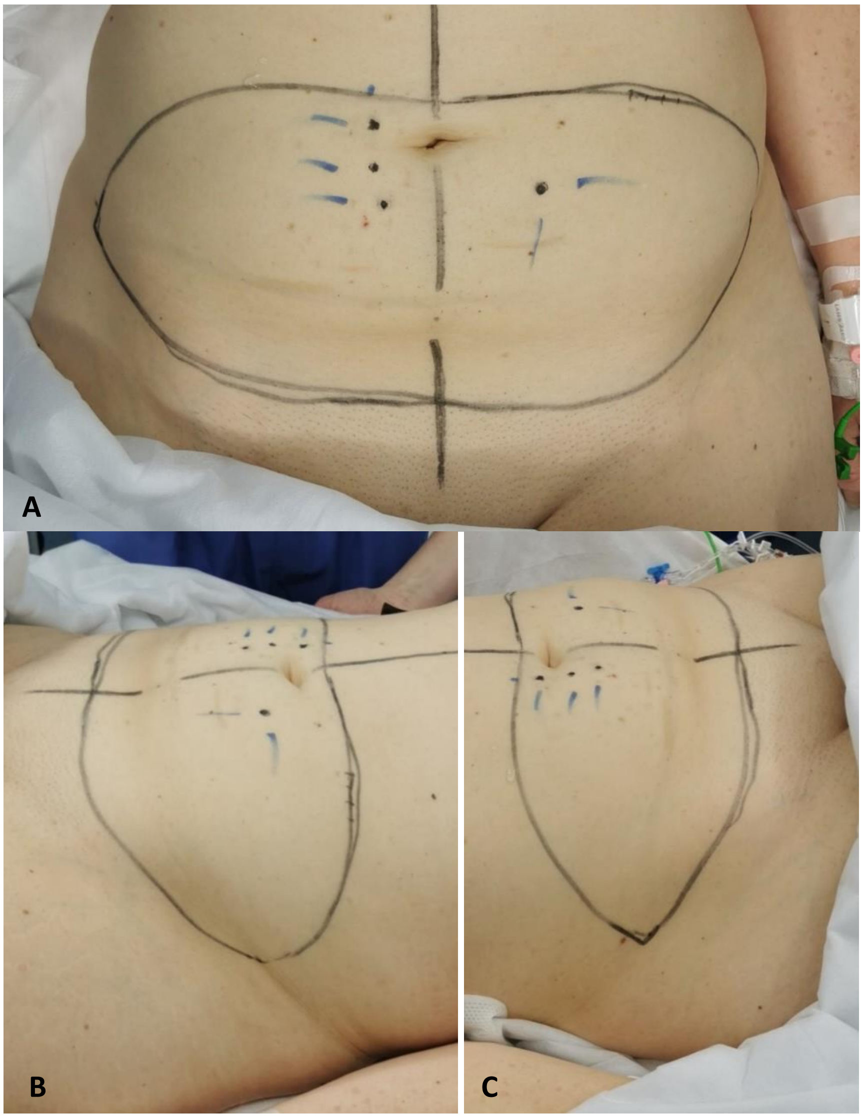

Figure 6. Example of 2D images captured with a mobile phone. Shown is a drawn DIEP flap delineation, a vertical midline and perforators (dots with blue lines). A. Frontal view. B. Lateral left view. C. Lateral right view.

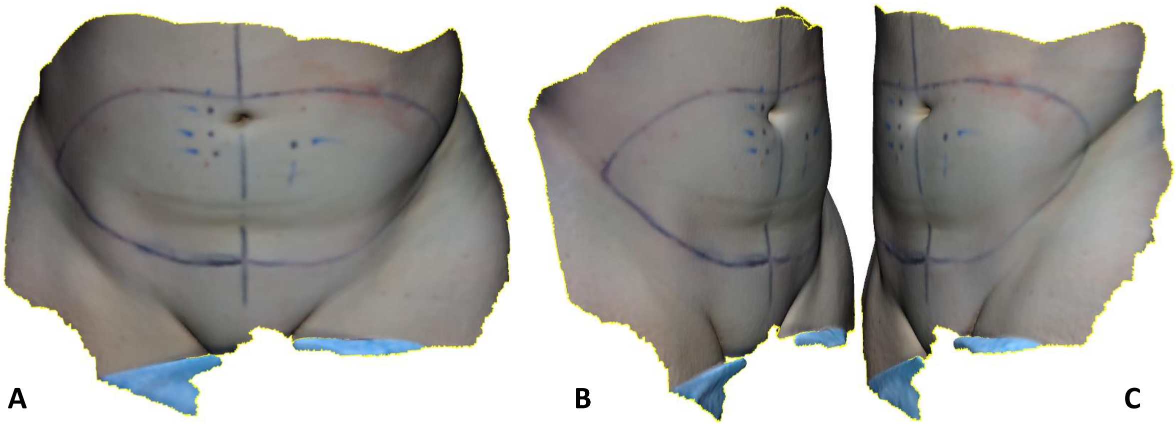

Figure 7. Example of a 3D scan of Revopoint POP 2 of the same patients as Figure 6. Shown is a drawn DIEP flap delineation, a vertical midline and perforators (dots with blue lines). A piece of the blanket is visible on the 3D scan as well.

2.2 Pre-processing: segmentation

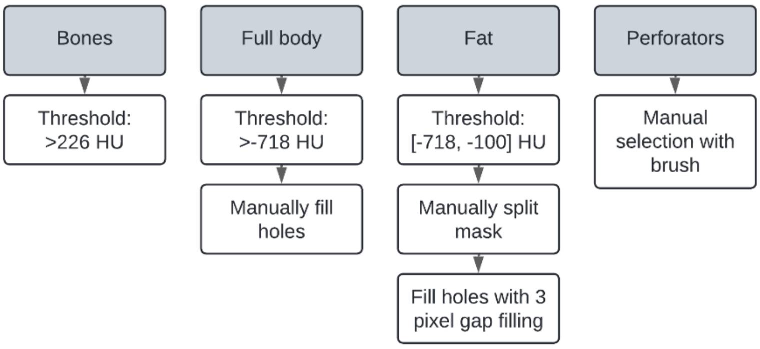

Figure 8. Flowchart of segmentation and used parameters.

Segmentation of the CTA scans was performed in Mimics (Materialise, Leuven, Belgium), see also Figure 8. The bones were segmented with the standard threshold, of >226 Hounsfield Units (HU), visible in Figure 10A. HU are the relative quantitative measurement of radio density of CTA images.[52] The full body was segmented using a threshold of >-718 HU, illustrated in Figure 10B and E. Holes were manually filled and if necessary, underwear was manually removed by various methods, like thresholding or region growing of the underwear and Boolean subtraction. With the current protocol, there is no underwear, but incidentally, an edge of the towel must be removed. The fat layer was segmented with a threshold of -718 to -100 HU, resulting in Figure 9. This segmentation was further processed by manually splitting into the subcutaneous layer of fat and the visceral fat. Holes were filled using a 3-pixel gap filling. The final fat segmentation is visible in Figure 10C and F. Perforators were manually segmented using the *Smart brush* function around the point the perforator leaves the muscle into the fat layer, as shown in Figure 10D, E and F. The full body segmentation of the CTA will be referred to as CTA model.

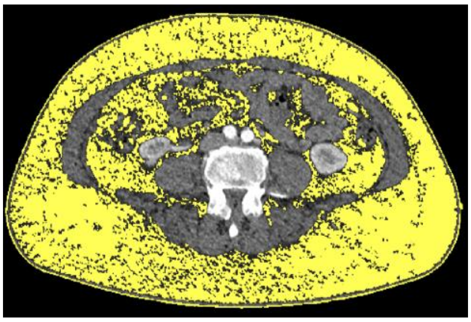

Figure 9. Fat segmentation after thresholding without further processing. The visceral fat is removed by manual mask splitting, the holes are filled by an automatic 3-pixel gap filling.

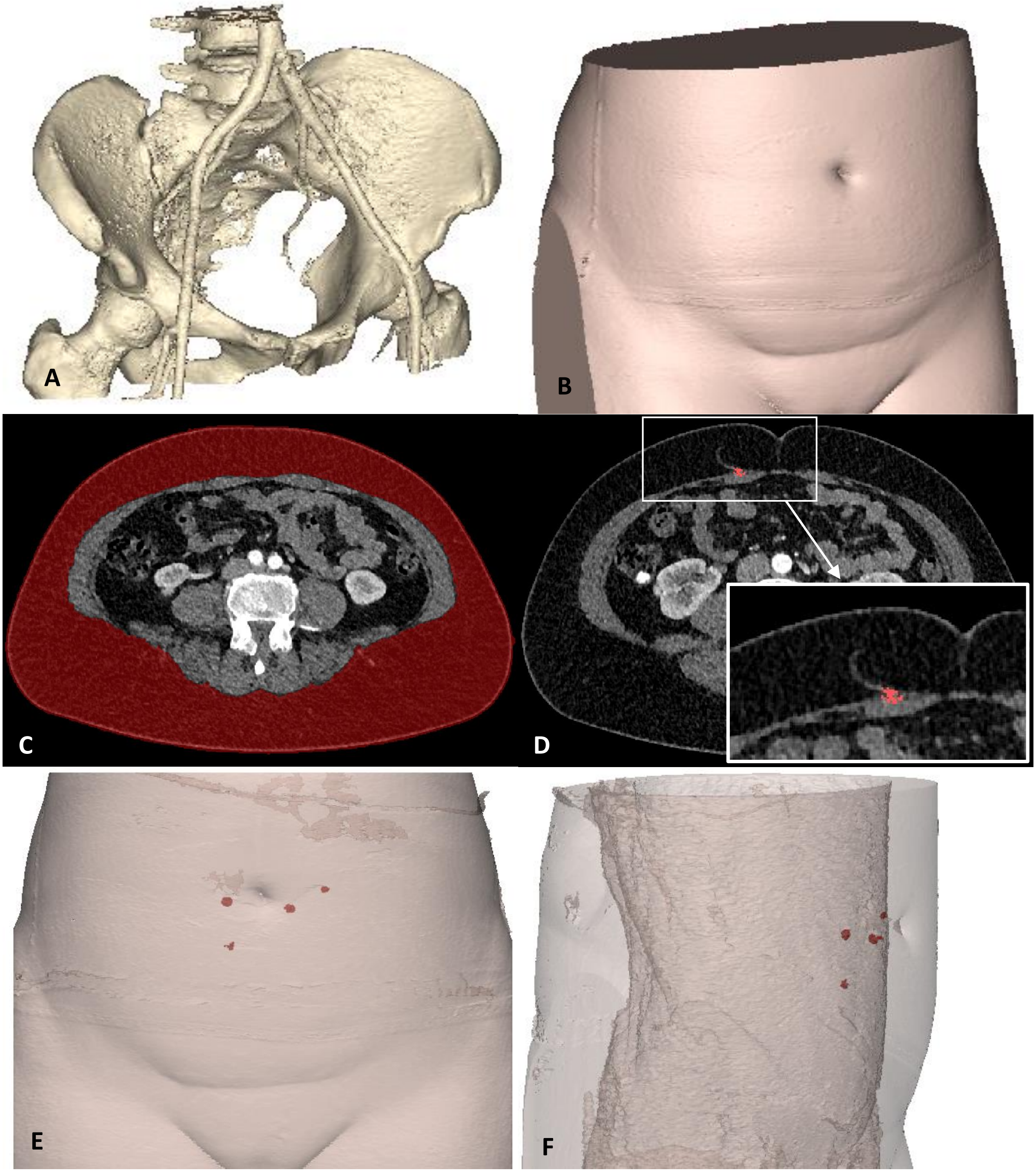

Figure 10. Segmentation of the CTA scan of a random patient. A: Bones segmentation. B: Full body segmentation. C: Fat segmentation (red) of an axial slice. D: Perforator location segmentation (red) of an axial slice, with a close-up. E. Perforator location segmentation visualization in a transparent full body segmentation, front view. F. Perforator location segmentation visualization in a transparent fat segmentation, lateral right view.

Chapter 3 Semi-automatic DIEP flap delineation and volume planning

To virtually plan a DIEP flap volume, various steps must be taken. Initially, a DIEP flap delineation for the abdominal incision has to computed, and subsequently the corresponding volume of the delineation must be calculated. The delineation will be semi-automatically determined, while adhering to the guidelines as described in 1.2, after which the volume for that delineation will be calculated. This chapter describes the development of this semi-automatic algorithm and the clinical volume validation for the algorithm that was performed.

3.1 Design of semi-automatic planning algorithm

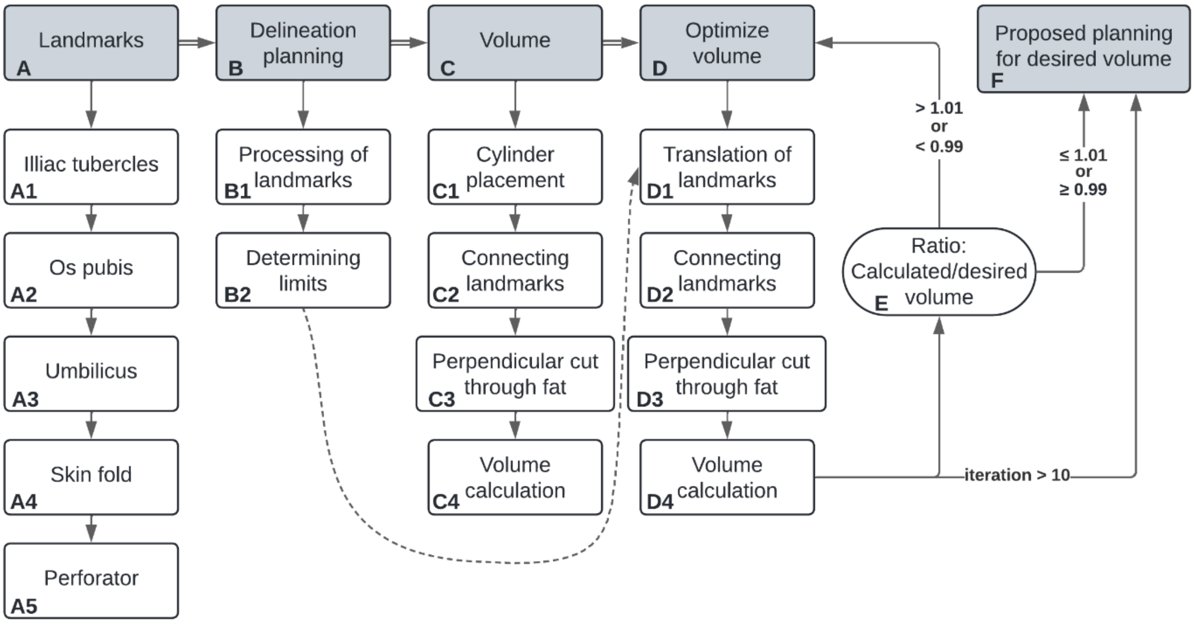

Figure 11. Flowchart of the algorithm used to create delineations with a corresponding volume for DIEP flap breast reconstructions. The dashed line represents a dependency of the translations of landmarks of the limits that were determined.

The semi-automatic DIEP flap delineation was done using scripting in 3-Matic (Materialise, Leuven, Belgium) and is summarized in Figure 11. The delineation is based on various landmarks (A track in Figure 11): umbilicus, symphysis, tubercles of the iliac crest, perforator locations and skin folds, as illustrated in Figure 12. These landmarks are manually selected and some of those are further processed. The symphysis and tubercles of the iliac crest are selected on the bone segmentation. Since the middle of the symphysis in cartilage, it is not visible on the segmentation of the bones. Due to this, the symphysis is determined with two clicks, by selecting a point directly left and right of the symphysis and averaging it. The iliac tubercles are chosen to determine how high the lateral corners of the delineation should be. In reality, this is also based on the skin folds of a standing person.[15,53] However, the CTA scan is made while the patient is lying down, so these skin fold are not visible. Another guideline that was used, was the location of the iliac tubercle, so this was used as a substitute.[54] This landmark was adjusted to be located on the coronal plane, and thus in the exact middle of the body of the person. The symphysis and iliac tubercle landmarks were translated two centimetres cranial as this was the approximate guideline used (B1 in Figure 11).[15,53,54] The umbilicus and skin folds are selected on the full body segmentation. The skin fold landmark is only selected when a skin fold around the caudal incision is visible, and it is placed on a vertical line drawn between the umbilicus and symphysis to improve the symmetry of the delineation. The perforator location of the most cranially located perforator is selected with the perforator segmentation, illustrated in Figure 12D. The cranial incision is dependent on the umbilicus, it cannot go on under the umbilicus, so a limit is based on this (B2 in Figure 11). However, since the cranial incision should also be at least two to three centimetres above the perforator to reduce the risk of complications, the limit is adjusted if the perforator is less than two centimetres below the umbilicus.[15]

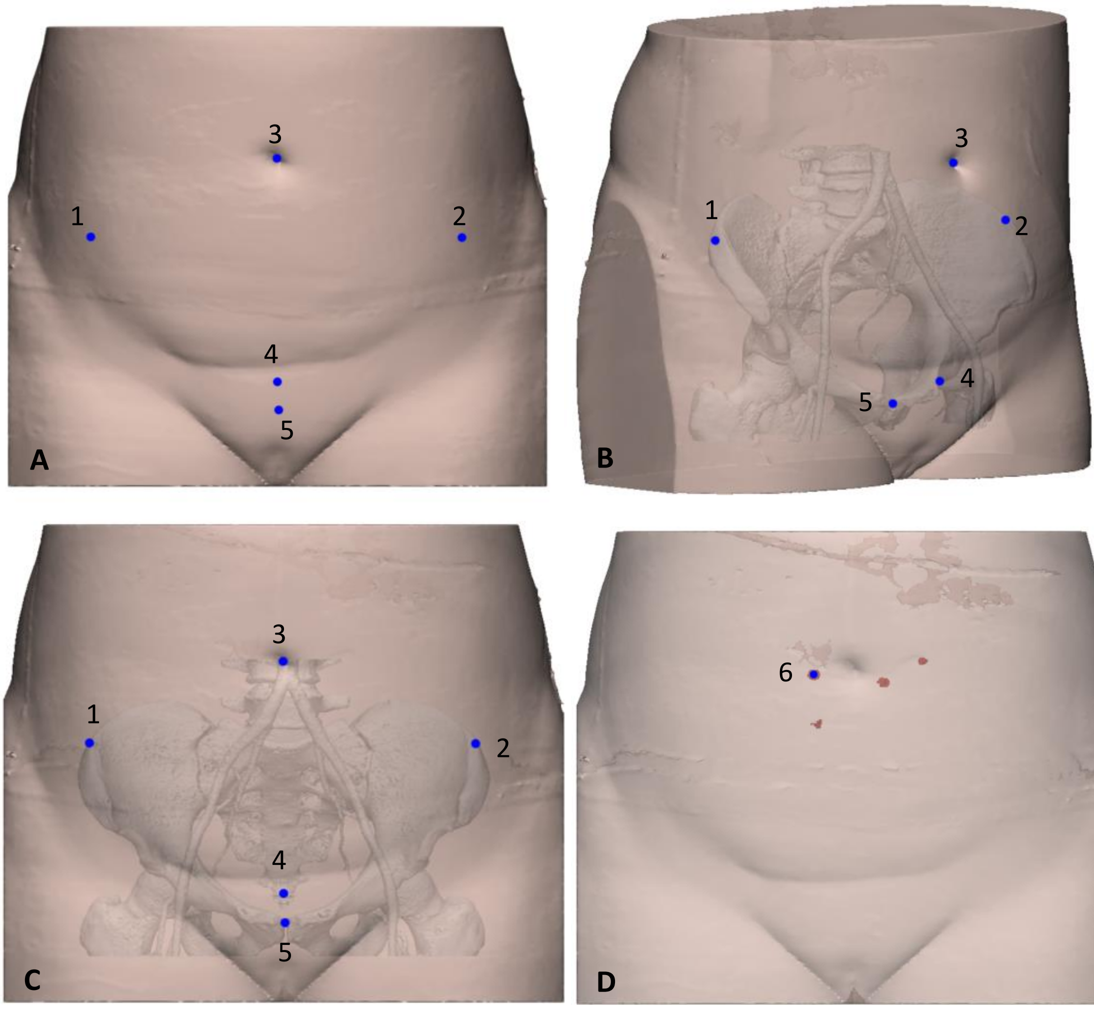

Figure 12. Landmark locations used by the planning algorithm. A in Figure 11. A. Full body visualization, front view. B. Transparent full body visualization with bones showing, side view. C. Transparent full body visualization with bones showing, front view. D. Transparent full body visualization with perforators showing in red, front view. Landmarks: 1. Right iliac tubercle. 2. Left iliac tubercle. 3. Umbilicus. 4. Lowest point of skin fold. 5. Symphysis. 6. Perforator.

An initial delineation is made on a cylinder of the same size as the patient's body (C1 in Figure 11), shown in Figure 14. Seen from a top view, the widest part of the cylinder is positioned in the middle of the patient's body to mimic the surgeon's cut as best as possible. The cut will be made approximately perpendicular to the skin of the patient, so the surface normal of the patient should be similar to the surface normal of the cylinder. Initially, the delineation was made on the CTA model, however, the surface of the CTA model was too rough for the extrusion step later in the process, even after smoothing, illustrated in Figure 13. To still be able to make a cut perpendicular to the skin, but also have the smooth surface that is required for a straight cut, the cylinder was chosen.

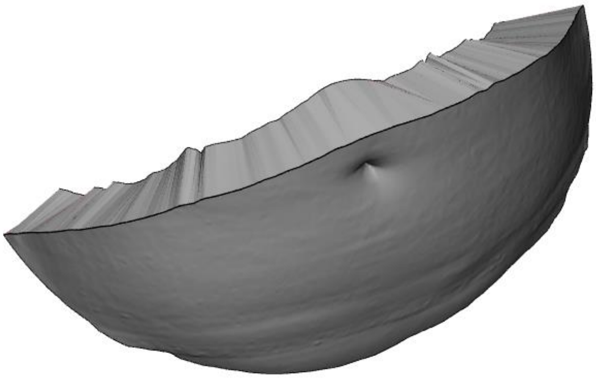

Figure 13. Extruded surface of CTA model, leading to rough edges instead of straight cut.

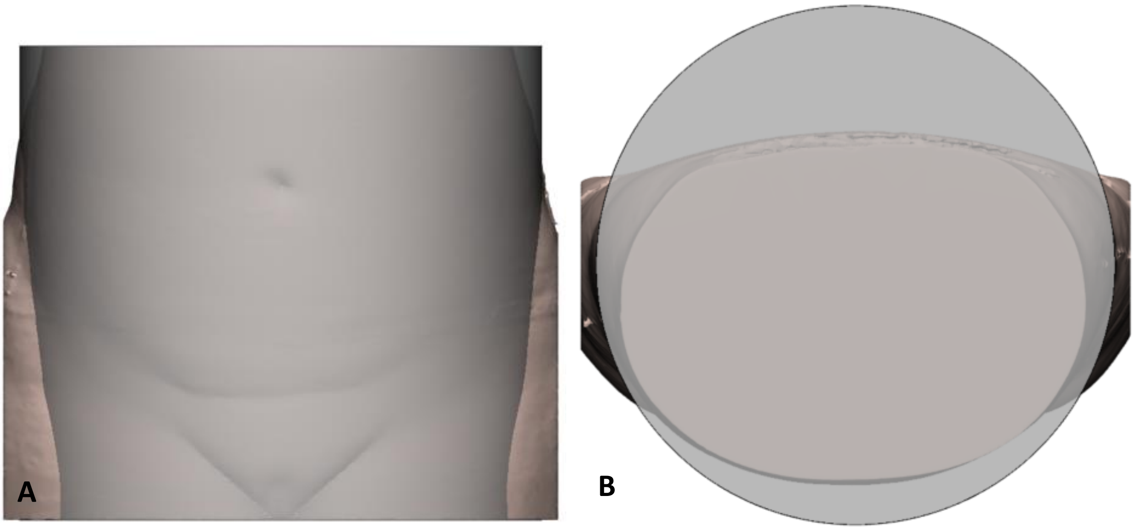

Figure 14. The cylinder used for the perpendicular cut. C1 in Figure 11. A. Frontal view. B. Cranial view. The cylinder is positioned to cover the entire 3D model (A) and with the widest part of the cylinder at the centre of the body (B).

The cranial part of the delineation is drawn from the translated iliac tubercle landmarks through a point two centimetres above the umbilicus landmark. The caudal incision goes through the skin fold landmark if present, and otherwise through the translated symphysis landmark (C2 in Figure 11). Figure 15 shows the initial delineation on the cylinder and Figure 16 shows how this delineation is extracted and extruded perpendicular to the faces of the surface of the cylinder to simulate the cut by the surgeon (C3 in Figure 11).

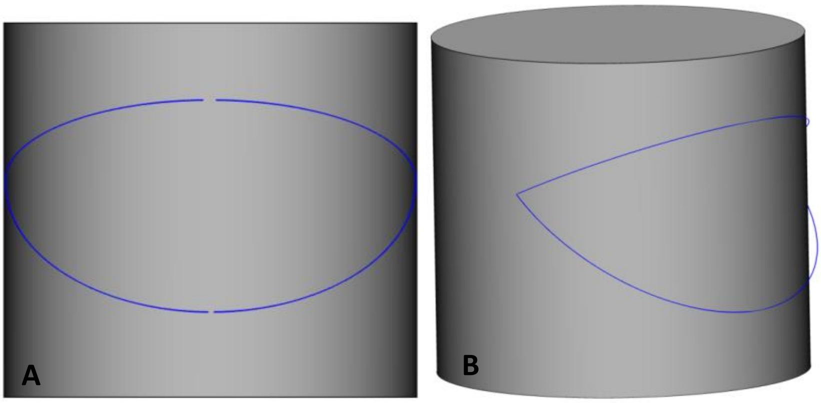

Figure 15. Cylinder with the connected landmarks for an initial flap planning. C2 in Figure 11. A. Front view. B. Front-lateral view

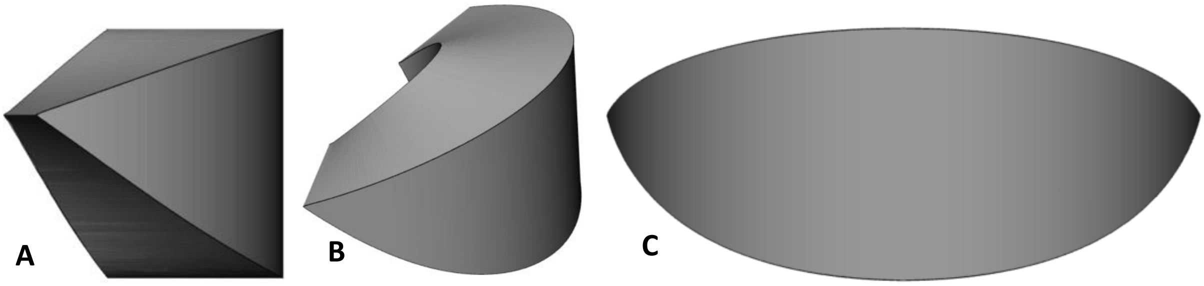

Figure 16. The extruded surface of the cylinder that will be intersected with the fat layer. C3 in Figure 11. A. Left lateral view. B. 3D view. C. Front view

A DIEP flap volume is created by the Boolean intersection of the segmentation of the fat and the cylinder, giving the result seen in Figure 17 (also part of C2 in Figure 11).

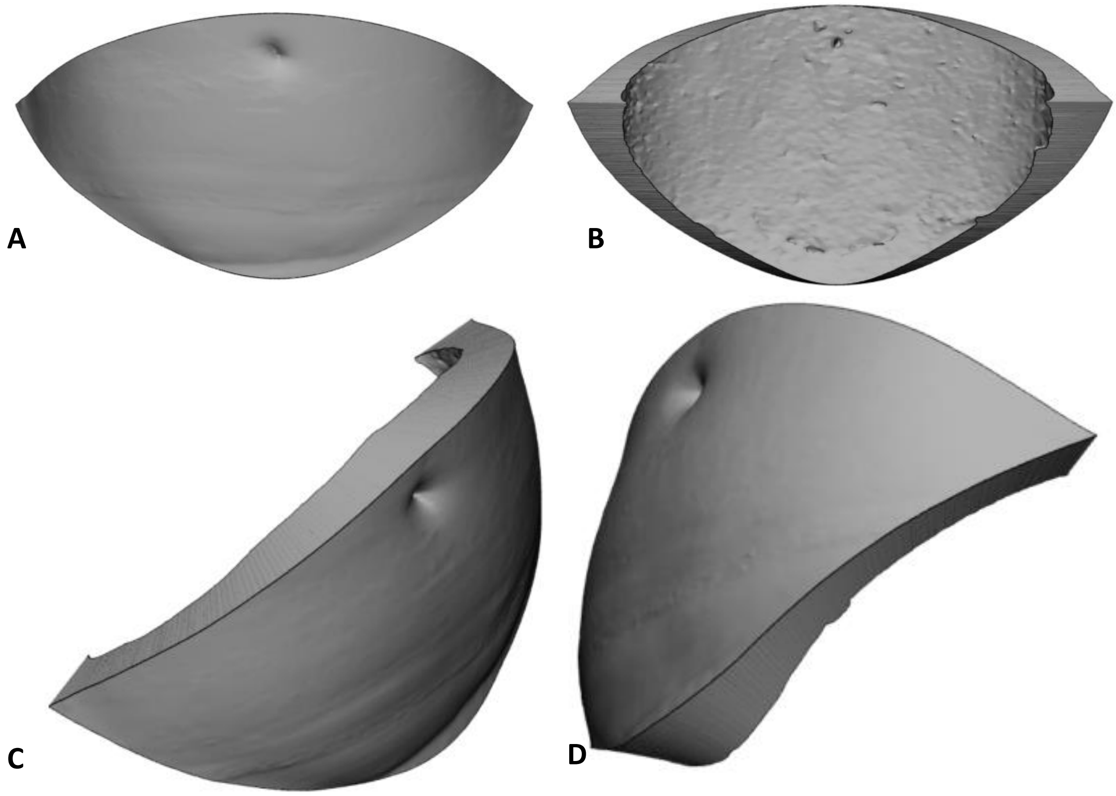

Figure 17. Final flap calculated by Boolean intersection of the extruded cylinder surface and the fat layer segmentation. C2 and F in Figure 11. A. Frontal view. B. Dorsal view. C/D. 3D view

The ratio between the volume of the calculated flap and the desired volume for the breast is calculated. Depending on the ratio, landmarks are automatically adjusted (D1 in Figure 11). When the calculated volume is less than the desired volume, the cranial incision is moved more cranial by translation of the umbilicus landmark. If the umbilicus cannot be moved more because the total height of the flap would become too large to close the wound, the lateral points of the delineation are translated towards to the dorsal side. The caudal incision is already at the lowest point possible and thus will not be changed. When the calculated volume is more than the desired volume, the umbilicus landmark is translated caudally, to move the cranial incision in that direction. Changing this incision will reduce the volume the most and keep the scar as low as possible. When the cranial incision is as low as possible, the caudal incision can be moved more cranial, but this will affect the scar location. Preferences about this should be discussed with operating surgeon and the patient. After translation, the same process as described above, meaning connecting the landmarks, extrusion of the cylinder surface and intersection with the fat layer, is performed (D2-D4 in Figure 11).

Translation of the landmarks is done iteratively (E in Figure 11), until the volume has less than 1% deviation from the desired volume, or when the landmarks reach their limits, or after ten iterations. After ten iterations, only slight changes to the delineation are observed, and the landmarks are reaching their limits. Figure 18 shows how the planning changes for the various iterations. After the iterative process a final flap is determined, equal to Figure 17 (F in Figure 11). The various drafts of the algorithm were discussed with the plastic surgeons and improved based on the feedback.[15,53]

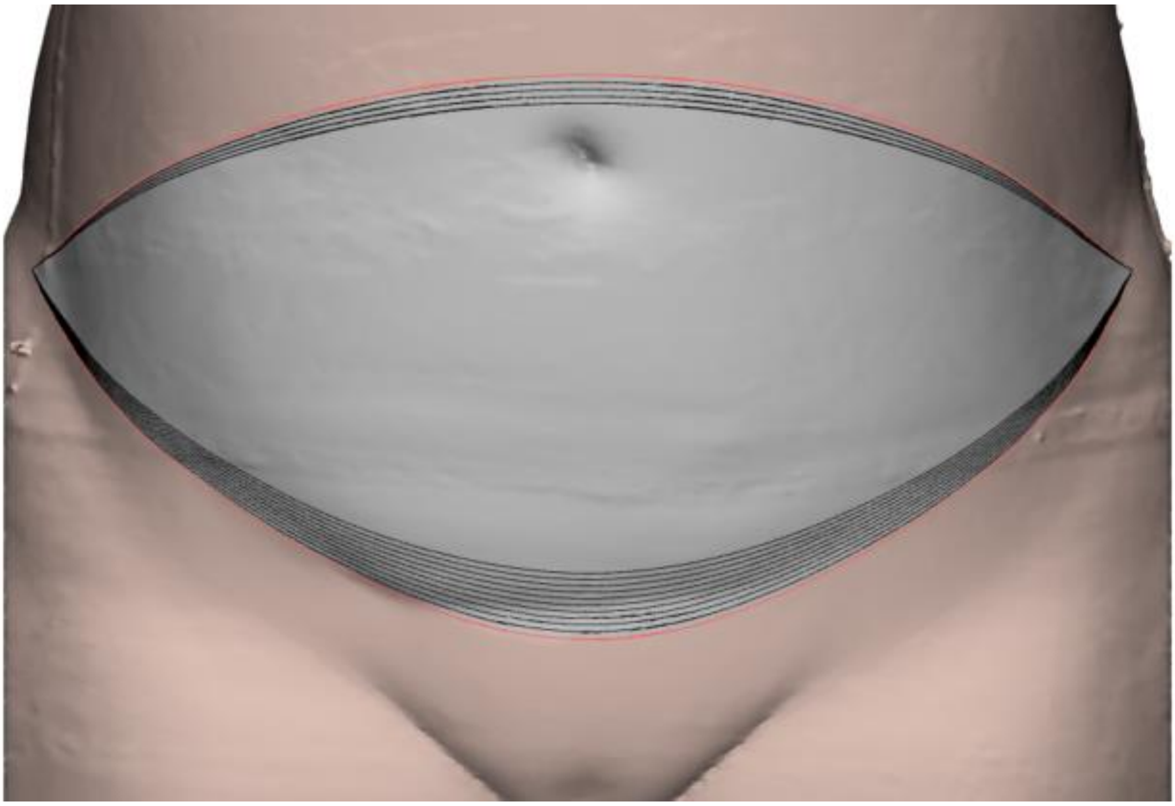

Figure 18. Different iterations of the same planning. The initial planning (red) gave a too large volume. The algorithm adjusted to delineation towards a smaller volume. The final distance between the cranial incision and the umbilicus in this planning it higher than regular for a flap with too much volume due to a cranial positioned perforator. E in Figure 11.

An initial step has been taken towards enhancing planning for unilateral reconstructions. This involves planning the portion of the flap that will provide the desired volume to be implanted in the breast. For this planning, two additional incision lines are planned: the midline cut and the lateral corner. Based on the desired and current volume, iterative adjustments and other constraints, either the midline cut, or the entire flap delineation is modified to reach to desired volume. While the current algorithm does provide a volume for this part of the flap, the process must be improved by optimizing which incision should be changed to get to the desired volume. Since this depends on the optimal delineation of the entire flap as well, more results about the correctness of the entire flap delineation should be acquired before this optimization can be done efficiently.

3.2 Volume validation

To be able to compare the per-operative delineation to the virtual delineation, either the actual per-operative delineation must be transferred to the CTA model, or the virtual delineation must be transferred to the patient. Transferring the actual delineation to the CTA model has the benefit of not interfering with the workflow of the plastic surgeons. This method imposes no additional burden on the patient and the plastic surgeons cannot be affected by additional knowledge. Furthermore, the data can be analysed retrospectively. To validate the volume predicted by the tool for a certain delineation, the 3D scans of the delineation were used to create a digital flap which was compared to the per-operative weight of the flap. Given inherent variations in factors like breast size and exact dissected weight, the aim is to predict the DIEP flap volume within a 10% deviation.[15]

3.2.1 Methods

Volume validation was performed in 3-Matic (Materialise, Leuven, Belgium) with a workflow that follows the same steps as the planning algorithm with regard to mimicking the surgeon's cut, but uses 3D scans to determine the delineation. The workflow is summarized in Figure 19.

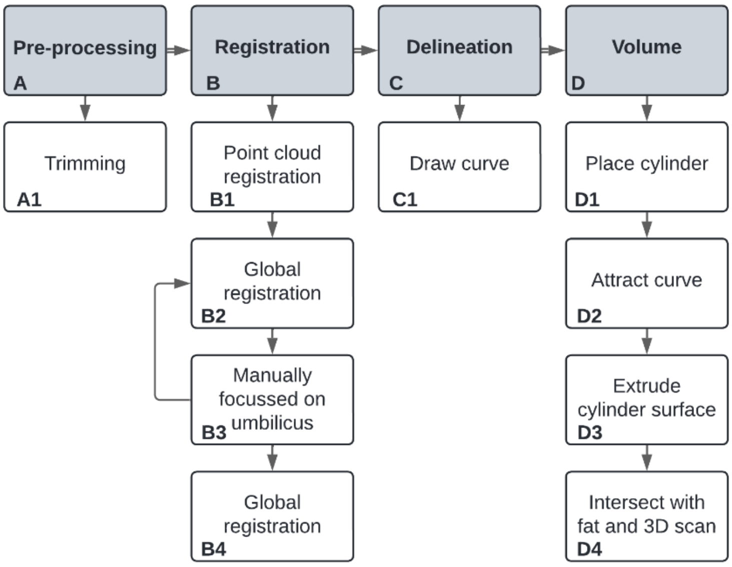

Figure 19. Flowchart of the process to validate the volume using 3D scans.

3.2.1.1 Participants

The population consists of the participants acquired in 2.1.1, which were patients going for a DIEP breast reconstruction, both unilateral or bilateral and both immediate and delayed, included in Ziekenhuisgroep Twente (ZGT) hospital.

3.2.1.2 Registration

Initially several methods were explored to match the per-operative images with the delineation to the CTA model. This included photogrammetry and projection of 2D images. Those are elaborated on in Appendix D. Unfortunately, these methods did not achieve the required level of accuracy. An alternative approach investigated was using 3D scans obtained with the Revopoint POP 2 to transfer the delineation to the CTA model. Despite inherent limitations of this method, amongst others the deviation on the lateral sides shown in Figure 52 in Appendix D, this option was chosen as best option.

The per-operative 3D scans were trimmed to eliminate confounding data like arms and legs (A1 in Figure 19). Then, the 3D scan was registered on the CTA model (B track in Figure 19). This was done by a rigid point-cloud registration of the umbilicus and SIAS, or other easily identifiable landmarks, like the pubic area. The result of this can be seen in Figure 20. Optimalisation was done using the *Global registration* function.

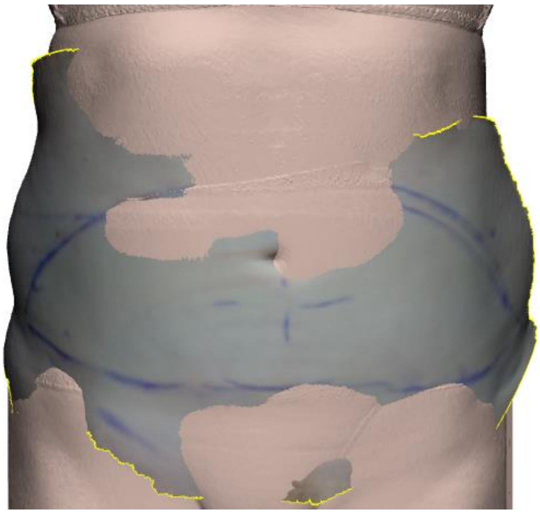

Figure 20. Result of rough registration using point-cloud registration of CTA model and 3D scan. B1 of Figure 19.

The umbilicus was used as a ground truth for optimal registration. Manual correction of the registration was performed when the umbilicus was not registered correctly, as can be seen in Figure 21 to Figure 23. Another *Global registration* was performed, unless the umbilicus did not remain properly registered. The average distance error as given by Materialise 3-Matic during *Global registration* was noted.

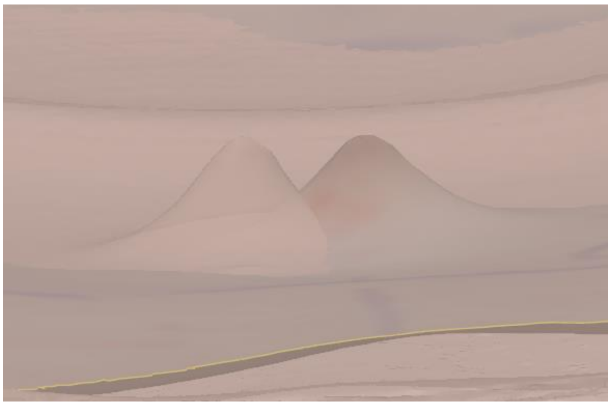

Figure 21. Umbilicus position as seen from the top after rough registration using point-cloud registration of CTA model and 3D scan. Umbilicus of CTA model is left on the image, Umbilicus of 3D scan on the right. B3 of Figure 19.

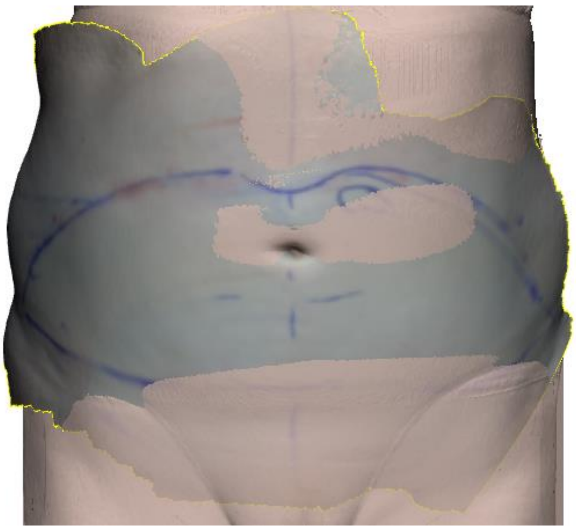

Figure 22. Registration after manual translation and rotation while focusing on the umbilicus. B3 of Figure 19.

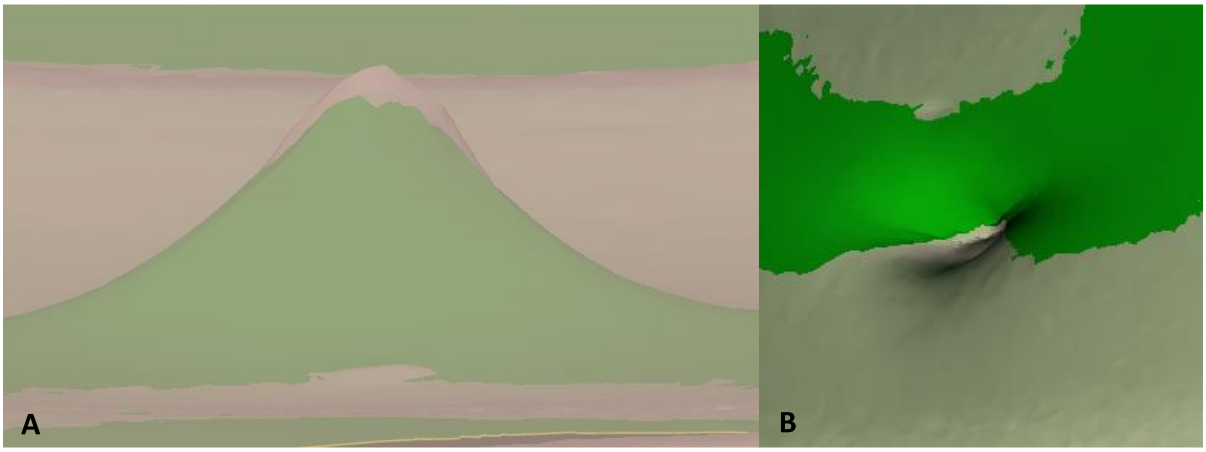

Figure 23. A. Top view of umbilicus after registration. Green is the 3D scan. Beige is the CTA model. B. Umbilicus after registration from a dorsal-lateral view to the inside of the abdomen. Green is the 3D scan; lighter green is the CTA model. B3 of Figure 19.

3.2.1.3 Transferring of delineation

Some 3D scans were of a bad quality, for example with holes in the umbilicus or skin folds. These holes were repaired using *Fill Hole Freeform.* After registration and possible restauration of the 3D scan, the delineation of the 3D scan was manually traced using 3-Matic (C in Figure 19), see Figure 24, and attached to a cylinder, similar to Figure 14, that was fit to the CTA model as seen in Figure 25 and Figure 26 (D1-D2 in Figure 19). Attaching of the delineation to the cylinder was done using a minimisation of the distance between the 3D objects.

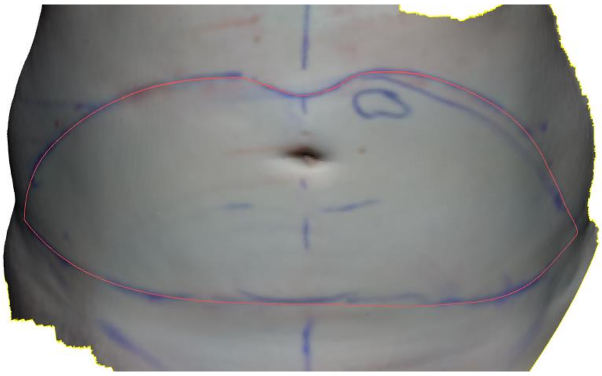

Figure 24. 3D scan with a manually drawn curve in red following the blue delineation made by the plastic surgeon during surgery. C of Figure 19.

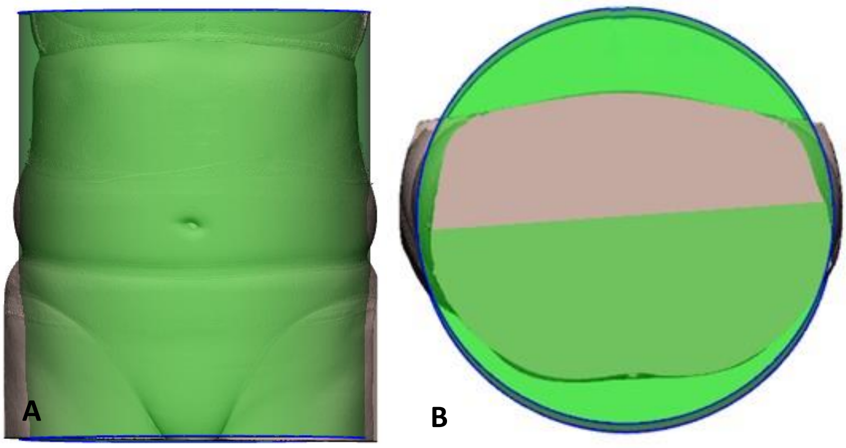

Figure 25. The cylinder used for the perpendicular cut. A. Frontal view. B. Cranial view. The cylinder is positioned to cover the entire 3D model (A) and with the widest part of the cylinder at the centre of the body (B). D1 of Figure 19.

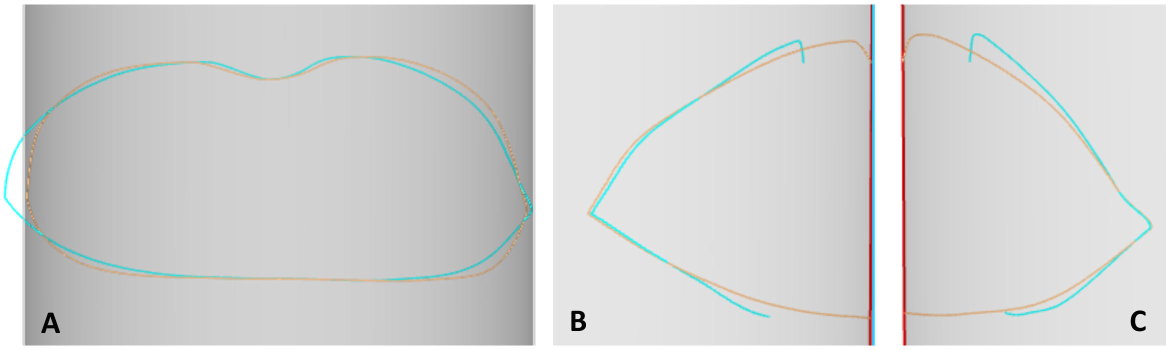

Figure 26. Close-ups of the attracted curve on the cylinder. Blue: Manual delineation on 3D scan (red curve of Figure 24). Orange: The curve on the surface of the cylinder transferred using a minimal distance attraction. D2 of Figure 19. A. Front view. B. Left view. C. Right view.

Similar to Figure 16, the surface of the cylinder within the delineation was separated and extruded perpendicular to the surface (D3 in Figure 19), as shown in Figure 27 and Figure 28. The delineation had to be transferred to the cylinder to ensure the same cut as used in the algorithm. This leads to the consideration whether the difference in delineation between the 3D scan and the cylinder would be negligible, especially as the delineations seem to vary in certain 2D views, as illustrated in Figure 26. This was investigated by ensuring the extrusion did not only reach the fat layer, but also the 3D scan, as seen in Figure 29. The intersection of the extruded cylinder surface was assessed by visual inspection of the lines and the difference in surface area was determined.

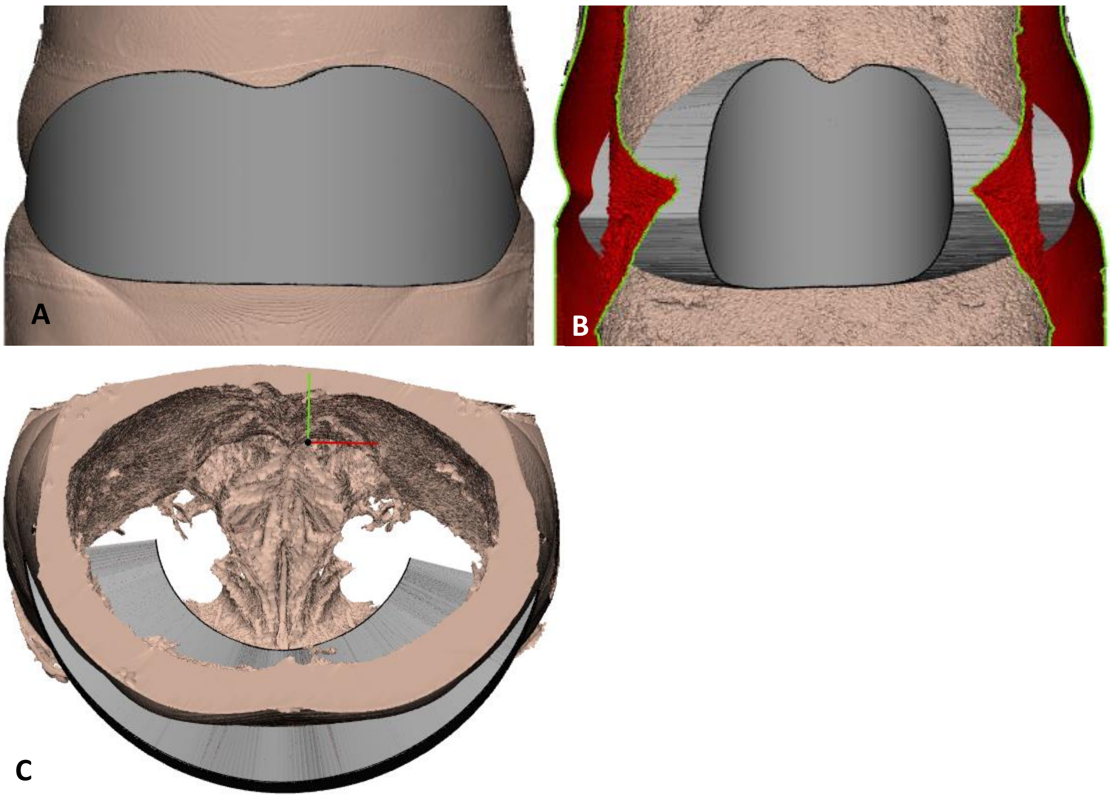

Figure 27. View of how the cylinder surface is extruded to fully cross the fat layer for intersection. D3 of Figure 19. A. Front view. B. Back view (from inside) C. Top view

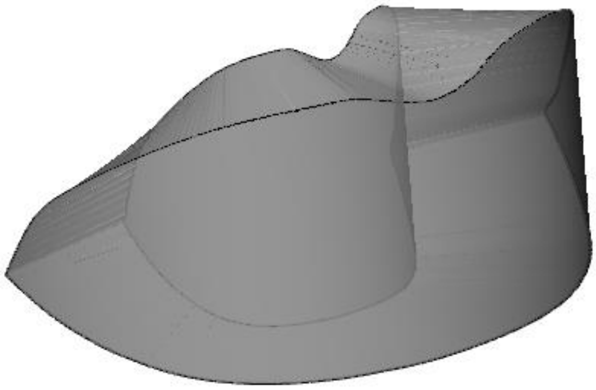

Figure 28. Transparent 3D view of the extruded cylinder surface used for Boolean intersection. D3 of Figure 19.

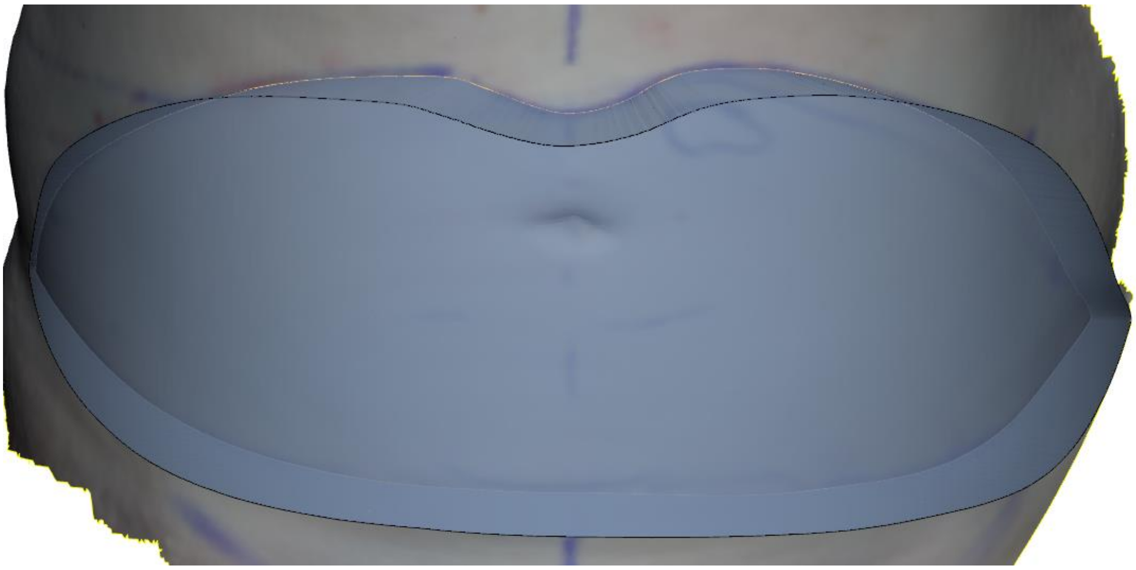

Figure 29. View of how the cylinder surface is extruded to fully cross the 3D scan, front view.

3.2.1.4 Volume

The DIEP flap of Figure 30 was created by the Boolean intersection of the segmentation of the fat and the extruded cylinder (D4 in Figure 19). This volume was converted to weight using the density of 0.89 g/mL (1.12 mL/g).[51] The per-operative weight of the harvested flap and the calculated weight of virtual flap were compared, as well as the surface area of the delineation of the 3D scan and the virtual flap.

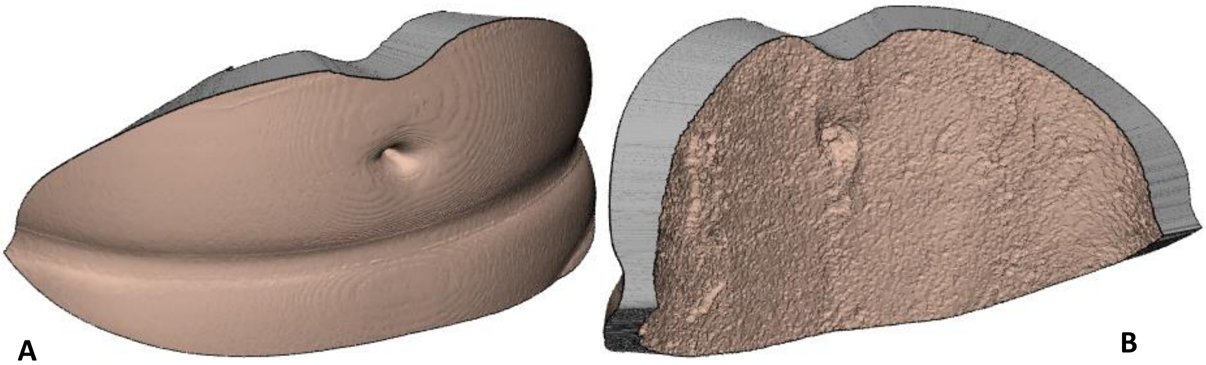

Figure 30. The calculated flap. D4 of Figure 19. A. Frontal view. B. Dorsal view

3.2.2 Results

The patient demographics, results of accuracy of the registration and the results of the volume measurements are shown below.

3.2.2.1 Participants

A total of twenty-four patients were initially included to validate the volume. Nine of those were excluded due to a missing 3D scan of the per-operative delineation, while another two were excluded due to insufficient quality of the 3D scan, leaving n=13. Among the included patients, one underwent a stacked DIEP flap procedure for unilateral reconstruction. In one patient breast reconstruction was not performed, as the quality of the acceptor vessels was insufficient. This patient was not included in the flap weight of Table 2, since only the total flap weight was known, and not the discarded and implanted weight. The flap weights are also visualized in Figure 31. With the aim of 10% deviation, for the average weight of 1417 grams for the harvested flaps, this would equate to a permissible deviation of 141 grams.

Table 2. Patient demographics. Underwear is graded as follows: – no underwear, +/- underwear, but negligible effect, + underwear with effect, ++ severe effect of underwear. Examples of these grades are shown in Figure 4. Leg position indicates if the legs were raised during CTA acquisition or not. CTA age indicates the time between the date the CTA was made, and the surgery performed. Status at the start indicates the status of the breast before reconstruction. Breast volume indicates the volume of the breast that went for surgery. Since ablated breasts without implants have no volume, they were excluded. Another distinction was made between natural breasts and prostheses or tissue expanders (TE). The discarded and implanted flap weights are determined per implanted flap, which means two flaps were obtained out of one harvested flap for the bilateral reconstructions. The changed caudal incision indicates if the caudal incision was changed after acquiring the images of the delineation due to the expected difficulty with closing the wound.

	Bilateral reconstruction (n=6)	**Unilateral reconstruction (n=7)**	**All (n=13)**
Age (mean years ± SD)	46.3 ± 4.5	53.0 ± 5.0	49.9 ± 5.8
BMI (mean ± SD)	29.0 ± 3.0	28.8 ± 2.9	28.9 ± 2.9
Reconstruction type (n=)			
Delayed	4	3	7
Direct	2	4	6
Underwear (n=)			
-	0	2	2
+/-	1	1	2
+	3	3	6
++	2	1	3
Leg position CTA (n=)			
Raised	2	5	7
Down	4	2	6
CTA age (mean days ± SD)	239.5 ± 162.2	40.1 ± 40.4	132.2 ± 151.3
Status at start (n=)			
No breast	0	1	1
Natural breast	2	4	6
Prothesis	3	1	4
TE	1	1	2
Breast volume (mean cc ± SD)			
All breasts	416 ± 80 (n=12)	557 ± 168 (n=6)	463 ± 131 (n=18)
All natural breasts	430 ± 40 (n=4)	534 ± 197 (n=4)	482 ± 143 (n=8)
Flap weight (mean grams ± SD)			
Harvested	1428 ± 363 (n=5)	1409 ± 474	1417 ± 413 (n=13)
Discarded	48 ± 76 (n=10)	758 ± 333	340 ± 417 (n=17)
Implanted	666 ± 169 (n=10)	652 ± 213	660 ± 182 (n=17)
Changed caudal incision (n=)	3	2	5

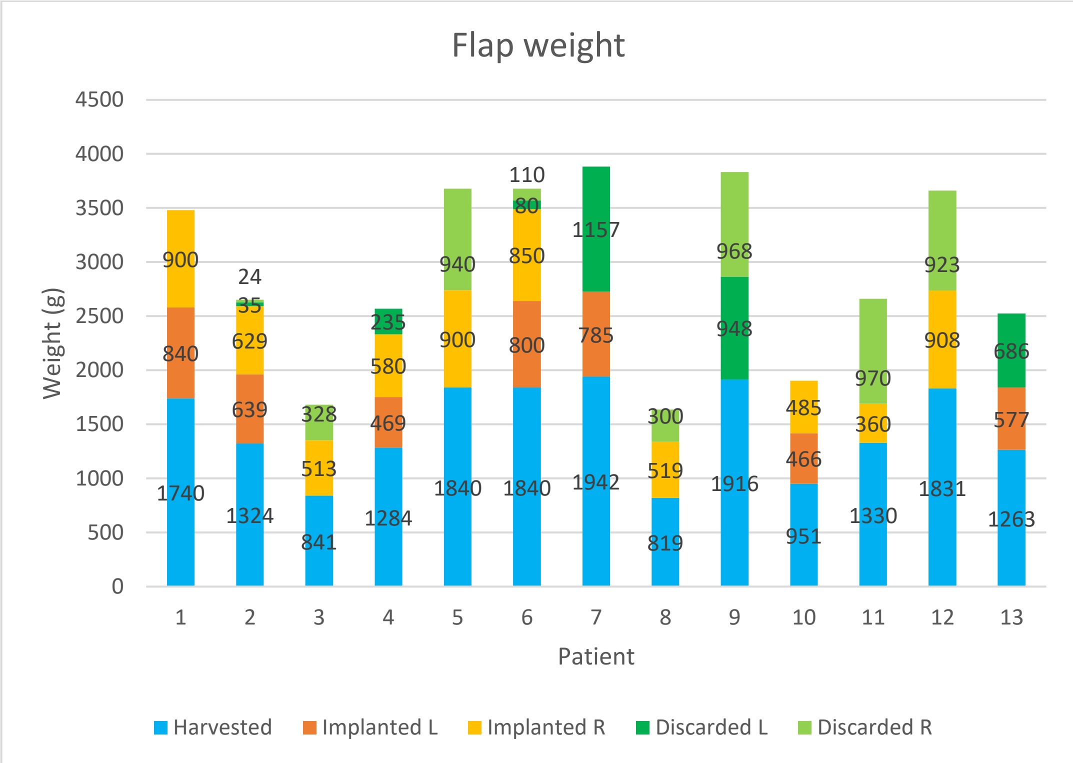

Figure 31. Flap weight per patient, giving the harvested weight, the implanted weight and the discarded weight. For bilateral reconstructions, the implanted and discarded weight is divided in the left and right side.

3.2.2.2 Registration and transferring of the delineation

The quality of the registration was assessed by determining the surface area of the delineation in the 3D scan, the surface area of extruded cylinder surface that intersects with the 3D scan and the surface area of the delineation on the CTA model. The scatterplot of these results is shown in Figure 33. An example of the visual assessment is shown in Figure 32, as well as Figure 53 and Figure 54 in Appendix F. The visual assessment of the other subjects showed similar results. Furthermore, the mean average distance error between the CTA and trimmed 3D scan was found to be 0.9 ± 0.1 mm. More details about the results are shown in Table 6 in Appendix E.

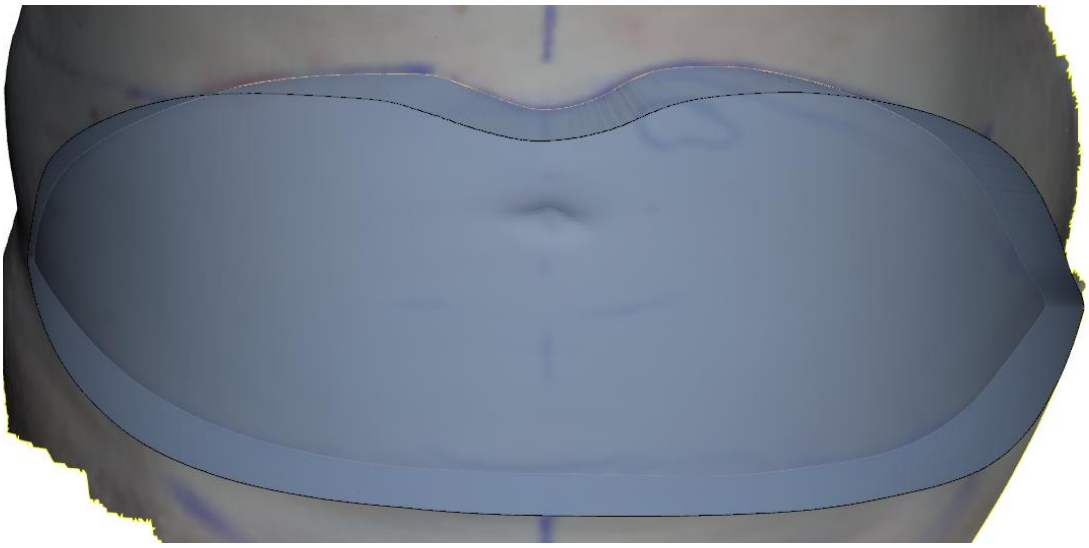

Figure 32. Visualization of how the extruded cylinder surface follows the original delineation of the 3D scan. In orange the traced delineation.

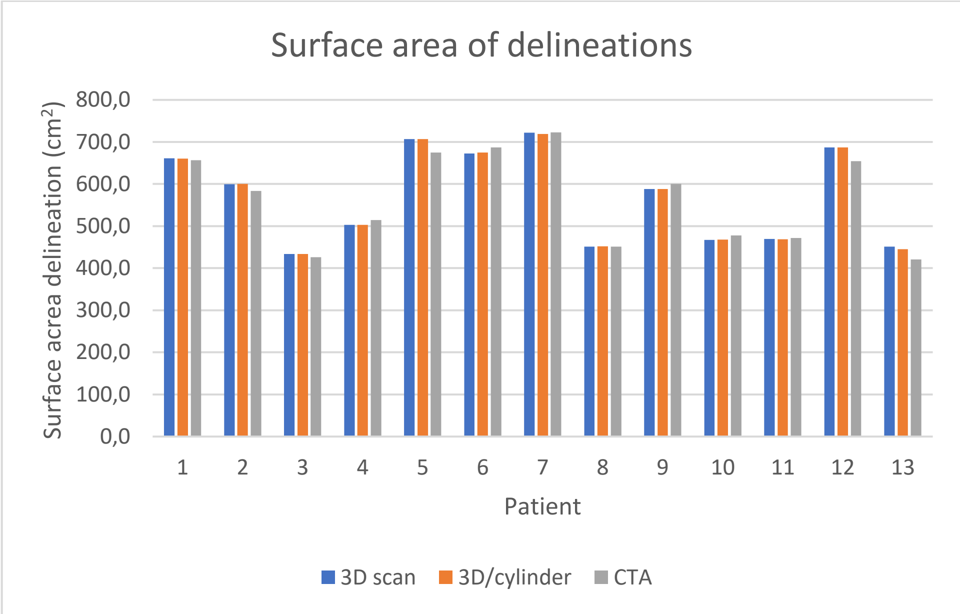

Figure 33. Bar chart of the surface area within the delineation of the surgeon as manually drawn on the 3D scan and the surface area of the virtual delineation projected on the CTA model. The 3D/cylinder bar shows the surface area of the delineation as given by the intersection of the extruded cylinder surface and the 3D scan, as seen in Figure 29.

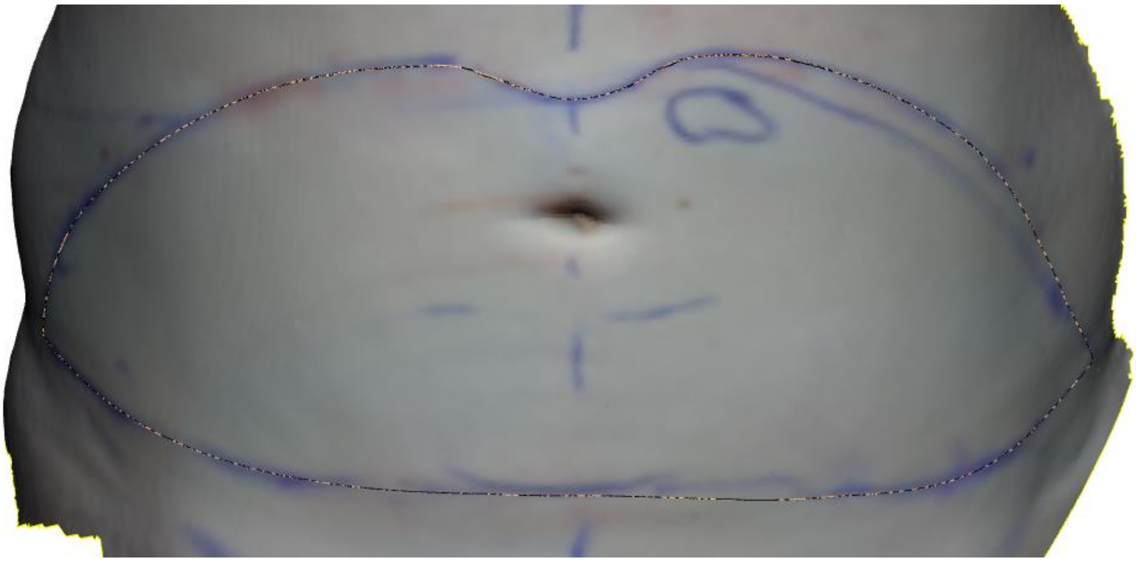

Figure 34. Visualisation of how the delineations align and overlap. In orange the original curve that was manually traced over the delineation. In black the curve that was made by Boolean intersection of the extruded cylinder surface and 3D scan.

3.2.2.3 Volume

Comparison of the harvested flap weight and the virtual flap weight is shown in the scatterplot of Figure 35. The mean difference in weight between the harvested and actual weight when taking the absolute values is 11.9% and 166,6 grams, with more details shown in Table 7 in Appendix E. Comparing the relative and absolute difference between weight of the actual flap and the virtual flap shows a linear trend, seen in Figure 55 in Appendix E. Due to the linear trend between the absolute and relative difference in weight, only the figures showing the relative weight difference are shown. The results regarding the absolute weight difference can be found in Appendix E.

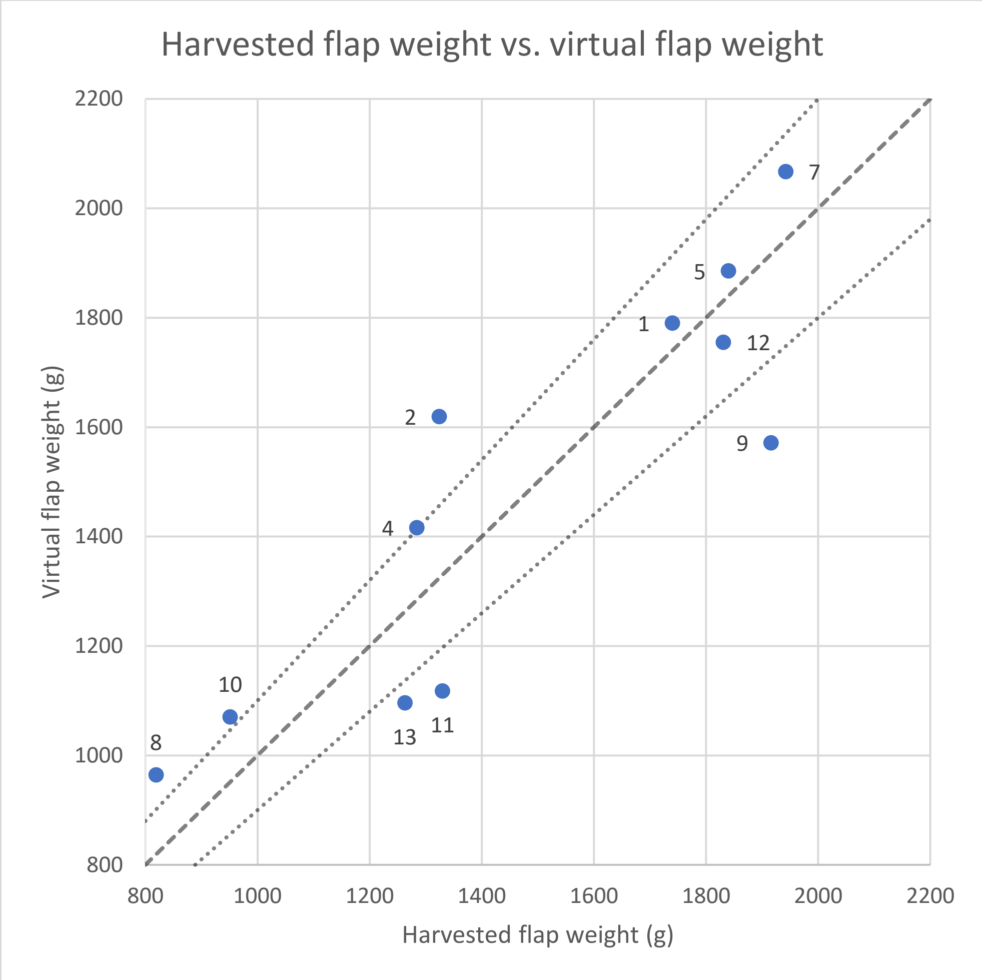

Figure 35. Scatterplot of the harvest flap weight versus the virtually determined flap weight, with dashed lines for the expected trend and 10% deviation. The numbers indicate the patient.

Various scatterplots and boxplots were made to compare the difference in harvested and virtual flap weight to the various demographic factors. Figure 36 shows scatterplot of the CTA age versus the flap weight difference. After dividing the CTA ages in 'very recent' (<21 days), 'recent' (<100 days) and 'old' (≥ 100 days), a boxplot could be made which is shown in Figure 57 in Appendix E. A significant difference was found for the difference in flap weight compared to CTA ages. A significant difference was also found for the difference in weight between the various underwear grades, shown in the boxplot of Figure 37.

Having raised legs during the CTA or having a changed caudal incision during surgery did not result in significant difference in either the relative of absolute difference between weight of the actual flap and the virtual flap, as determined with the boxplots in Figure 59 and Figure 60 in Appendix E. Additionally, scatterplots analysing the relationship between the difference in flap weight and various parameters, including the difference in surface area of delineation between the 3D scan and CTA models, BMI, and the harvested flap weight, did not reveal any discernible trends. These scatterplots are also available for reference in Appendix E.

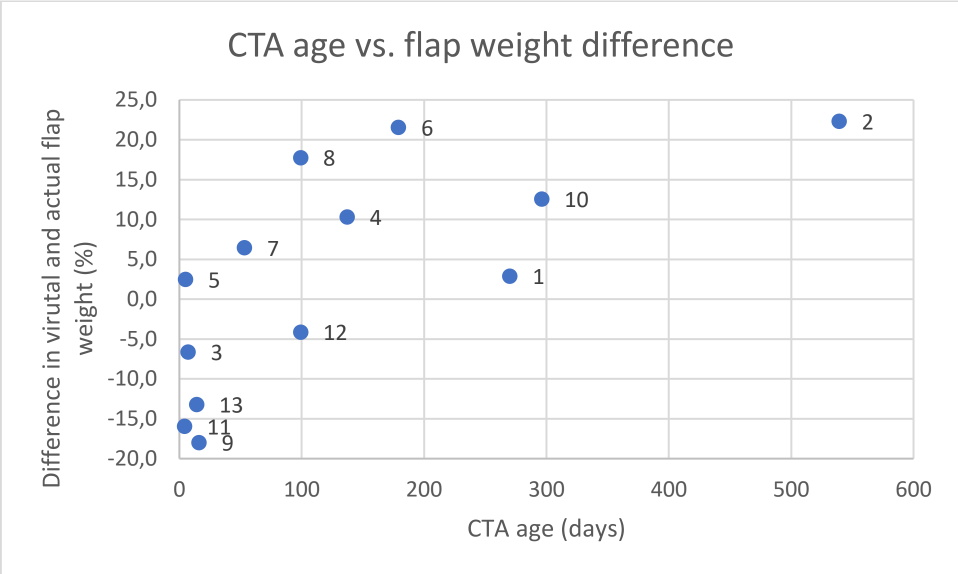

Figure 36. Scatterplot of CTA age in days versus flap weight difference. The numbers indicate the patient

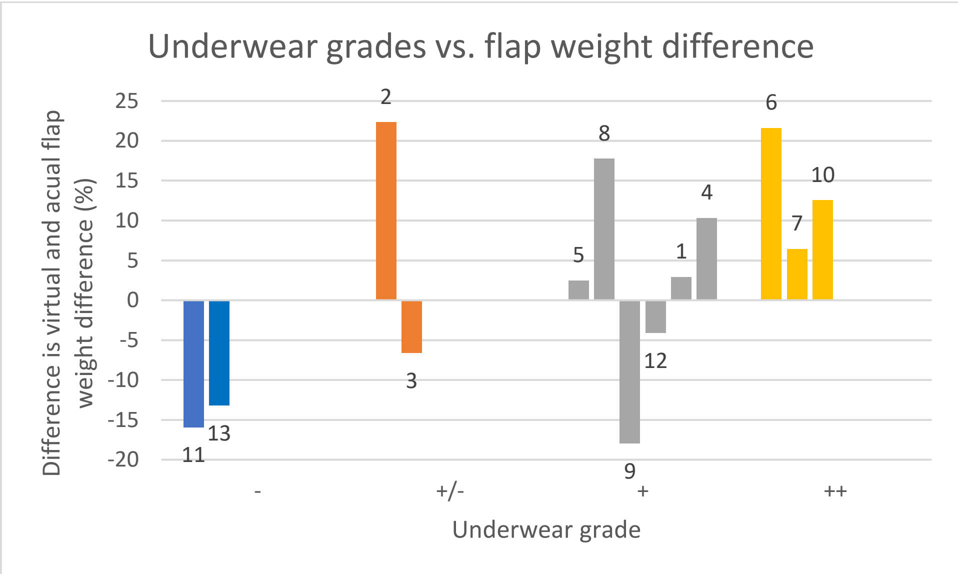

Figure 37. Bar chart of underwear grades versus flap weight difference. The numbers indicate the patient

3.2.3 Discussion

The aim to predict the flap weight with a maximum deviation of 10% was not reached, with a mean difference in weight between the harvest and actual weight of 11.9% and 166,6 grams and even higher deviations when looking at individual cases. Various options have been explored to identify where this deviations stems from. Confouding factors from the patient demographics mainly showed no significant difference, with an exception for the underwear grades and CTA age. Interestingly, it could be expected that the very recent CTA scans and the scans made without underwear would yield better results. Nevertheless, they showed relatively large deviations, with the algorithm mostly giving an underestimation of the flap weight, which was significantly different from the other CTA ages and underwear grades. It should be noted that the two subjects with underwear grade '-' were both also in the 'very recent' CTA age. Both differences could possibly be lead back to those subjects. Furthermore, one of those subjects had a bad quality 3D scan where holes needed to be repaired.

Additionally, patient 2 and 9 appear as outliers in Figure 35 till Figure 37. No definitive reasons were found for this, however both patients have some noticeble characteristics. Patient 2 is remarkable due to notably long interval between the CTA scan and the surgery. While no correlation was identified between flap weight difference and CTA ages exceeding 21 days, it remains noteworthy. On the other hand, patient 9 exhibited regular data across all investigated aspects; however, she experienced a significant complication during surgery where the DIEP flaps could not be implanted due to inadequate recipient vessel quality. The impact of this complication on the data is unknown, however it could have influenced factors such as tissue hydration due to fluid administration. A hypervolemic state in patient might have led to an increased flap weight due to amount of tissue hydration. Nonetheless, no measurements to validate or refute this theory were obtained during this study.

A factor that could not be objectively evaluated was the registration of the 3D scans on the CTA models. This was mainly based on the umbilicus, however, not all participants had a clearly visible umbilicus. Some where shallow or compressed by underwear which made it hard to use them for a reliable registration. Visual assessment of registration showed deviations between the 3D scan and CTA model, shown in Figure 52 in Appendix D. Several hypotheses were proposed to explain these discrepancies. Firstly, a difference in body position during acquisition of the CTA and 3D scan. Secondly, it was speculated that the Revopoint POP 2 3D scanner, which is developed for making highly detailed 3D objects of small objects, might introduce errors when used for larger structures. A study done by Leilis did not support the latter hypothesis, but different body positions seemed to result in deviations of the scans.[55] With the collected data, this could not be verified for this study.

Since the data showed a deviation higher than the aim, but no explanations could be found, it can be assumed that one of the major causes for the deviation lies within data that was not collected, such as the accuracy of the registration of the 3D scans of the CTA models. This is supported by the visual assessment showing deviations between the 3D scan and CTA model. Leilis made a start with identifyng the causes of the deviation, but with a small population. Future research should focus on either quantifying the accuracy of the registration and 3D scan quality, or removing those factors all together.

3.2.4 Conclusion

With retrospective analysis of the algorithm, no definitive conclusion could be drawn due to the large error margins. Reducing the error margins can improve the reliability of the results. Transferring the delineation from the patient to the CTA model appeared to be the most challenging part. The use of a more robust ground truth than the 3D scans could aid in solving that issue. Moreover, transferring of the planning to the patient will be necessary to implement the planning in the future. Finding a suitable and accurate transfer method is thus required.

Chapter 4 Feasibility study: assessing the DIEP planning algorithm and transferral to the patient through a 3D printed mould

4.1 Introduction

To be able to plan and use a DIEP flap virtual planning, the planning must be transferred to the patient and the planned flap volume should be identical to surgically obtained flap volume. Previous validation efforts did not provide conclusive evidence regarding the correlation between the planned and surgically obtained flap volumes due to significant error margins. A major contribution to the error margins appeared to be registration of the 3D scan to the CTA model, which could not be reliably evaluated. Furthermore, this process deviated from the intended workflow and only gave values for the volume prediction of the planning, but not the quality of the delineation. These issues can be addressed by transferring the planning to the patient to reduce the error margins of registration and collect more data about the quality of the delineation. Moreover, transferring of the planning to the patient will be necessary to implement the planning in the future. A suitable and accurate transfer method is thus required.

Various options are available to transfer a virtual planning to a patient, which can be roughly divided into two groups: navigation and physical moulds. Navigation includes electromagnetic tracking, projection or augmented reality. Physical moulds are i.e. 2D printed templates on paper or 3D printed moulds.

Augmented reality is ultimately the preferred method by plastic surgeons, due to the possibility of viewing the planning and other useful information like perforator trajectories in 3D and on the patient. Multiple options are available like wearables or projection, which are already used to visualize perforators. [17,36,40,43,56–58] A limitation of wearables is that visualisation is only visible for the surgeon wearing the device. Hummelink et al. used a projector, which is visible for everyone present, but can only show the anatomy on the skin of the patient instead of in 3D.[40] Augmented reality is a suitable option, however, this technology is not readily available in this hospital.

On the contrary, 3D printing is already used and thus available and easy to add to the current workflow. Using 3D-printed moulds during autologous breast reconstruction is not new. Various studies used a 3D-printed breast mould.[18,39,41] Furthermore, Chae et al. used a 3D-printed template to show the perforators.[16] Geurts did a pilot study for a 3D printed mould for transfer of a DIEP planning, which showed that a 3D print is a robust way to get digital planning visualized in real-time, although positioning can be a challenge.[59] Despite the challenging positioning, 3D was assumed to be more reliable in the position due to the lack of landmarks on the abdomen and CTA model. Using a 3D printed mould has the benefit of using shape as landmark. Furthermore, a physical mould has minor impact on the current workflow compared to augmented reality or other navigation methods, which makes implementation smoother. Downsides includes the material costs and printing time.

This feasibility study attempts to determine the quality of the planning and transferal of the planning. This will be done by assessing how the delineation differs from the plastic surgeon's final delineation, as well as the correlation between the planned flap volume and the surgically obtained flap volume. Furthermore, the use of a 3D printed mould will be evaluated using observations and expert opinions about the strengths, difficulties and shortcomings.

4.2 Methods

4.2.1 Data collection and processing

A subgroup of the participants described in 2.1.1 and their obtained data was used for this feasibility study. Patients from all plastic surgeons were eligible. The acquired CTA scan and 3D photos were processed as described in 3.1 resulting in a patient specific planning. A couple of plannings and corresponding delineations were made and shown, together with images of the patient, expected volume and weight of the flap and perforator locations, to the plastic surgeon who was going to perform the surgery. An example of a summarizing image shown to the plastic surgeon is shown in Figure 38, the other shared information is seen in Appendix F. Remarks about the planning were noted and the planning was altered accordingly, after which the planning is discussed again until all remarks are solved.

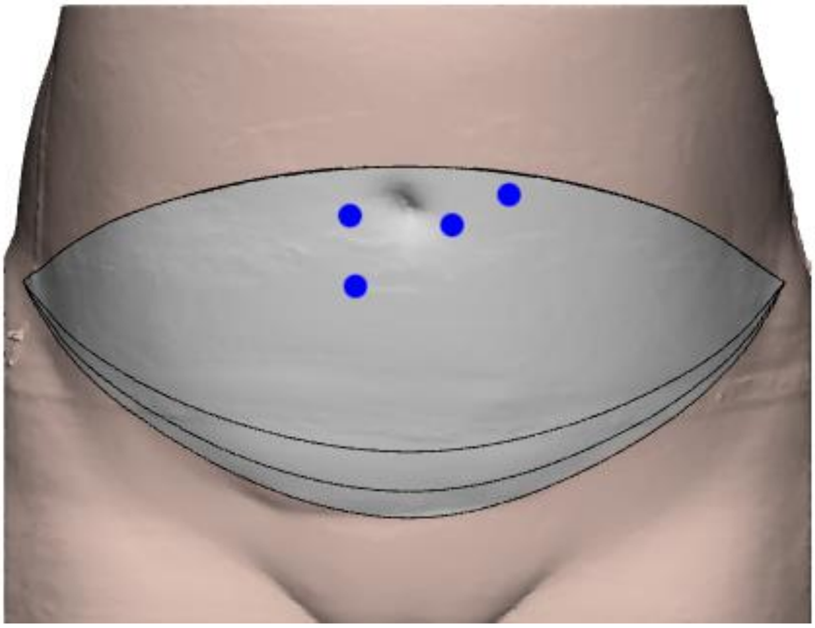

Figure 38. Summarizing image showed to surgeon to discuss the plannings. CTA model with three plannings shown in grey with a black line surrounding it. The blue dots represent the perforators.

4.2.2 3D printed mould

Figure 39 shows how the virtual planning was made into a virtual mould that can be 3D printed. The mould, see Figure 40A, consists of the delineation, the umbilicus and both SIAS as landmarks and some connections for stability if necessary. The delineation was extruded for one centimetre over the surface of the abdomen to the centre and one centimetre perpendicular to the surface to give the mould a thickness. The surgeon can draw the delineation around the outside of the mould. The umbilicus landmark was made by separating the surface of the umbilicus and extruding this one centimetre perpendicular to the surface. This means that the umbilicus landmark is shaped exactly like the umbilicus of the patient. The SIASs were indicated on the mould by a cylinder pointing to the SIAS. For stability, a connection was made from the umbilicus to the middle of the lower half of the mould. The edges of the mould were rounded to increase patient comfort. The mould was printed in an Ultimaker S5 (Ultimaker, Utrecht, Nederland) with white polylactic acid (PLA). Later models also include markers for the perforator locations, which were also indicated by cylinders.
Since various plannings were made, separate extensions were made that could be attached to the initial mould using a pin-and-hole system. The pin-and-hole system is located towards the lateral sides of the mould and placed at a location where the initial mould and extension touch. The holes were made in the initial mould, so that the delineation can still be made around the outside of the mould if an extension is taken off. Figure 40 shows a mould, with and without the extension that was incorporated.

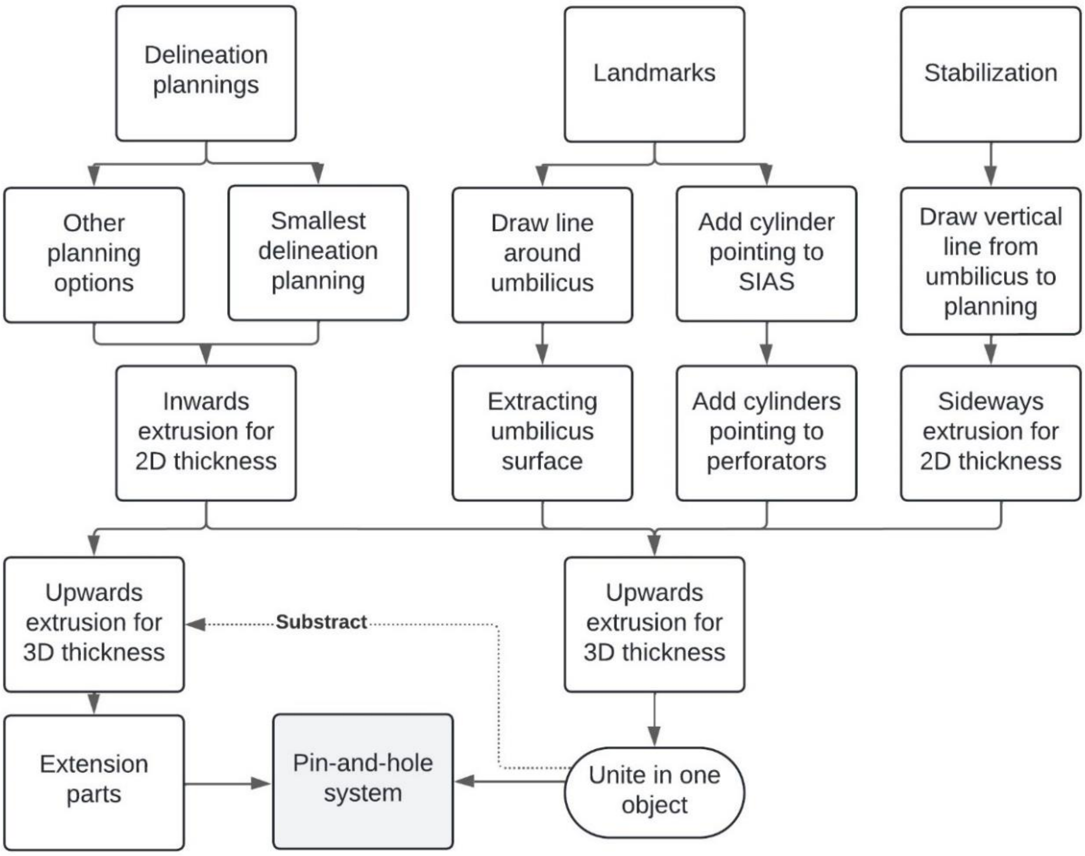

Figure 39. Flowchart for making of the 3D printed patient specific mould from the virtual planning.

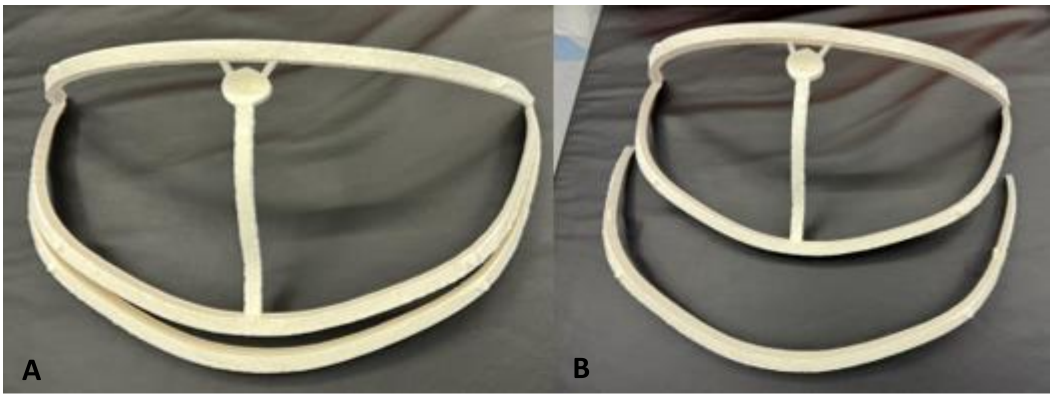

Figure 40. An example of a mould with (A) and without (B) the extension attached. The extension gives the option to choose the planning that suits the patient best.

4.3 Results

4.3.1 Patient demographics

Table 3 shows the demographics of the subgroup of patients that were included for this study. Patients from all plastic surgeons where eligible, but eventually patients of two different surgeons were included. They will be referred to as A and B.

Table 3. Patient demographics. The plastic surgeon indicates who was the main plastic surgeon who performed the surgery. Underwear is graded as follows: – no underwear, +/- underwear, but negligible effect, + underwear with effect, ++ severe effect of underwear. Examples of these grades are shown in Figure 4. Leg position indicates if the legs were raised during CTA acquisition or not. CTA age indicates the time between the date the CTA was made, and the surgery performed. Status at the start indicates the status of the breast before reconstruction. Breast volume indicates the volume of the breast that went for surgery. Since ablated breasts without implants have no volume, they were excluded. Another distinction was made between natural breasts and prostheses. The changed caudal incision indicates if the caudal incision was changed after acquiring the images of the delineation due to the expected difficulty with closing the wound.

Patient	1	2	3	4
Age	42	52	46	53
BMI	24.0	29.7	30.8	26.9
Plastic surgeon	A	A	B	B
Reconstruction type	Delayed	Delayed	Direct	Direct
Reconstruction type	Bilateral	Unilateral	Unilateral	Unilateral
Underwear	++	+	-	-
Leg position CTA	Down	Down	Raised	raised
CTA age (days)	296	99	40	14
Status at start	Protheses	No breast	Natural	Natural
Breast volume (cc)	442/324	-	923	430
Flap weight (grams)				
Harvested	951	1831	1630	1263
Discarded	0/0	923	720	686
Implanted	466/485	908	910	577

4.3.2 Planning and transfer quality

The results of the planned and surgical weight, as well as changed made to the planning are shown in Table 4. The mean difference in weight between the planning and the actual weight is visualized in Figure 41.

Table 4. Results of the planning and mould. The planned weight is the weight for the used option of the mould. Alterations to the plannings describes how the plastic surgeon adjusted the planning during the delineation of the incision, if adjustments were made. The corrected weight is the weight after altering the delineation in the algorithm to match the alterations made by the surgeon during surgery. The difference in weight is determined with the corrected weight.

Patient	Planned weight (g)	Alterations to planning	Corrected weight (g)	Actual weight (g)	Difference in weight (%)	Difference in weight (g)
1	1133	The caudal incision moved up, umbilicus indentation	967	951	1.7	16
2	1733	no	-	1831	-5.4	-98
3	1562	no	-	1630	-4.2	-68
4	1002	The cranial incision moved up, wider caudal incision	1174	1263	-7.0	-89

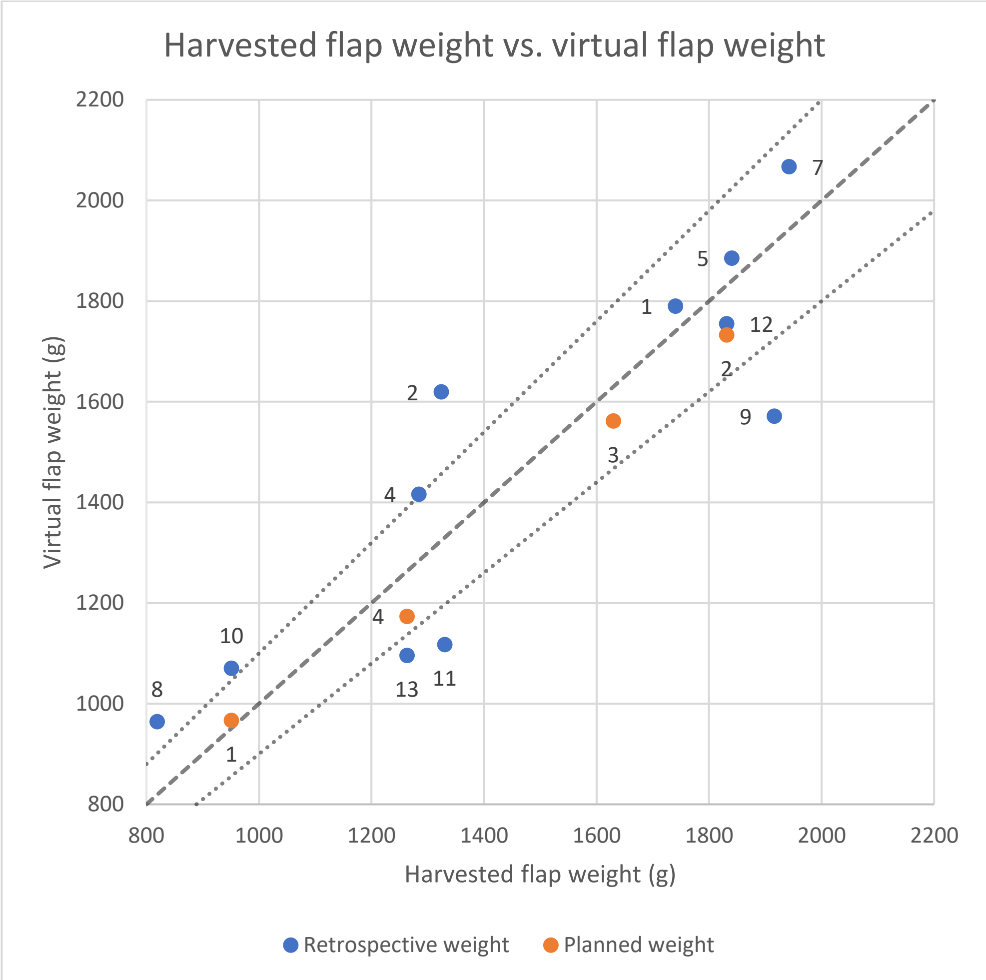

Figure 41. Scatterplot of the harvest flap weight versus the virtually determined flap weight, with dashed lines for the expected trend and 10% deviation. The numbers indicate the patient. This is the same scatterplot of Figure 35, but with the data of this chapter added in orange. Patient 1, 2 and 4 of this chapter are identical to patient 10, 12 and 13 of Chapter 3 respectively. Patient 3 was excluded in Chapter 3.

The moulds are shown in Figure 42. There were some alterations made to the delineations by the surgeons, also listed in Table 4. For patient 1 the caudal incision was moved more cranial as the abdomen would not yield a lot of volume below that point and decreasing the height of the flap would ease wound closure. For patient 4 the incision was moved up because a perforator that would potentially be harvested could be cut if the planning of the mould would be used. The changed delineation is shown in Figure 43, which also illustrates the comparison between the planning and the obtained 3D scan. If the delineation had been maintained, the perforator would indeed have been severed. However, the perforator was ultimately not utilized for the anastomosis.

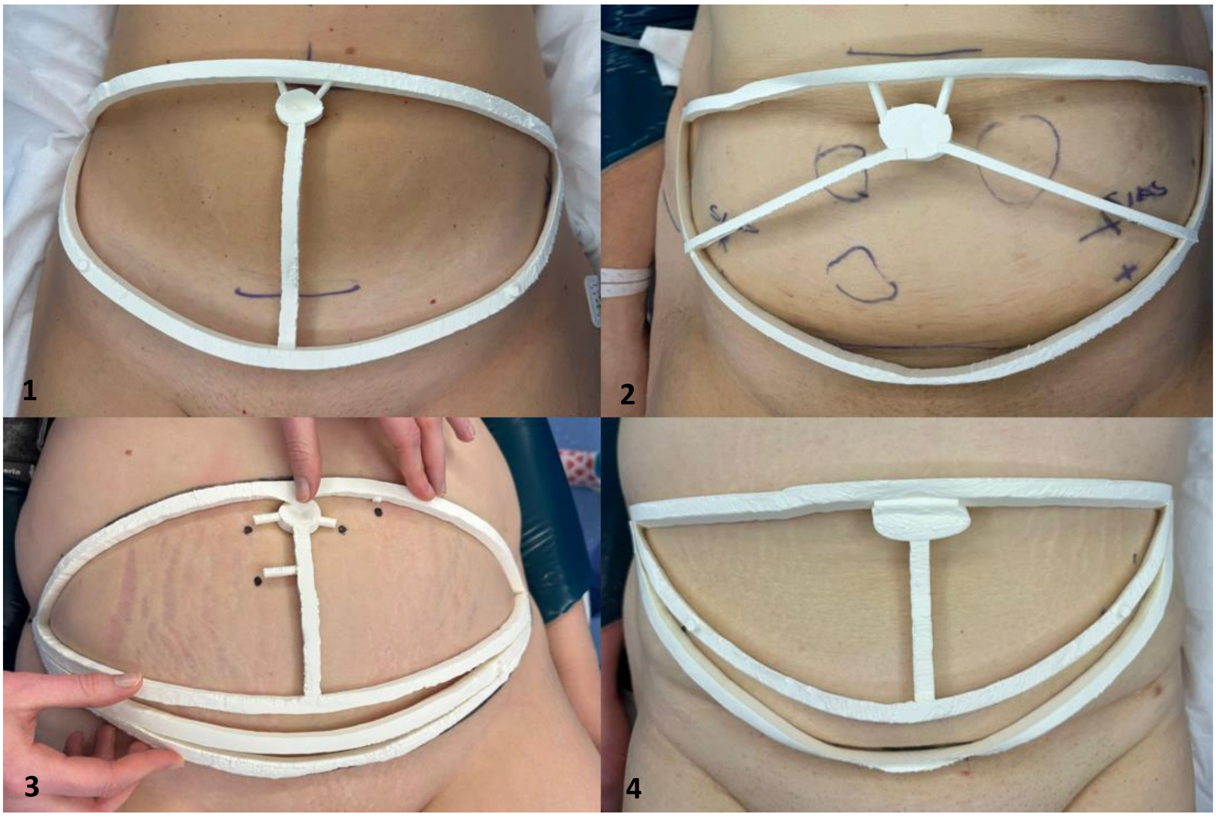

Figure 42. The four 3D printed moulds, numbered by their case. All moulds show an umbilicus landmark and a planning. The small cylinders on top were used to indicate the most anterior point around the SIAS. Patients 1, 3 and 4 have a vertical midline stabilization. Patient 2 has two more horizontal stabilization to give better access to the SIAS. Patients 3 and 4 have extension on the mould that were used during delineation. Patient 3 has cylindrical indicators for the perforator locations, with the black dots that were made using those indicators.

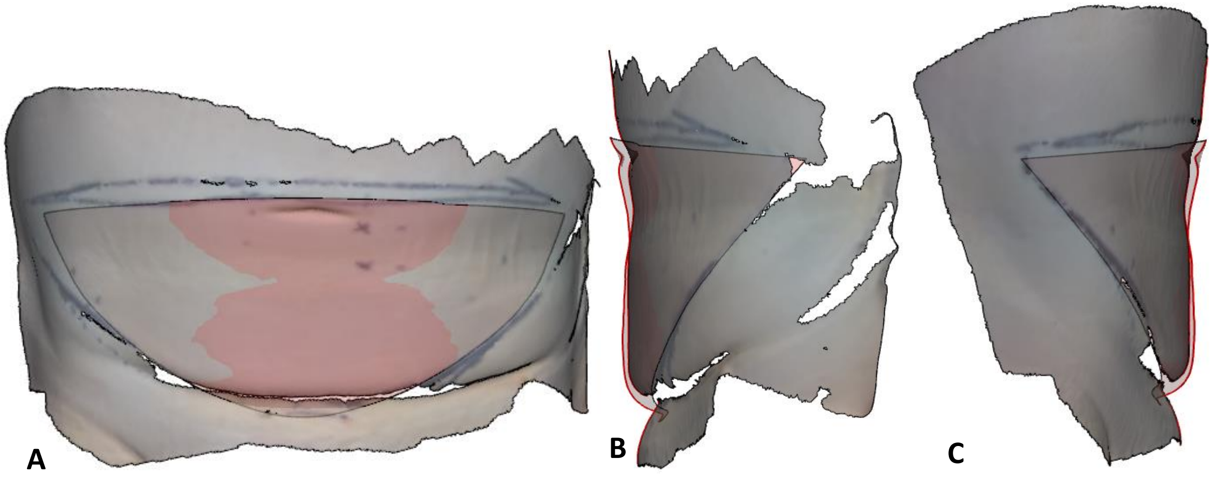

Figure 43. Visualization of the changed delineation of patient 4. The red surface is the original planning on the CTA segmentation, the black lines around that are the delineation used by the surgeon as captured with a 3D scan. A. Frontal view. B. Left lateral view. C. Right lateral view.

4.3.3 Observations regarding the 3D printed mould

The plannings were discussed with the plastic surgeon performing the surgery prior to the creation of the moulds. Although the option to adjust the planning was offered, no changes were made in any of the cases as the plans were deemed suitable. Patients 3 and 4 did get the note that the smallest option was probably not the one that would be used, as that would result in a too high scar location. This turned out to be the case during the procedure. Underlying causes will be discussed in the discussion section of this chapter.

Figure 42 demonstrates that the moulds fitted the patients, although the moulds of patients 1 and 2 did not lay flat on the skin. There was a gap between the mould and the ventral side of the patients, while the lateral sides of the mould touched the patient. Both these patients wore underwear during the CTA scan. The mould of patient 3 and 4 did not lay fully flat either, despite not wearing underwear, but they adhered more closely to the body compared to those of patients 1 and 2, as can be seen in Figure 44. A deep, hollow umbilicus provided a stable anchoring point for the mould. The SIASs were also located at the position of the indicators on the mould. Patient 4 had a relatively flat umbilicus, but a very pronounced skin fold that aided in the positioning. All moulds would lay flat on the body when applying pressure. For patients with loose or excessive skin, like patient 2, the skin tends to stretch when pressure is applied with a marker, which leads to a less smooth delineation.

Figure 45 shows a video of a mould with perforator indicators and the Doppler signals found at those locations. The perforators shown in the video were located at the presumed locations. The perforators next to the umbilicus were small and harder to detect with Doppler, but they were found. One of the major perforators was missed during the segmentation of the CTA scan due to human error.

Figure 44. Lateral view of the mould of patient 4 without applying pressure, showing some distance between mould and skin at the cranial part. As seen at the bottom of the image, a gel pad was placed around the arm.

Figure 45. Link to a video showing the Doppler signals found at the perforator locations given by the mould for patient 3. Please scan the QR code or click the image to follow the link.

4.3.3.1 Expert opinion

In general, the plastic surgeons expressed positive feedback regarding the use of the mould. Furthermore, the extensions were deemed useful, as they give more freedom in choosing which mould would yield the best flap. Moreover, the plastic surgeons were enthusiastic about the perforator indicators to find the perforators faster and this was an addition they would like to see in the future moulds as well. A specific suggestion for improvement was the addition of an indentation towards the umbilicus. Furthermore, one of the surgeons preferred a straighter caudal incision.

4.3.3.2 3D printing

The larger moulds were close to maximal printing size of the Ultimaker, which is 330 x 240 x 300 mm. Most moulds were over thirty-three centimetres wide, necessitating a tilt to fit within the Ultimaker. This tilting resulted in an increased need for support structures, thereby extending the printing time to over a day in some instances. Due to the elongated appearance of the mould, the print could become unstable despite the support, leading to minor printing errors. These errors manifested as misaligned layers, where layers were not placed correctly on the layer below due to a small translation of the print, shown in Figure 46. The extensions were especially challenging to 3D print due to instability of the object in the 3D printer, which made it susceptible to breaking. One of the moulds was less than 33cm wide, so it fitted flat on the building plate. This decreased the amount of support needed, and thus reducing printing time approximately by half, as well as improving the stability, so no printing errors were observed.

Figure 46. Printing error made in one of the extensions due to the instability of the object.

The pin-and-hole system functioned effectively, but the accuracy of the Ultimaker using 0.2mm layers led to some manual correction like sanding down of the pins and holes to ensure a proper fit. As the pins and holes were placed in a fully touching part, this did not affect the planning.

For patient 2, a stabilization connection was designed to extend laterally from the umbilicus to the lower half of the mould, rather than vertical stabilization, as shown in Figure 42. This was done to avoid long and thus unstable indicators for the SIAS landmarks. On the other moulds, the SIAS landmarks were located closer to one of the incision lines so the indicators could be incorporated there.

4.4 Discussion

The quality of the planning and transferal of the planning are evaluated based on the delineation, volume correlation and other observations, which will be elaborated below.

4.4.1 Planning and transfer quality

The delineation differed from the plastic surgeon’s delineation for two patients. For patient 1 the change in thickness of the fat layer that caused the changed incision could be identified on the CTA model and thus should have been added to the options. The protocol has been changed to also include minor skin folds like in this patient as option for the planning. The planning for patient 4 was adjusted based on perforator locations. Safeguards are in place in the algorithm to prevent this, but the protocol has to be clarified on which perforators are potentially suitable, so all suitable perforators are within the safeguards. Furthermore, the preferences about the planning given by the plastic surgeons should be incorporated in the planning where possible.

However, it remains challenging to estimate the height of the flap with the lowest possible scar location for which the abdomen can be fully closed on the CTA model. Plastic surgeons are used to feeling the amount of stretch of the skin when they pre-operatively determine the incision and that information is lost during the presentation of the planning on the CTA model. This was addressed by incorporating smaller options in the mould. A pinch test can also provide an estimate for the amount of stretch of the skin to help solve this issue. However, even with the pinch test, it remains unsure how much the skin can stretch exactly after dissection and how much lifting of the legs will help with closing. The extend of lacking information of CTA models, as well as other possible issues due to misinterpretation of the CTA should be identified.

The predicted volume and the actual volume are all within the 10% deviation range given as acceptable limit. The not adjusted plannings showed a remarkably similar difference and if that trend would remain the same in a larger population, a correction factor could be applied. The adjusted plannings showed a more diverse deviation. Within the current population it is not possible to say if that is due to errors made with the retrospective correction of the planning, or with the actual planning algorithm or transferal of the planning.

4.4.2 3D printed mould

The mould had a decent, but not a perfect fit, with some space observed between the mould and the patient's skin. The presence of underwear during acquisition of the CTA scan seemed responsible for the larger deviations in fit. A study done by Leilis indicated that the difference in position of the CTA scan with arms lifted and the surgical position with gel pads contribute to a change in amount of fat observed on the lateral sides of the abdomen.[55] This was consistent with visual assessment of the contact points of the mould. Putting pressure on the mould eliminated all space between the skin and mould, but did introduce some added pressure from the mould on the lateral sides of the patient. The correct positioning of the mould is supported by the perforator indicators that located the perforators. In addition, as the perforator indicators were positioned correctly on the mould, they could aid in finding the perforators in the future.

The plastic surgeons responded positively to the use of the moulds, expressing enthusiasm and willingness to use them. No complaints were reported about the use of mould by the plastic surgeons or other personnel. However, improvements can be made to increase the stability and integrity of the mould during and after printing, as well as decrease printing time and material costs.

4.5 Conclusion

The virtual plannings based on a CTA segmentation and a desired breast volume seem to be accurate enough to be used, especially with the allowance of minor adjustments. Nonetheless, further optimization is imperative to mitigate the requirement for such adjustments during surgery. The virtual planning, transferred to the patient using a 3D printed mould, can determine the volume of a DIEP flap within the given permissible deviation of 10%, based on this feasibility study. However, due to the small sample size, more research is needed to reliably quantify the deviation.

Chapter 5 Discussion and conclusion

5.1 Discussion

This study aimed to virtually plan a DIEP flap volume pre-operatively using CTA and a desired volume. It explored a novel approach to achieve this goal by developing a semi-automatic workflow and algorithm. The data was collected to validate and optimize the workflow and algorithm. Additionally, a more reliable validation process was initiated, as well as a feasibility study with a 3D-printed mould to transfer the planning to the patient.

5.1.1 Delineation

This study showed that it is possible to semi-automatically plan a DIEP flap volume for autologous breast reconstruction with a CTA scan and other available imaging like 3D photos of the breast. The delineation of the flap is based on the guidelines that are known for DIEP flap delineation and the observations of the work and discussion with plastic surgeons.[12,15,53,54] As seen in Appendix A there is not a general shape for a DIEP flap delineation. Differences in width and length ratio can be seen, as well as variations in the curve of the caudal incision and the umbilicus deviation. Due to this, an objective comparison between the planning of the tool and the surgeon's delineation could not be given. Visual comparison of the delineations of Appendix A and Figure 18 show similarities and differences. However, those same differences seem to be present when looking solely at the delineations made by plastic surgeons shown in Appendix A. Furthermore, the delineation or the algorithm follows the rough guidelines, concerning the minimal position of the perforators from the edge of the flap and factors that improve aesthetic outcomes such as following skin folds when possible. Furthermore, the various drafts of the planning were discussed with the plastic surgeons and improved based on the feedback.[15,53] The feasibility study of Chapter 4 revealed more improvements, due to the more direct method of feedback. A point of feedback given by both surgeons was to incorporate an indentation for the umbilicus. Nevertheless, half of the plannings made for the feasibility study of Chapter 4 were used without adjustments and the other half with minor adjustments. So even though no objective measurements can be given about the quality of the delineation, the plannings seems to be accurate enough to be used, especially when minor adjustments can be made.

A limitation in the quality of the planning is that the CTA scan cannot provide the same information as physical examination of the patient. Furthermore, interpretations of the CTA model can be wrong. This became apparent in patient 1 of Chapter 4 where a minor skin fold was not taken into consideration, but which did have an effect. Furthermore, the amount of stretch of the skin remains uncertain with just the CTA model. To adjust for this and the possibility of not being able to close the wound, smaller options were incorporated in the moulds.

5.1.2 Transferal

The first attempt to validate the volume predicted by the planning relied on the transfer of the actual per-operative delineation to the CTA model. As shown in Appendix D, finding the right method to transfer the per-operative delineation to the CTA model remains challenging. Photogrammetry failed to produce a usable 3D object. The 2D projection lacked sufficient landmarks for accurate registration resulting is noticeable deviations, particularly in the lateral corners of the delineation. Similarly, 3D projection proved hard to register properly due to a lack of landmarks. No objective measurements were obtained for the accuracy of the registration of the 3D scans. Furthermore, visual assessment indicated deviations between the CTA model and 3D scan, mainly on the lateral sides of the patient, which was supported by a study done by Leilis.[55] While definitive conclusions cannot be drawn without precise measurements, it is likely that registration errors contributed to differences in flap weight measurements.

The utilization of 3D printed moulds largely addressed these challenges. The 3D printed mould proved to be a viable solution for transferring of the virtual delineation to the patient. The moulds fitted the patients and the gap between the mould and the skin was eliminated when light pressure was applied to the mould. While objective measurements were not conducted to verify the precise placement of the mould on the body, the correct positioning of all three landmarks simultaneously suggested accurate placement. Moreover, the perforator indicators successfully located the perforators, further indicating the correct placement of the moulds.

The main limitation with the transferral is the lack of objective measurements to quantify the error. Due to this, the effect of registration on the outcomes remains uncertain.

5.1.3 Volume correlation

To be able to determine the correlation between the planned flap volume and the surgically obtained flap volume, the algorithm was applied to the data in two studies. The study of 3.2 used 3D scans to transfer the delineation of the plastic surgeon to the CTA model, while the feasibility study of Chapter 4 used a 3D printed mould to transfer the virtual delineation to the patient. The first study resulted in a deviation between virtual and surgically obtained weight that was outside of the given limit of 10%. The feasibility study yielded better results with all deviations remaining within the limit.

No obvious reason was found for the large deviation in the study of 3.2, however, many factors had an impact on the accuracy of the volume besides the performance of the algorithm. This included the age of the CTA scans, the deformity of fat tissue, per-operative alterations from the delineation to the final incision and other confounding factors in the population, the variable density of fat tissue, simplification of the segmentation and algorithm, and the quality of the images made of the delineations, as well as registration of those images to the CTA model.

Older CTA scans would seem less precise than more recent scans because the patient could have gained or lost weight, which would lead to a different amount of fat in the delineated flap on the CTA scan and during the surgery. However, this was not proven. On the contrary, the results showed that recent CTA scans led to an underestimation of the volume, whereas older CTA scans were more likely to overestimate the volume. A similar deviation was seen for the deformity of fat tissue due to underwear. No underwear would theoretically lead to a more accurate volume, because the fat is not deformed compared to the surgical situation. Nevertheless, the group without underwear had an underestimation of volume as well. It is, however, important to notice that the two patients in the no underwear group also had very recent CTA ages. It could be possible that the correlation with CTA ages in these patients led to a bias in the results for the underwear. Another factor of deformity of fat tissue was shown by Leilis.[55] This study showed a deformation of the lateral sides of patients between the CTA scan position with arms raised and the surgical position with the arms next to body and secured with gel pads.

Other identified possible confounding factors that were quantified in the study of 3.2 such as BMI, change of caudal incision, raised legs during acquisition of the CTA scan for a more similar position to the surgical position, harvested flap size or quality of registration of 3D scan and CTA model did not yield significant differences.

A limitation that should be noted, is the difference in surgically obtained flaps being measured as weight, while the virtual flap is measured in volume. This was corrected using the density of abdominal fat tissue, however, studies done to determine the density of fat tissue have shown a high range. Van der Pot et al. found a mean specific density of 1.12 mL/g, with a range of 1.02 to 1.32 mL/g.[51] Razzano et al. found a similar density of 1.19 mL/g, with a of range: 1.10 - 1.32 mL/g.[21] Deviations in the volume could also be caused by variations in the fat density.

In addition, the simplification of the segmentation may have introduced some inaccuracies. The segmentation of the fat is quicker when the skin and umbilical stalk are also segmented, even though the umbilical stalk and usually most of the skin are not part of the implanted flap. This deviation was assumed insignificant. Another estimation was made by assuming that the cut through the fat layer is perpendicular to the surface of the cylinder. In reality, there will be some deviations from this, as well as some slanted edges can be made to reduce the chance of fat necrosis.[53] These differences were also considered insignificant. However, if further data collection reveals a consistent trend of overestimating volume compared to the actual weight due to the inclusion of skin, umbilical stalk or not slanted edges, corrective measures can be implemented. This may involve refining the segmentation process and algorithm steps or applying a modifier to adjust the predicted weight accordingly.

Furthermore, it remained unsure how accurate the used 3D scanner was. Previous research showed that the Revopoint POP 2 was accurate when making scans of breasts.[60,61] However, the scans of the abdomen showed unexplainable deviations. Various hypotheses were evaluated, and it appeared that the deformation of the fat due to a different position of the patient during the CTA and the surgical situation can be responsible for some of the deviation.[55] However, the sample size in these studies was too low for definitive conclusions.

To summarize, while the results of the volume validation of 3.2 show a deviation of more than the given 10% between the actual weight and the predicted weight, it could be possible this is mostly due to the limitations of the data set and the challenges with the transfer of the delineation to the CTA model, instead of errors in the planning algorithm. The feasibility study of Chapter 4 supports the statement, with all differences between the planned and actual weight remaining under the 10%. Due to the small sample size, no conclusions can be drawn yet. Nevertheless, the results show a more consistent deviation than 3.2 when limitations like registration errors are mitigated.

5.1.4 Future perspectives

The current workflow and algorithm have not been tested and optimized enough for clinical implementation. Nevertheless, after further improvement and testing, it can be used to improve the information provided to patients for shared decision-making. It can also increase the aesthetic results of DIEP flap breast reconstruction by improving symmetry and possibly reduce the risk of complications by decreasing the surgical site area and operating time. The planning process provides an objective measure of the amount of fat that can be obtained from the abdomen. This information can be shared with the patient to give them a better idea of the size of the breast that can be achieved. If the abdomen has relatively little fat, the patient can be given choices. They can opt for a smaller breast size than before for bilateral reconstructions, or undergo mamma reduction on the other breast for unilateral reconstructions. Another option is to raise the entire flap cranially to achieve a higher volume, but with the risk that the scar will be above the underwear. Informing the patient of the various options and outcomes can help with achieving better patient satisfaction, as they know better what to expect and can choose the option that suits them best.

To achieve this clinical relevance, the validation and implementation of the 3D printed mould of Chapter 4 should be continued to ensure the planning can correctly predict the volume, as well as follow the DIEP flap design to the wishes of the plastic surgeons. As described before, the CTA scans lack an important piece of information, namely the amount of stretch of the skin. This was dealt with by offering smaller options of the planning. For the population in this study, these smaller options turned out to be too conservative. Therefore, further research is required to determine the appropriate size of the smaller options. A pinch test offers a preliminary assessment of skin stretch, but uncertainties arise when surgeons aim for larger flaps beyond the limits suggested by this test. It remains unsure how much the skin can stretch after dissection and how much elevation of the legs will help with wound closure. Setting up a study to examine the correlation between the results of the pinch test, the height of the flap and the ease of closing the wound would aid in solving this problem.

Furthermore, due to the different preferences of the plastic surgeons, it would be appreciated to incorporate these differences like a straighter caudal incision. On the other hand, a more uniform workflow would generate more uniform results. It would be interesting to discuss personal preferences of the surgeons to identify which changes should be integrated into the general workflow, which options can be kept as personal preferences and which options are not used for the planning.

Moreover, improvements can be made to make the planning more applicable. First, the volume must be corrected for the lateral corners that are removed from the DIEP flap during surgery. Knowing which part of the flap should be discarded is even more important for unilateral breast reconstructions, as this could help achieve a more symmetrical breast and reduce the time needed to trim the flap to the right volume. Knowing which part of the DIEP flap gives the same volume as the other breast would improve the workflow and possibly the aesthetic outcome.

5.2 Conclusion

A virtual planning for DIEP flap volume using CTA scans and other available imaging could be made. No definitive conclusions about volume accuracy can be drawn when transferring a plastic surgeon's delineation to the CTA model using a 3D scan. The delineation made by the planning is suitable and in half of the cases no adjustments were required. Nevertheless, further improvement is needed to reduce the number of adjustments. Transferring of a virtual planning using a 3D printed mould could predict the volume of a DIEP flap within a 10% deviation according to a feasibility study with four patients. However, due to the small population, more research is required to reliably quantify the accuracy of virtual DIEP flap planning.

References

1. Smorenburg CH, Boersma LJ, Hairwassers D, et al. Borstkanker - Algemeen. Published 2020. Accessed July 10, 2023. https://richtlijnendatabase.nl/richtlijn/borstkanker/algemeen.html
2. NKR Cijfers | Incidentie - Grafiek. Accessed July 17, 2023. https://nkr-cijfers.iknl.nl/#/viewer/056fbc0a-94c6-4ab3-9048-c5058f909924
3. Behandeling borstkanker. Accessed July 17, 2023. https://iknl.nl/kankersoorten/borstkanker/registratie/behandeling
4. Farhangkhoee H, Matros E, Disa J. Trends and concepts in post-mastectomy breast reconstruction. *Journal of Surgical Oncology*. 2016;113(8):891-894. doi:10.1002/jso.24201
5. Kouwenberg CAE, de Ligt KM, Kranenburg LW, et al. Long-Term Health-Related Quality of Life after Four Common Surgical Treatment Options for Breast Cancer and the Effect of Complications: A Retrospective Patient-Reported Survey among 1871 Patients. *Plastic and Reconstructive Surgery*. 2020;146(1). doi:10.1097/PRS.0000000000006887
6. Howes BHL, Watson DI, Xu C, Fosh B, Canepa M, Dean NR. Quality of life following total mastectomy with and without reconstruction versus breast-conserving surgery for breast cancer: A case-controlled cohort study. *Journal of Plastic, Reconstructive & Aesthetic Surgery*. 2016;69(9):1184-1191. doi:10.1016/j.bjps.2016.06.004
7. Engel J, Kerr J, Schlesinger-Raab A, Sauer H, Hölzel D. Quality of Life Following Breast-Conserving Therapy or Mastectomy: Results of a 5-Year Prospective Study. *The Breast Journal*. 2004;10(3):223-231. doi:10.1111/j.1075-122X.2004.21323.x
8. Guyomard V, Leinster S, Wilkinson M. Systematic review of studies of patients' satisfaction with breast reconstruction after mastectomy. *The Breast*. 2007;16(6):547-567. doi:10.1016/j.breast.2007.04.004
9. Mureau MAM, Van der Hulst R, Smorenburg CH, Willems C, Ligtenberg D. Reconstructietechnieken bij ablatieve behandeling. Accessed August 15, 2023. https://richtlijnendatabase.nl/richtlijn/borstreconstructie/reconstructietechnieken_bij_ablatieve_behandeling.html
10. Platt J, Zhong T. Patient-Centered Breast Reconstruction Based on Health-Related Quality-of-Life Evidence. *Clinics in Plastic Surgery*. 2018;45(1):137-143. doi:10.1016/j.cps.2017.08.011
11. Casey WJ, Chew RT, Rebecca AM, Smith AA, Collins JM, Pockaj BA. Advantages of preoperative computed tomography in deep inferior epigastric artery perforator flap breast reconstruction. *Plast Reconstr Surg*. 2009;123(4):1148-1155. doi:10.1097/PRS.0b013e31819e23e1
12. DIEP Flap Microsurgical Breast Reconstruction. Accessed July 24, 2023. https://www.microsurgeon.org/diepbreastreconstruction
13. Allen RJ, Treece P. Deep Inferior Epigastric Perforator Flap for Breast Reconstruction. *Annals of Plastic Surgery*. 1994;32(1).
14. Levine JL. DIEP Flap Breast Reconstruction Procedure. Accessed August 10, 2023. https://centerforbreastreconstruction.com/breast-reconstruction-procedure-options/diep-flap-breast-reconstruction-procedure/
15. Rakhorst H. Personal correspondence (plastic surgeon).
16. Chae MP, Hunter-Smith DJ, Chung RD, Smith JA, Rozen WM. 3D-printed, patient-specific DIEP flap templates for preoperative planning in breast reconstruction: a prospective case series. *Gland Surgery*. 2021;10(7):2192-2199. doi:10.21037/gs-21-263
17. Hummelink S, Verhulst AC, Maal TJJ, Hoogeveen YL, Schultze Kool LJ, Ulrich DJO. An innovative method of planning and displaying flap volume in DIEP flap breast reconstructions. *Journal of Plastic, Reconstructive and Aesthetic Surgery*. 2017;70(7):871-875. doi:10.1016/j.bjps.2017.04.008
18. Tomita K, Yano K, Hata Y, Nishibayashi A, Hosokawa K. DIEP Flap Breast Reconstruction Using 3-dimensional Surface Imaging and a Printed Mold. *Plastic and Reconstructive Surgery – Global Open*. 2015;3(3):e316. doi:10.1097/GOX.0000000000000288
19. Woo KJ, Kim EJ, Lee KT, Mun GH. A Novel Method to Estimate the Weight of the DIEP Flap in Breast Reconstruction: DIEP-W, a Simple Calculation Formula Using Paraumbilical Flap Thickness. *J Reconstr Microsurg*. 2016;32(7):520-527. doi:10.1055/s-0036-1581078
20. Demiri E, Dionyssiou D. Combined Autologous Breast and Lymphedema Reconstruction with a Predesigned DIEP and Lymph-Node Flap. In: *Clinical Scenarios in Reconstructive Microsurgery: Strategy and Operative Techniques*. ; 2022:665-672. doi:10.1007/978-3-030-23706-6_107

21. Razzano S, Taylor R, Schonauer F, Figus A. How to assess the volume of a DIEP flap using a free online calculator: The DIEP V (volume) method. *Journal of Plastic, Reconstructive & Aesthetic Surgery*. 2018;71(10):1410-1416. doi:10.1016/j.bjps.2018.04.018
22. Nelson JA, Voineskos SH, Qi J, et al. Elective Revisions after Breast Reconstruction: Results from the Mastectomy Reconstruction Outcomes Consortium(MROC). *Plast Reconstr Surg*. 2019;144(6):1280-1290. doi:10.1097/PRS.0000000000006225
23. Liker JK. *The Toyota Way: 14 Management Principles From the World's Greatest Manufacturer*. McGraw Hill Professional; 2003.
24. Ries E. *The Lean Startup: How Today's Entrepreneurs Use Continuous Innovation to Create Radically Successful Businesses*. Crown; 2011.
25. Cheng H, Clymer JW, Po-Han Chen B, et al. Prolonged operative duration is associated with complications: a systematic review and meta-analysis. *J Surg Res*. 2018;229:134-144. doi:10.1016/j.jss.2018.03.022
26. Cheng H, Chen BPH, Soleas IM, Ferko NC, Cameron CG, Hinoul P. Prolonged Operative Duration Increases Risk of Surgical Site Infections: A Systematic Review. *Surg Infect (Larchmt)*. 2017;18(6):722-735. doi:10.1089/sur.2017.089
27. Hummelink S, Gerrits JGW, Schultze Kool LJ, Ulrich DJO, Rovers MM, Grutters JPC. The merits of decision modelling in the earliest stages of the IDEAL framework: An innovative case in DIEP flap breast reconstructions. *Journal of Plastic, Reconstructive & Aesthetic Surgery*. 2017;70(12):1696-1701. doi:10.1016/j.bjps.2017.07.011
28. Varnava C, Wiebringhaus P, Hirsch T, Dermietzel A, Kueckelhaus M. Breast Reconstruction with DIEP Flap: The Learning Curve at a Breast Reconstruction Center and a Single-Surgeon Study. *Journal of Clinical Medicine*. 2023;12(8):2894. doi:10.3390/jcm12082894
29. Haddock NT, Teotia SS. Efficient DIEP Flap: Bilateral Breast Reconstruction in Less Than Four Hours. *Plast Reconstr Surg Glob Open*. 2021;9(9):e3801. doi:10.1097/GOX.0000000000003801
30. Sharma HR, Rozen WM, Mathur B, Ramakrishnan V. 100 Steps of a DIEP Flap—A Prospective Comparative Cohort Series Demonstrating the Successful Implementation of Process Mapping in Microsurgery. *Plastic and Reconstructive Surgery – Global Open*. 2019;7(1):e2016. doi:10.1097/GOX.0000000000002016
31. Issa CJ, Lu SM, Boudiab EM, et al. Comparing Plastic Surgeon Operative Time for DIEP Flap Breast Reconstruction: 2-stage More Efficient than 1-stage? *Plast Reconstr Surg Glob Open*. 2021;9(6):e3608. doi:10.1097/GOX.0000000000003608
32. Rozen WM, Garcia-Tutor E, Alonso-Burgos A, et al. Planning and optimising DIEP flaps with virtual surgery: the Navarra experience. *J Plast Reconstr Aesthet Surg*. 2010;63(2):289-297. doi:10.1016/j.bjps.2008.10.007
33. Granzow JW, Levine JL, Chiu ES, Allen RJ. Breast reconstruction with the deep inferior epigastric perforator flap: History and an update on current technique. *Journal of Plastic, Reconstructive & Aesthetic Surgery*. 2006;59(6):571-579. doi:10.1016/j.bjps.2006.01.004
34. Smit JM, Klein S, Werker PMN. An overview of methods for vascular mapping in the planning of free flaps. *J Plast Reconstr Aesthet Surg*. 2010;63(9):e674-682. doi:10.1016/j.bjps.2010.06.013
35. Clavero JA, Masia J, Larrañaga J, et al. MDCT in the preoperative planning of abdominal perforator surgery for postmastectomy breast reconstruction. *AJR Am J Roentgenol*. 2008;191(3):670-676. doi:10.2214/AJR.07.2515
36. Steenbeek LM, Peperkamp K, Ulrich DJO, Hummelink S. Alternative imaging technologies for perforator mapping in free flap breast reconstructive surgery – A comprehensive overview of the current literature. *Journal of Plastic, Reconstructive & Aesthetic Surgery*. 2022;75(11):4074-4084. doi:10.1016/j.bjps.2022.06.100
37. Chae MP, Hunter-Smith DJ, Rostek M, Smith JA, Rozen WM. Enhanced Preoperative Deep Inferior Epigastric Artery Perforator Flap Planning with a 3D-Printed Perforasome Template: Technique and Case Report. *Plastic and Reconstructive Surgery – Global Open*. 2018;6(1). doi:10.1097/GOX.0000000000001644
38. Hummelink SLM. *Technische Innovaties Bij Autologe Borstreconstructies*. [S.l.] : [S.n.]; 2018. Accessed August 22, 2023. https://repository.ubn.ru.nl/handle/2066/187344
39. Troost JB. Optimizing breast symmetry analysis using three-dimensional stereophotogrammetry images of Deep Inferior Epigastric Perforator flap reconstruction patients. Published online April 1, 2022. http://essay.utwente.nl/89808/
40. Hummelink S, Hoogeveen YL, Schultze Kool LJ, Ulrich DJO. A New and Innovative Method of Preoperatively Planning and Projecting Vascular Anatomy in DIEP Flap Breast Reconstruction: A Randomized Controlled Trial. *Plastic and Reconstructive Surgery*. 2019;143(6):1151E-1158E. doi:10.1097/PRS.0000000000005614

41. Hummelink S, Verhulst AC, Maal TJJ, Ulrich DJO. Applications and limitations of using patient-specific 3D printed molds in autologous breast reconstruction. *European Journal of Plastic Surgery*. 2018;41(5):571-576. doi:10.1007/s00238-018-1430-3
42. Renzulli M, Clemente A, Brocchi S, et al. Preoperative computed tomography assessment for a deep inferior epigastric perforator (DIEP) flap: a new easy technique from the Bologna experience. *Acta Radiol*. 2021;62(10):1283-1289. doi:10.1177/0284185120963899
43. Wesselius TS, Meulstee JW, Luijten G, Xi T, Maal TJJ, Ulrich DJO. Holographic Augmented Reality for DIEP Flap Harvest. *Plastic and Reconstructive Surgery*. 2021;147(1). doi:10.1097/PRS.0000000000007457
44. Ceron MA, Duque JL, Verdoy SB, et al. Characterization of the volume and thickness of DIEP flap by CTA image processing. In: ; 2021. doi:10.1109/STSIVA53688.2021.9592004
45. DIEP-lap borstreconstructie. Published online 2023. https://www.zgt.nl/media/folders/2jxdzira/diep-lap-borstreconstructie.pdf
46. Wood KL, Zoghbi Y, Margulies IG, Ashikari AY, Jacobs J, Salzberg CA. Is the Vectra 3D Imaging System a Reliable Tool for Predicting Breast Mass? *Ann Plast Surg*. 2020;85(S1 Suppl 1):S109-S113. doi:10.1097/SAP.0000000000002333
47. De Stefani A, Barone M, Hatami Alamdari S, et al. Validation of Vectra 3D Imaging Systems: A Review. *International Journal of Environmental Research and Public Health*. 2022;19(14):8820. doi:10.3390/ijerph19148820
48. O'Connell RL, Khabra K, Bamber JC, et al. Validation of the Vectra XT three-dimensional imaging system for measuring breast volume and symmetry following oncological reconstruction. *Breast Cancer Res Treat*. 2018;171(2):391-398. doi:10.1007/s10549-018-4843-6
49. Stern CS, Plotsker EL, Rubenstein R, et al. Three-Dimensional Surface Analysis for Preoperative Prediction of Breast Volume: A Validation Study. *Plastic and Reconstructive Surgery*. 2023;152(6):1153. doi:10.1097/PRS.0000000000010473
50. Fearn N, Meybodi F, Kilbreath S, et al. Reliability and Measurement Error of Breast Volume Calculation Using Three-Dimensional Surface Imaging. *Lymphatic Research and Biology*. 2023;21(3):296-303. doi:10.1089/lrb.2022.0015
51. van der Pot WJ, Kreulen M, Melis P, Hage JJ. Specific volume of female subcutaneous abdominal tissue as a reference in autologous breast reconstruction. *J Reconstr Microsurg*. 2010;26(3):185-188. doi:10.1055/s-0029-1243301
52. DenOtter TD, Schubert J. Hounsfield Unit. In: *StatPearls*. StatPearls Publishing; 2024. Accessed June 6, 2024. http://www.ncbi.nlm.nih.gov/books/NBK547721/
53. Wijbenga J. Personal correspondence (plastic surgeon).
54. Hendriks - Brouwer N. Personal correspondence (plastic surgeon).
55. Leilis C. Shape differences in subcutaneous abdominal fat between different body positions captured with 3D scans. Published online May 9, 2024.
56. Egozi D, Perkhulov V, Kouniavsky L, Di Via Loschope A, Benkler M, Benharush D. DIEP Flap Preoperative Planning Using Virtual Reality Based on CT Angiography. *Plastic and Reconstructive Surgery - Global Open*. 2022;10(3). doi:10.1097/GOX.0000000000004209
57. Freidin D, Singolda R, Tejman-Yarden S, et al. Using Virtual Reality for Deep Inferior Epigastric Perforator Flap Preoperative Planning. *Plastic and Reconstructive Surgery – Global Open*. 2023;11(1):e4773. doi:10.1097/GOX.0000000000004773
58. Phan R, Chae MP, Hunter-Smith DJ, Rozen WM. Advances in perforator imaging through holographic CTA and augmented reality: a systematic review. *Australasian Journal of Plastic Surgery*. 2022;5(1):32-38. doi:10.34239/ajops.v5n1.263
59. Geurts J. Digital pre-operative planning to operating room for a DIEP flap reconstruction. Published online 2023.
60. Lubbers N. The clinical applicability of 3D scanners as an alternative for the Vectra XT for improvement of reconstructive breast surgery. Published online 2022.
61. de Vries. Reproducibility of 3D surface imaging systems for female breast scans and influence of respiratory motion. Published online 2023.

Appendix A. Differences in delineations of surgeons

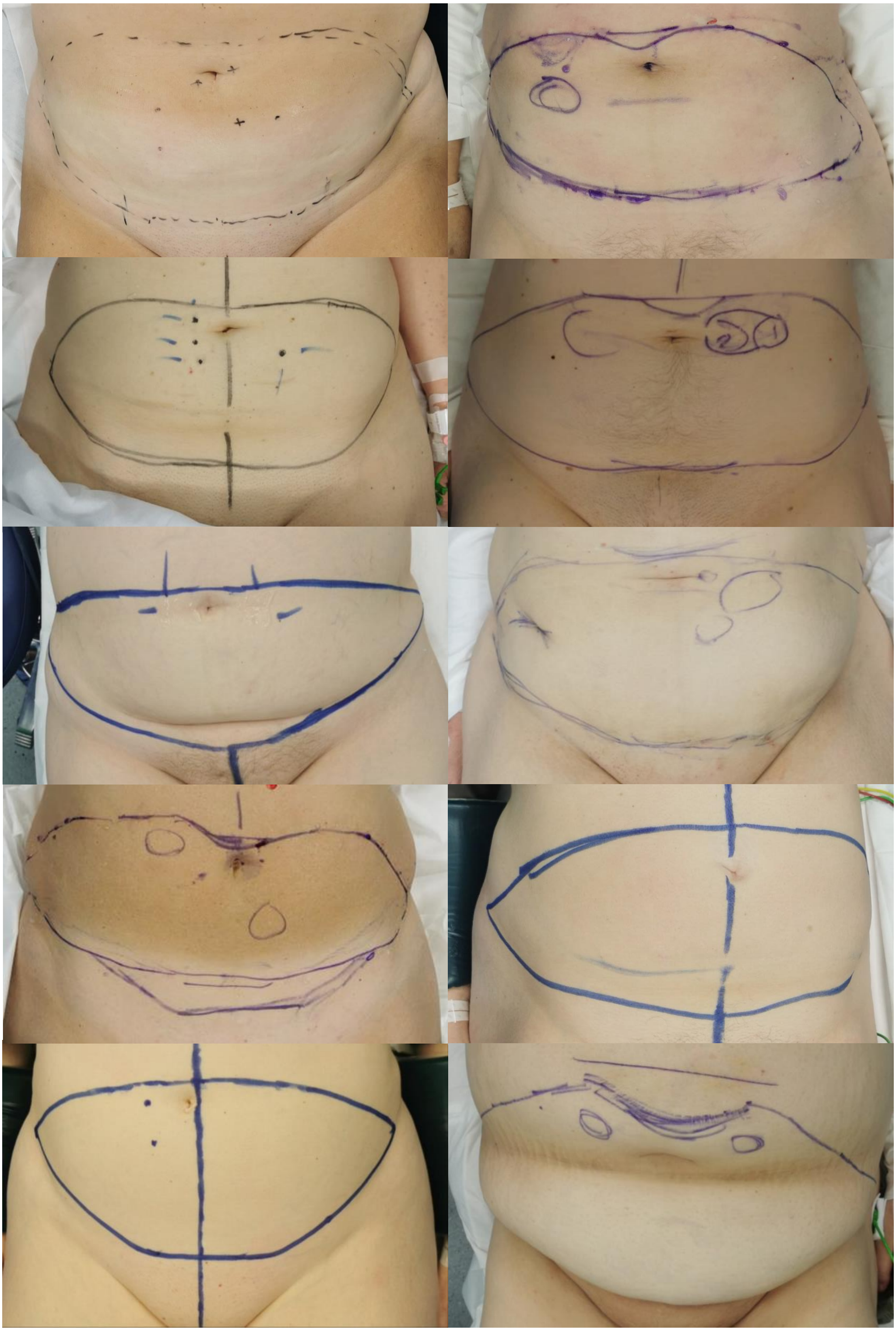

Appendix B. Breast Sculptor landmarks

LANDMARKS - Breast Sculptor					
Sn	Sternal notch	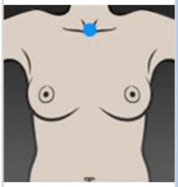			
MMF(r)	Medial Mammary Fold (Right)	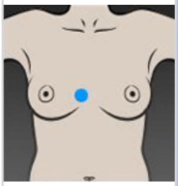	MMF(l)	Medial Mammary Fold (Left)	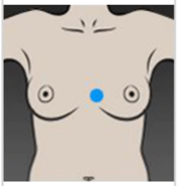
C(r)	Clavide (Right)	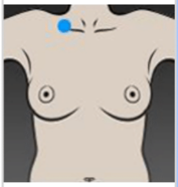	c(l)	Clavide (Left)	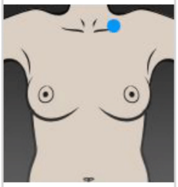
N(r)	Nipple (Right)	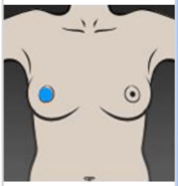	n(l)	Nipple (Left)	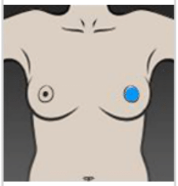
A(r)	Areola (Right)	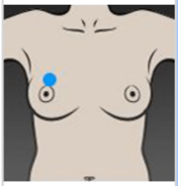	A(l)	Areola (Left)	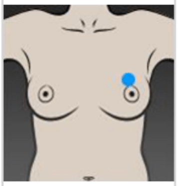
IMF(r)	Inframammary (Right)		IMF(l)	Inframammary (Left)	
LMF(r)	Lateral Mammary Fold (Right)	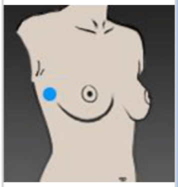	LMF(l)	Lateral Mammary Fold (Left)	

ESTHETEC info@esthetec.fr

Appendix C. Density experiment

Introduction

Literature states different values for the density of fat tissue. Two studies specifically looked at the abdominal fat tissue of women. Van der Pot et al. determined the density of the abdominoplasty specimens of thirty-two women. The mean specific density was 1.12 mL/g (range, 1.02 to 1.32 mL/g; standard deviation 0.04).[51] Razzano et al. found a similar density of 1.19 mL/g (range: 1.10 - 1.32 mL/g) assessing the contralateral side of DIEP flaps used for unilateral reconstructions.[21] This experiment was done to verify these values.

Methods

For three participants going for unilateral DIEP flap breast reconstruction of the population described in 2.1.1 were included for this experiment. The discarded side of the DIEP flap was weighted using a regular scale available in the operating room. The flap was then put in a measuring cup filled with water, which was put in a larger tub. The flap was pushed down until fully submerged. The water that flowed in the larger tub was weighed with the scale.

Results

Table 5 shows the collected data and the calculated density.

Table 5. Weight, volume and density of discarded side of the flap for unilateral breast reconstructions.

Case	Weight (g)	Volume (mL)	Density (mL/g)
1	590	647	1.10
2	570	631	1.10
3	328	336	1.02

Discussion

Two of the three patients gave comparable results to the values found by Van der Pot er al. Patient 3 had a larger deviation, but remained within the range Van der Pot et al. found as well.

The experiment was discontinued due challenges with the facilities regarding available space and storage. Furthermore, submerging the flap completely without also submerging the hands of the researchers proved to be difficult, which could have affected the result. Solving this problem within the already challenging facilities contributed to the discontinuation of the experiment.

Conclusion

The found values for the density for abdominal fat are in line with the 1.12 mL/g given by literature.

Appendix D. Matching of per-operative images to CTA model

Multiple options were explored for both acquiring useful images to compare delineations and to transfer the delineations from one modality to the other. This included photogrammetry and projections of 2D images and registration of 3D scans.

Photogrammetry

Photogrammetry was performed using Meshroom (AliceVision). Three images were captured of a resuscitation doll similar to the per-operative 2D images (see 2.1.5 Per-operative images). These images were processed according to the workflow shown in Figure 49. Unfortunately, Meshroom was unable to create a 3D object due to a lack of data because only a couple of pixels were reconstructed as shown in Figure 47. Aruco markers and additional images were added to make it easier to match the images. This did not change the outcome.

This led to a final test, a video of the abdominal area of the resuscitation doll was made and the frames were extracted and processed. The result is shown in Figure 48, with the corresponding workflow in Figure 50. This did yield a 3D object, however, there were many floating pixels and holes resulting in an unreliable mesh. Since the result was insufficient for further processing, photogrammetry was discarded as an option to process the data for comparison of the planning and actual situation.

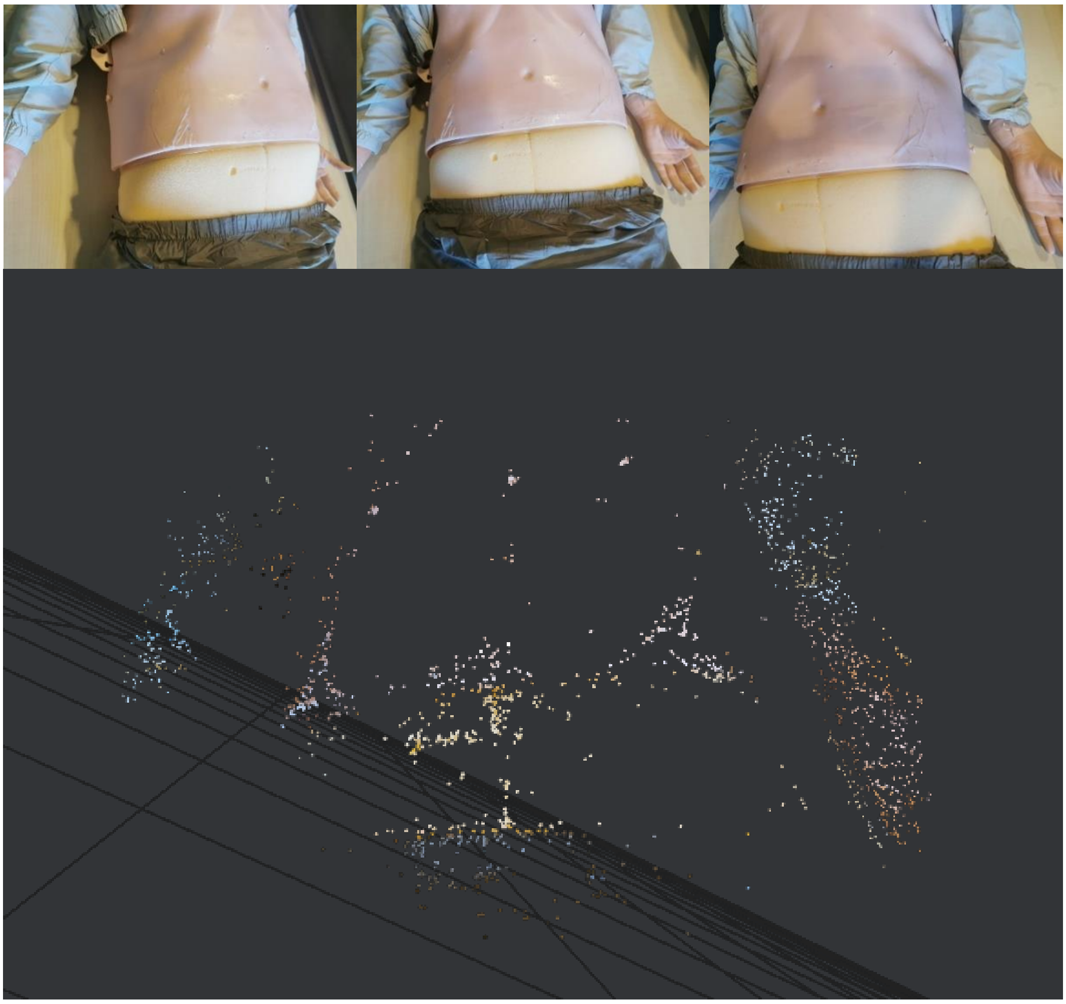

Figure 47. Output mesh when using the three shown images of the resuscitation doll.

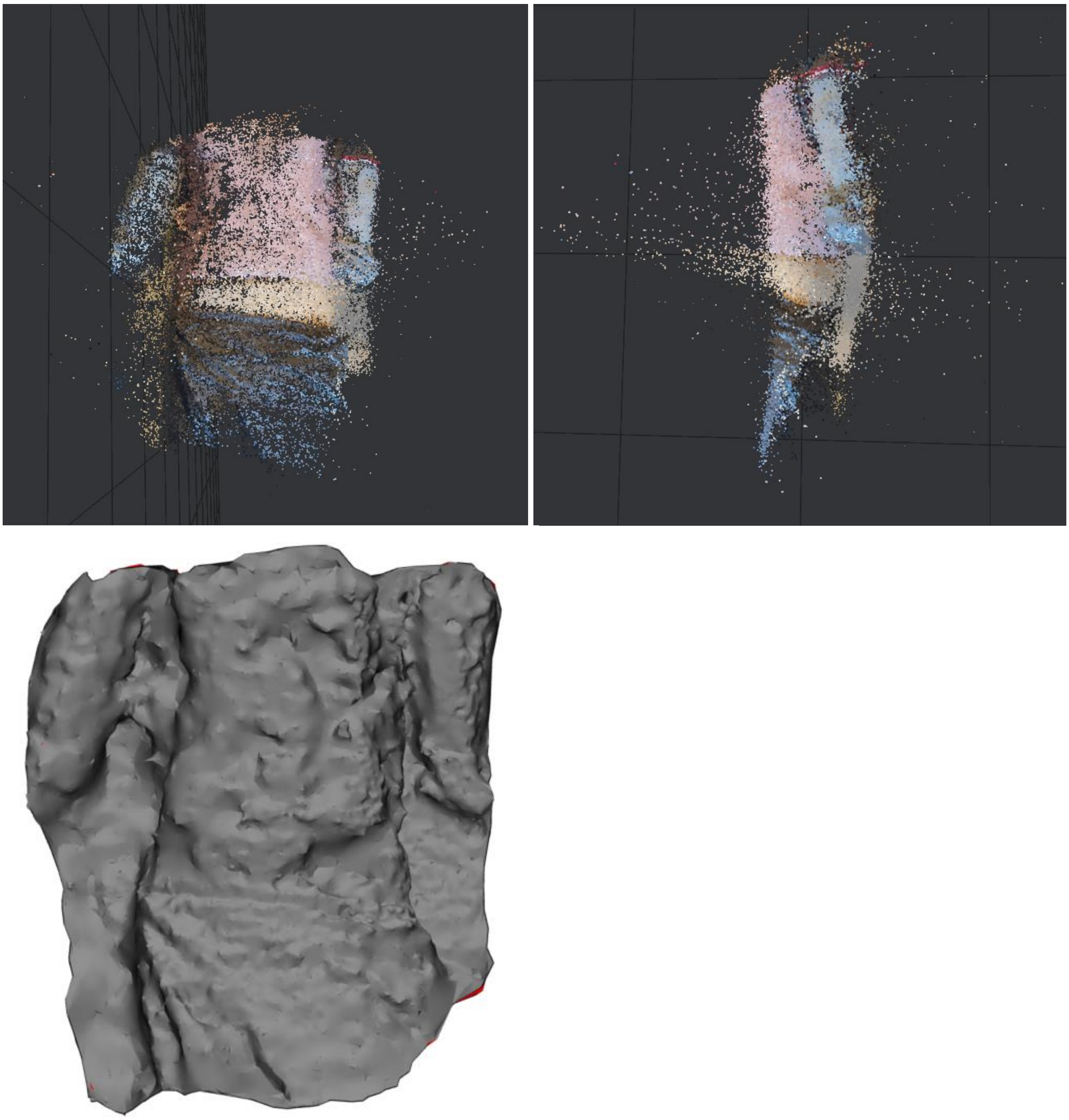

Figure 48. Photogrammetry of video frames. A. Frontal view 3D viewer Meshroom. B. Lateral view 3D viewer Meshroom. C. Frontal view of reconstructed, untextured mesh

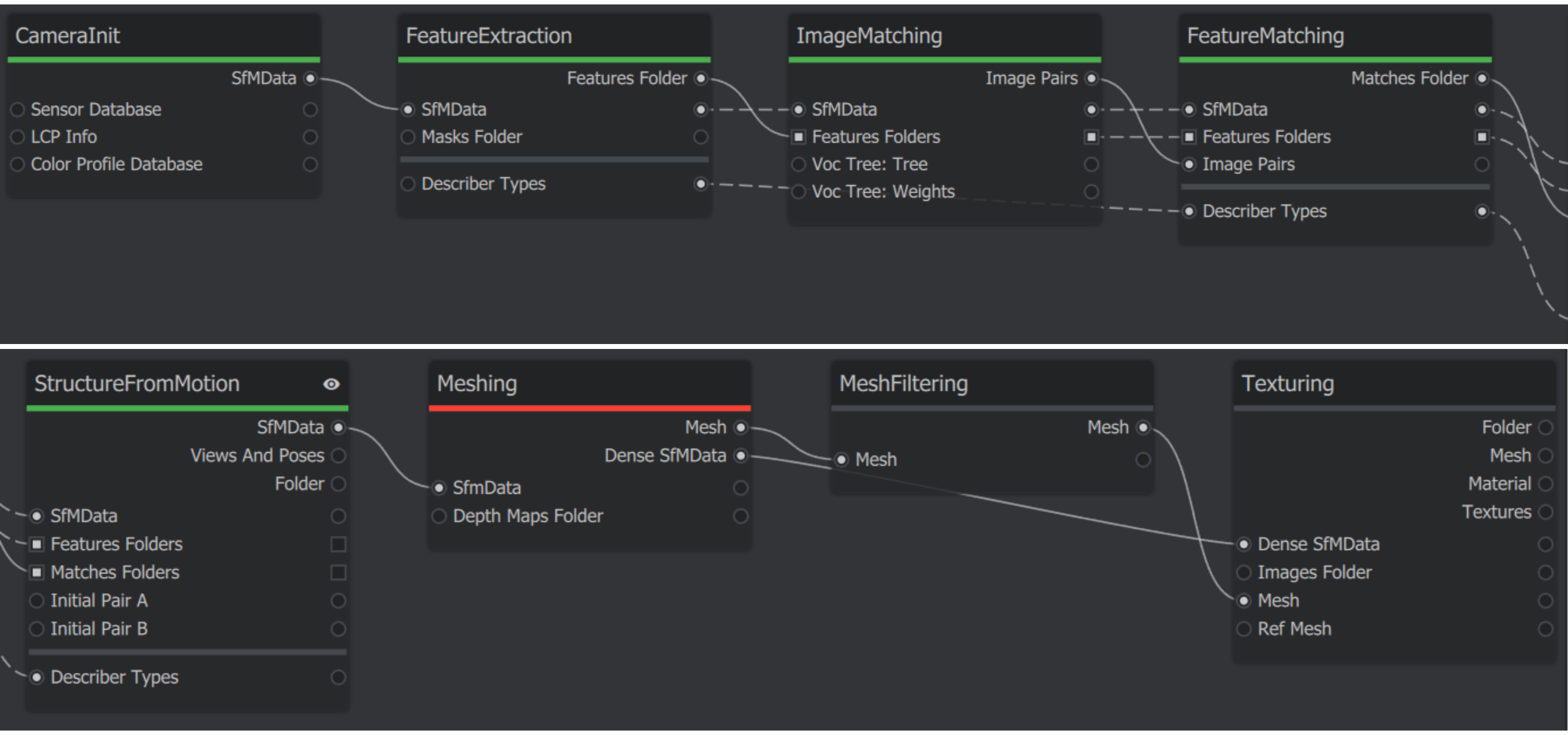

Figure 49. Meshroom workflow for single images

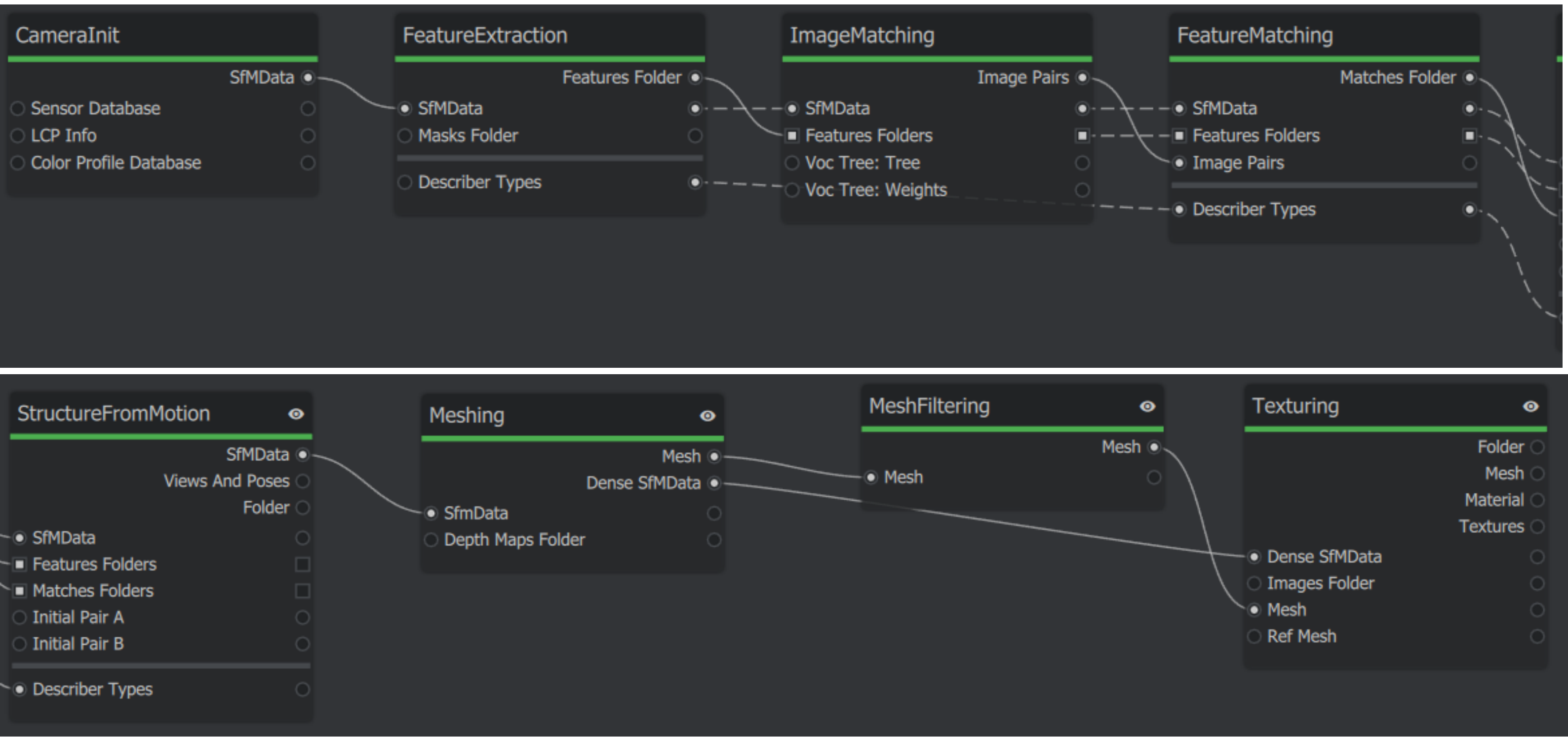

Figure 50. Meshroom workflow for videoframes.

2D projection

Projection of 2D images over the segmentation of the 3D scan was also attempted. This was done using the Photo Mapping option of Materialise Mimics. This function requires a selection of at least four landmarks on both the 2D image and the 3D object. A non-rigid registration is then performed. However, the abdomen provides few landmarks that are visible on both 2D images and the segmentation of the CTA scan. Landmark selection was done to the best of the researcher's abilities, but nevertheless, the registration remained somewhat unreliable. Furthermore, it became clear that the lateral corners got distorted in a way that could not be reliably corrected with the available options. Figure 51 shows how for example a skin fold can lead to an indent in the projected delineation, despite the actual delineation being a straight line.

The difference in surface area of the delineation of the flap was quantified for five randomly chosen participants. For three of the cases, the surface area of the projected 2D scan was 11% larger than the 3D scan. The fourth case was 23% larger, but further visual assessment and comparison to the 3D scan led to the conclusion that the projection was not done accurately enough due to the lack of landmarks. The fifth case was 7% smaller. Due to the difference being both positive and negative, the lack of accuracy due to the lack of landmarks and the distortion in the lateral corners led to the conclusion that projecting regular 2D photos on the CTA model is not a reliable method to transfer the delineation.

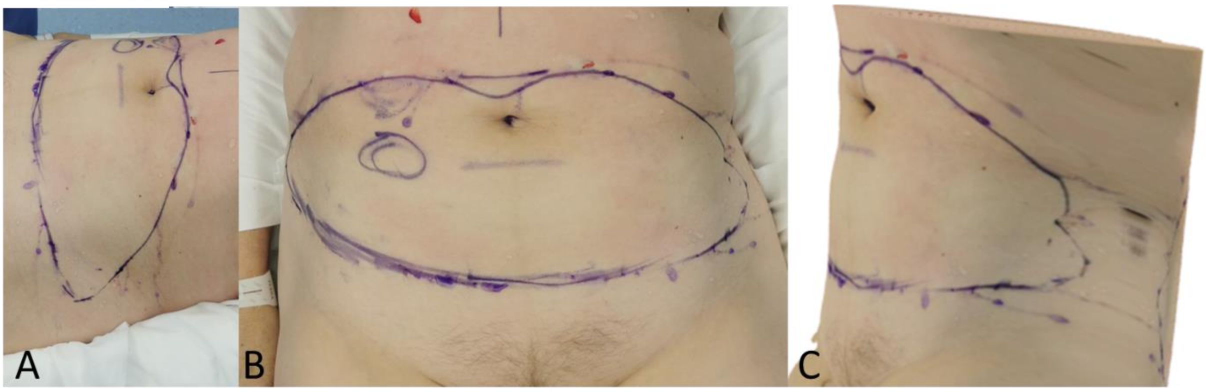

Figure 51. Projection 2D images of the delineation on the 3D segmentation of the CTA scan. A. Lateral view of the delineation. B. Frontal view of the delineation. C. Projection of image B of the CTA segmentation, showing a difference between A and C, due to the skin fold.

3D registration

3D registration as described in 3.2.1.2 gave the best results, however, as shown in Figure 52, deviation still occurred.

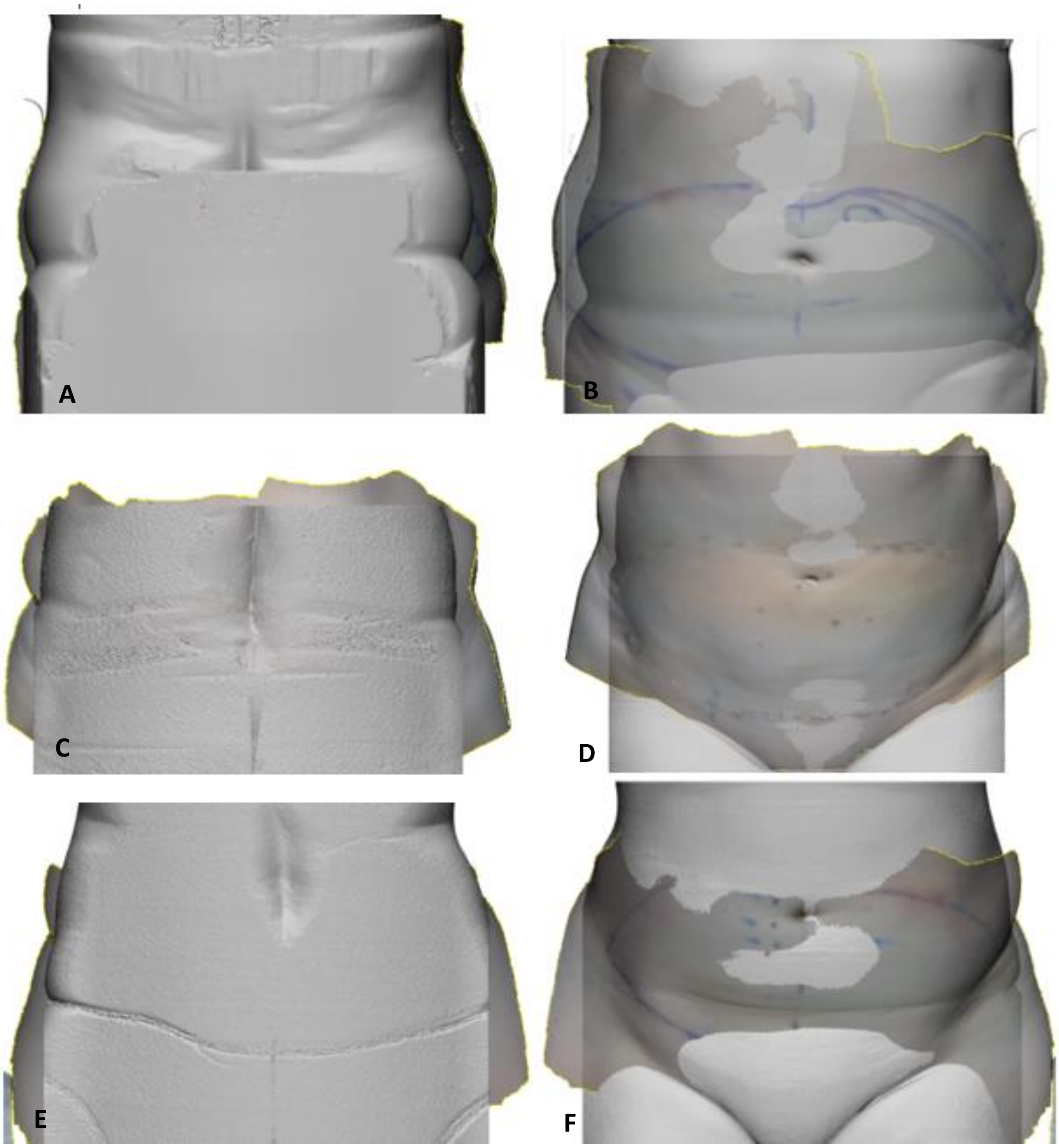

Figure 52. Visualization of 3D images of three random patients, showing deviations at the lateral sides between the 3D scan (skin coloured) and the CTA model (grey). A/B/E: Back view. B/D/F: Front view.

Appendix E. Additional results for volume validation

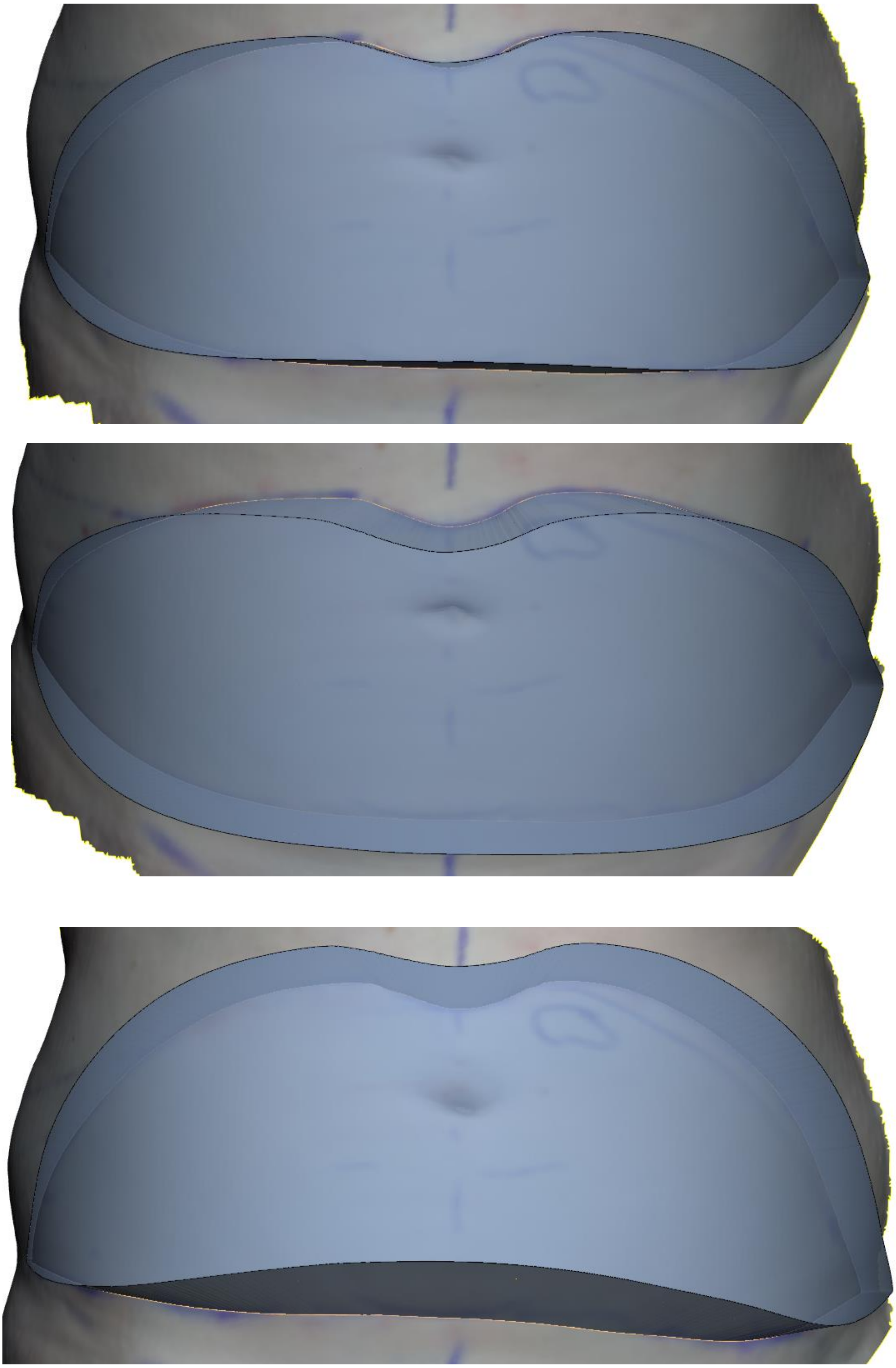

Figure 53. Visualization of how the extruded cylinder surface follows the original curve of the 3D scan. In orange the traced delineation.

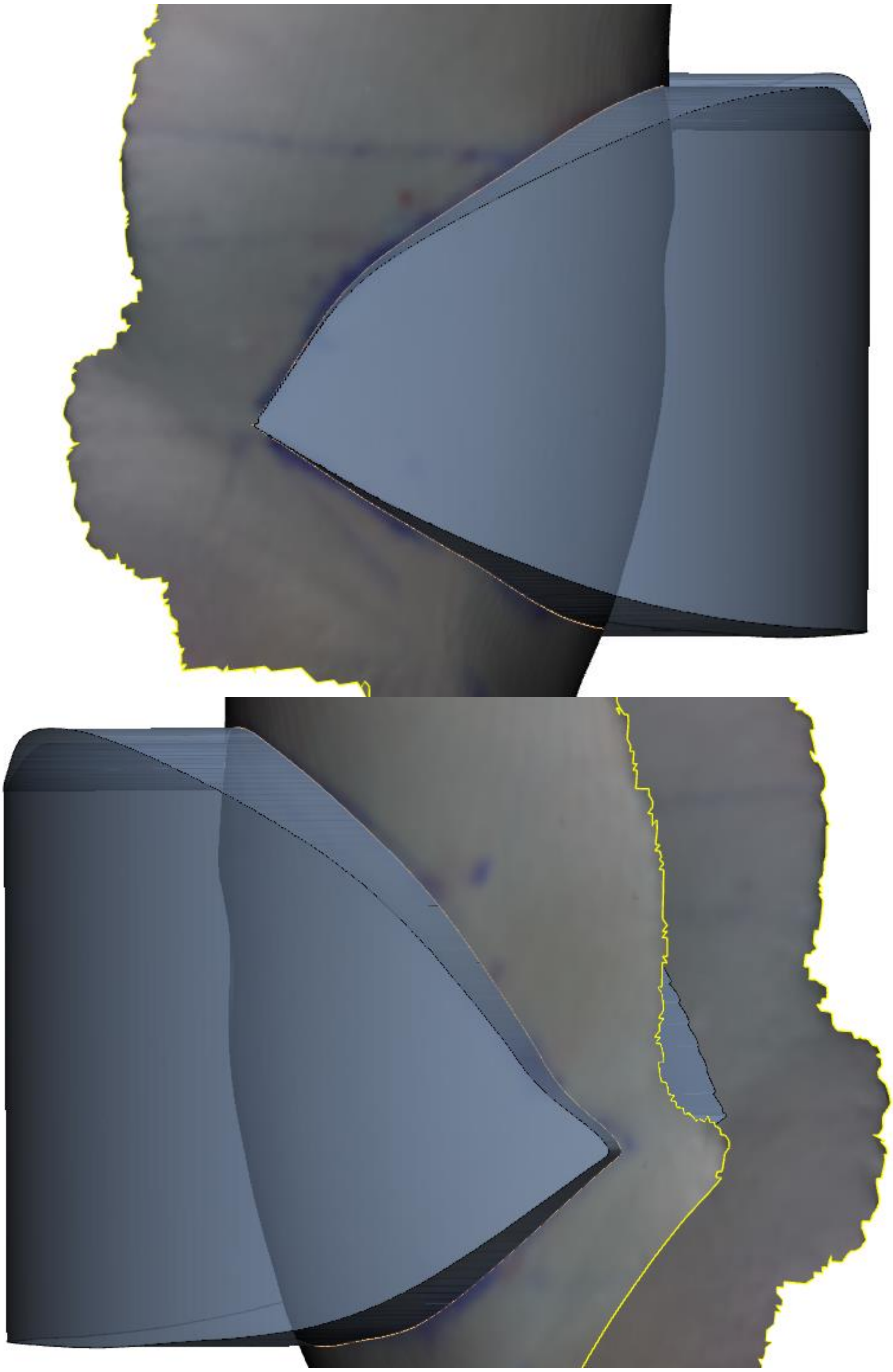

Figure 54. Visualisation of how the extruded cylinder surface follows the original curve of the 3D scan. In orange the traced delineation. Left and right view.

Table 6 Results of validation: surface areas. Mean of surface area difference cylinder = -0.1%. Mean of surface area difference CTA = -0.9%.

Case	Average distance error (mm)	Surface area 3D (cm^2)	Surface area cylinder (cm^2)	Surface area difference cylinder (%)	Surface area CTA (cm^2)	Surface area difference CTA (%)
1	0,74	661,0	660,8	0,0	656,9	-0,6
2	0,78	599,7	600,1	0,1	584,0	-2,6
3	0,94	433,6	434,0	0,1	426,1	-1,7
4	0,81	503,4	503,0	-0,1	514,7	2,2
5	0,77	706,8	706,8	0,0	675,0	-4,5
6	0,77	672,3	674,9	0,4	686,7	2,1
7	0,70	722,4	718,8	-0,5	723,1	0,1
8	1,05	451,6	452,3	0,2	451,4	0,0
9	1,08	588,4	588,6	0,0	600,3	2,0
10	0,88	467,3	468,0	0,1	477,7	2,2
11	0,85	469,9	468,8	-0,2	472,0	0,4
12	0,71	687,0	687,3	0,1	654,4	-4,7
13	1,10	451,6	445,2	-1,4	420,8	-6,8

Table 7 Results of validation: volume. The mean difference in weight when taking the absolute values is 11.9% or 166,6 g.

Case	Volume CTA (mL)	Weight CTA (g)	Weight per-operative (g)	Difference weight (%)	Difference weight (g)
1	2011,8	1790,5	1740	2,9	50,5
2	1819,8	1619,6	1324	22,3	295,6
3	882,4	785,3	841	-6,6	-55,7
4	1591,7	1416,6	1284	10,3	132,6
5	2119,0	1885,9	1840	2,5	45,9
6	2513,6	2237,1	1840	21,6	397,1
7	2322,8	2067,3	1942	6,5	125,3
8	1083,6	964,4	819	17,8	145,4
9	1765,9	1571,7	1916	-18,0	-344,3
10	1202,7	1070,4	951	12,6	119,4
11	1256,2	1118,0	1330	-15,9	-212,0
12	1972,6	1755,6	1831	-4,1	-75,4
13	1231,6	1096,1	1263	-13,2	-166,9

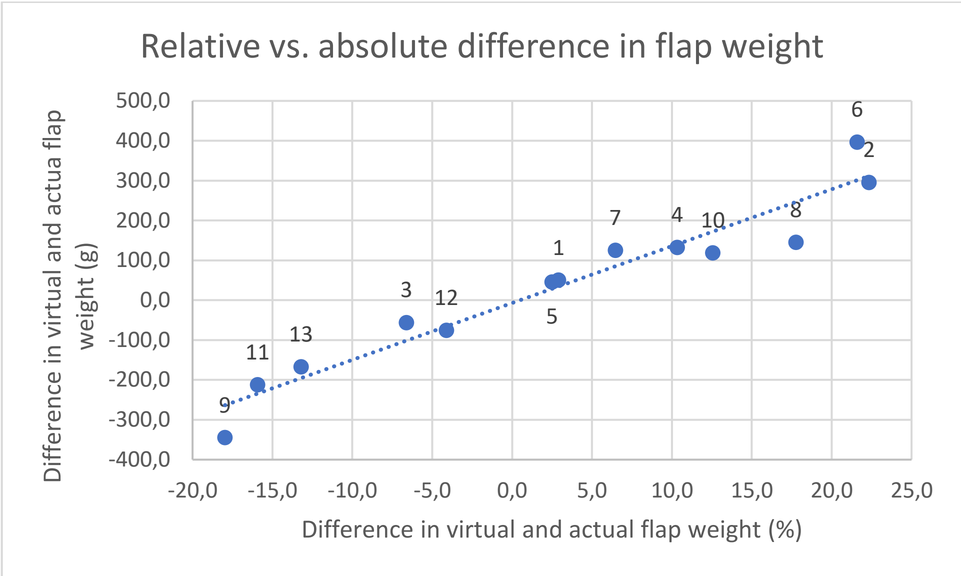

Figure 55. Plot of the relative and absolute difference in weight between the weighted per-operative flap and the virtually calculated flap.

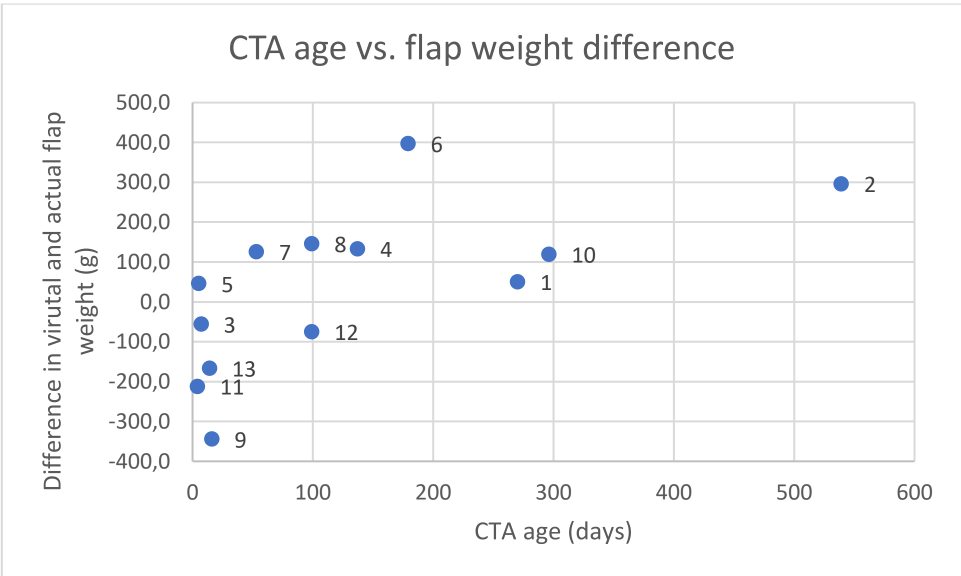

Figure 56. Scatterplot of CTA age in days versus the difference in flap weight of the harvested and virtual flap, with relative difference.

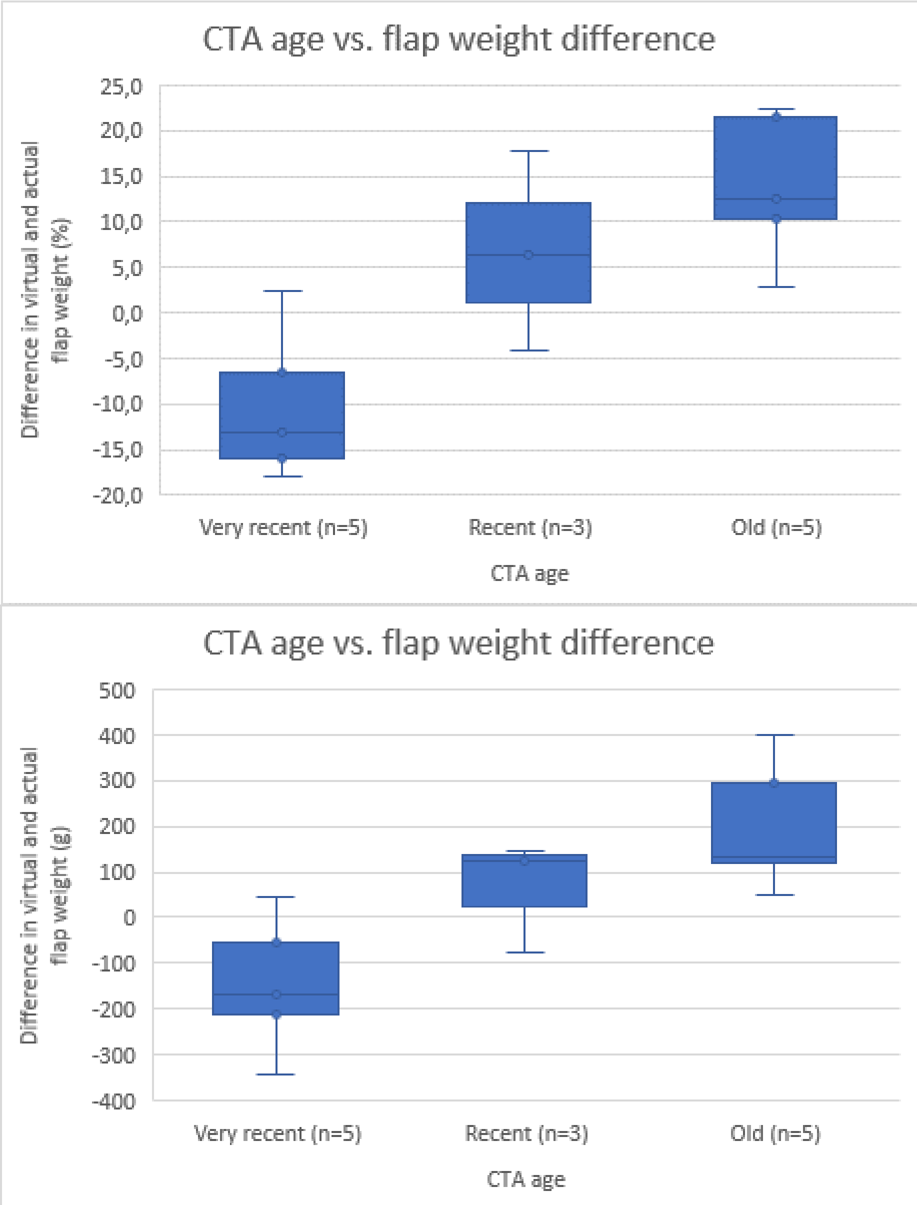

Figure 57. Boxplot of CTA age versus the difference in flap weight of the harvested and virtual flap, with relative difference shown in A, and absolute difference shown in B. Very recent: <21 days. Recent: <100 days. Old: ≥ 100 days.

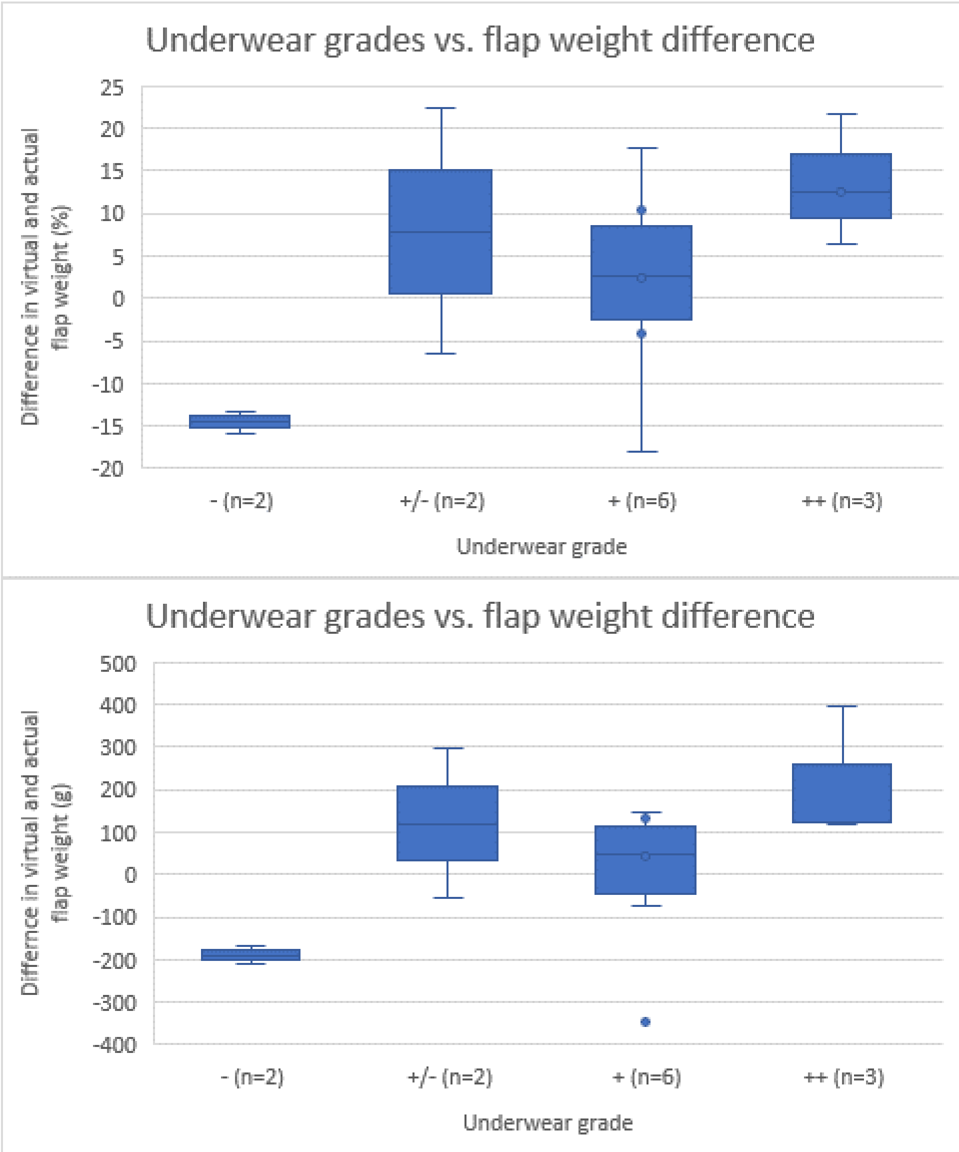

Figure 58. Boxplot of underwear grades versus the difference in flap weight of the harvested and virtual flap, with relative difference shown in A, and absolute difference shown in B..

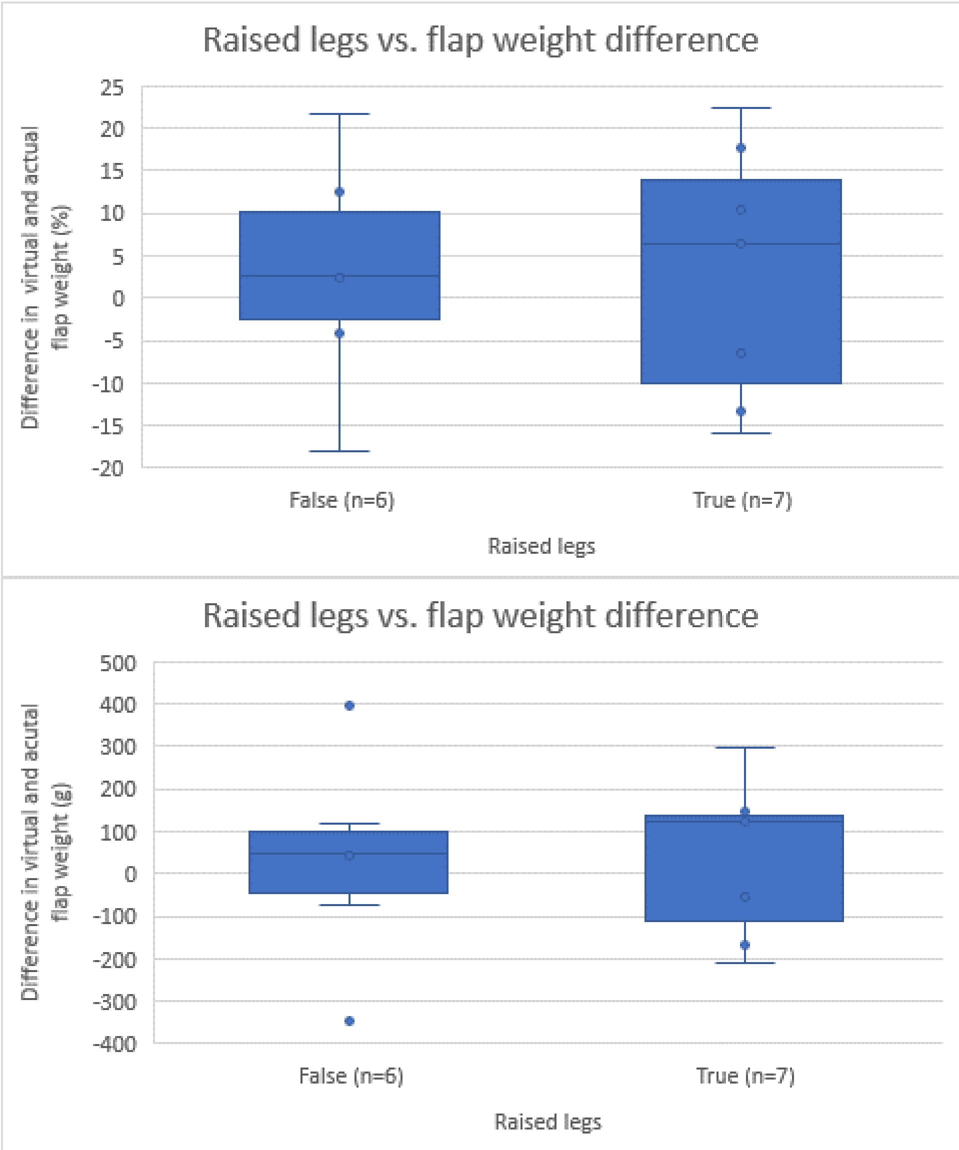

Figure 59. Boxplot of whether the legs of the participants were raised during the CTA versus the difference in flap weight of the harvested and virtual flap, with relative difference shown in A, and absolute difference shown in B.

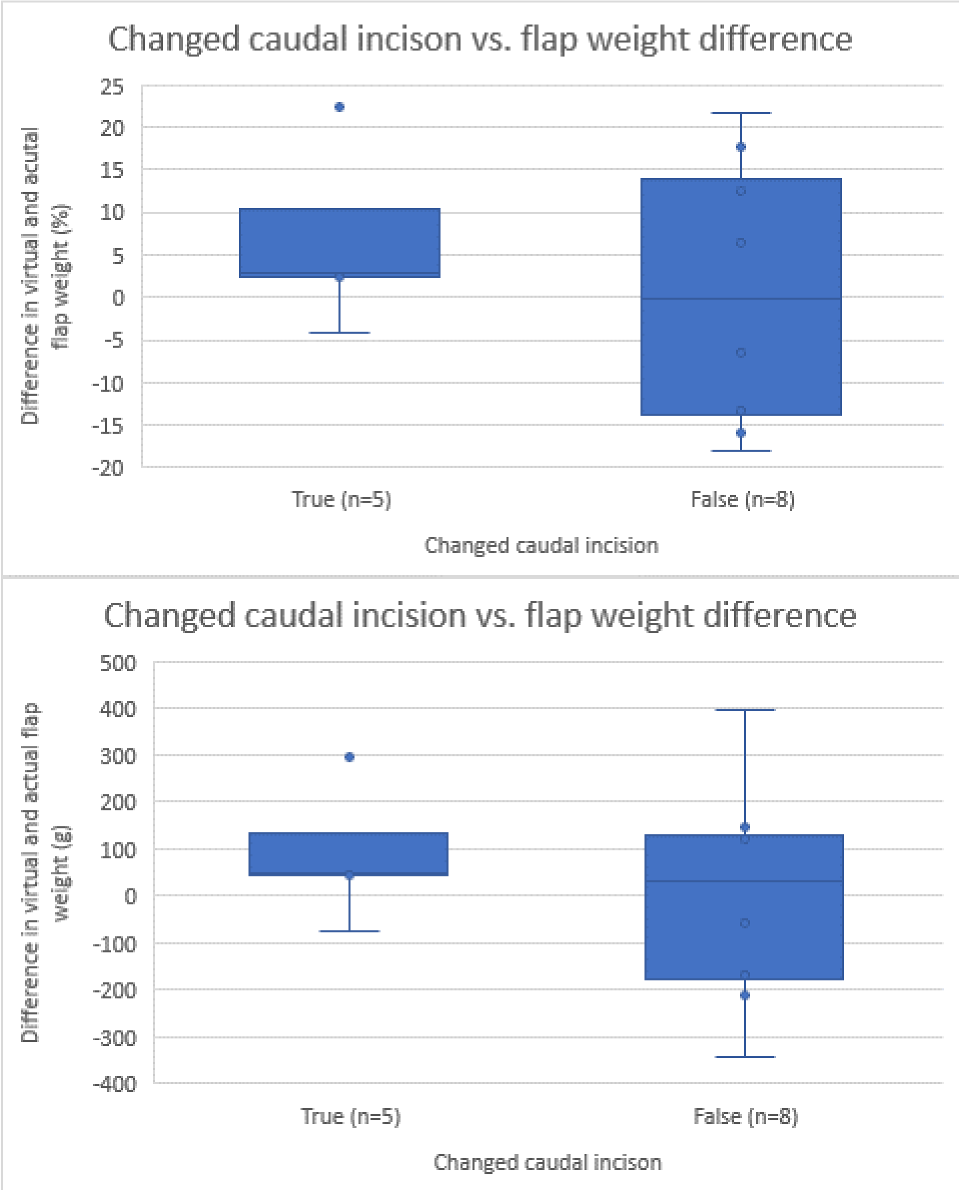

Figure 60. Boxplot of whether the caudal incision changed during surgery versus the difference in flap weight of the harvested and virtual flap, with relative difference shown in A, and absolute difference shown in B.

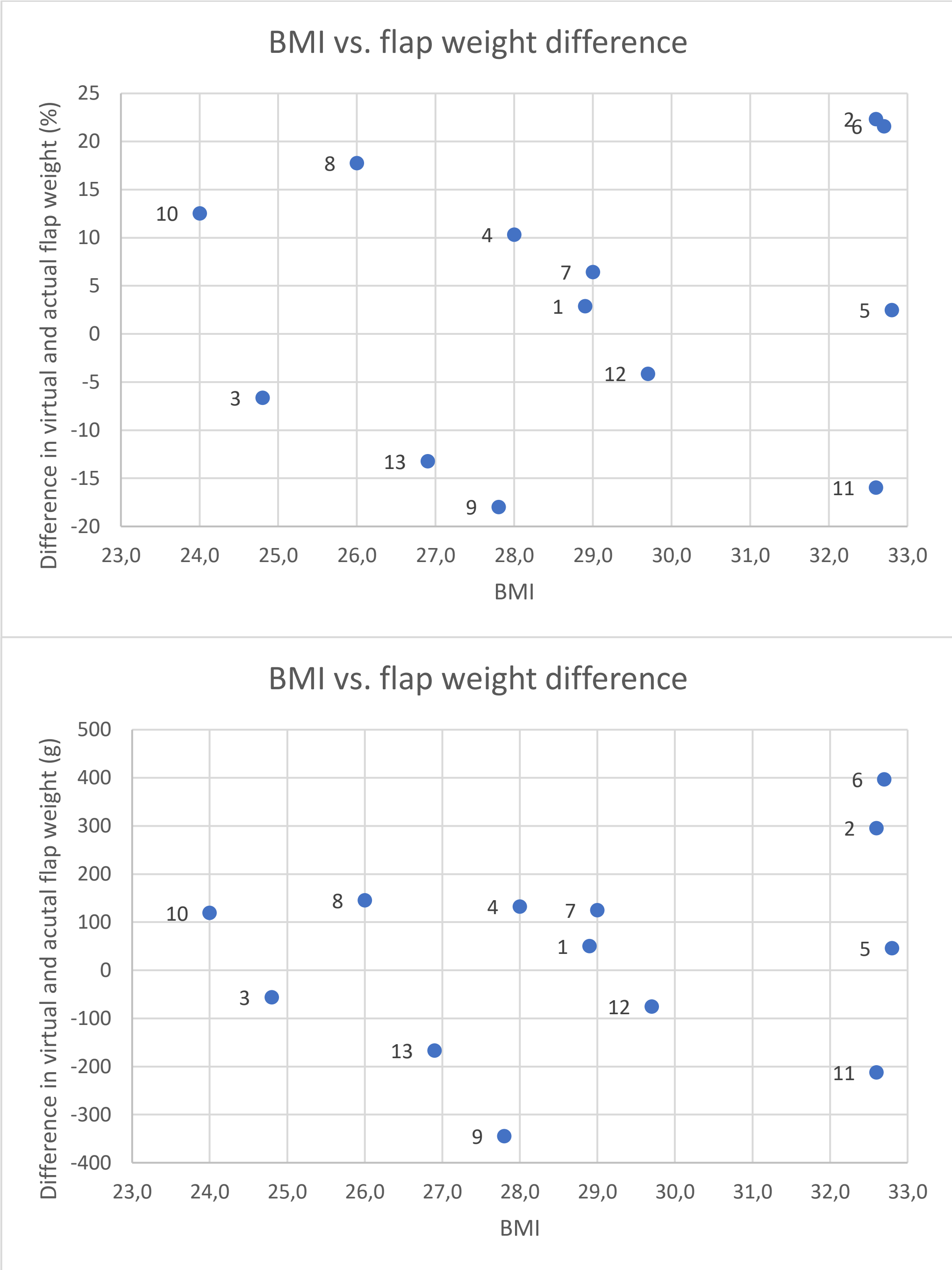

Figure 61. Scatterplot of the BMI of the participants versus the difference in flap weight of the harvested and virtual flap, with relative difference shown in A, and absolute difference shown in B.

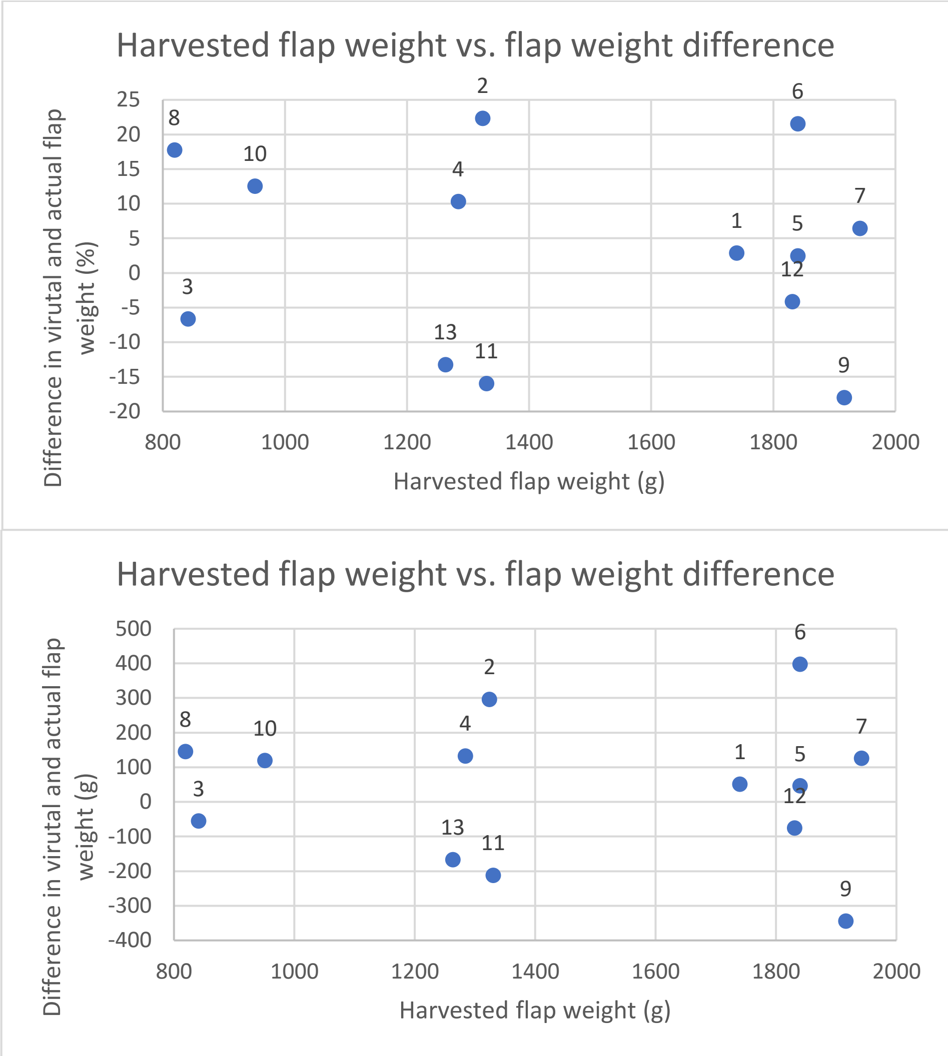

Figure 62. Scatterplot of the harvested flap weight vs the difference in flap weight of the harvested and virtual flap, with relative difference shown in A, and absolute difference shown in B

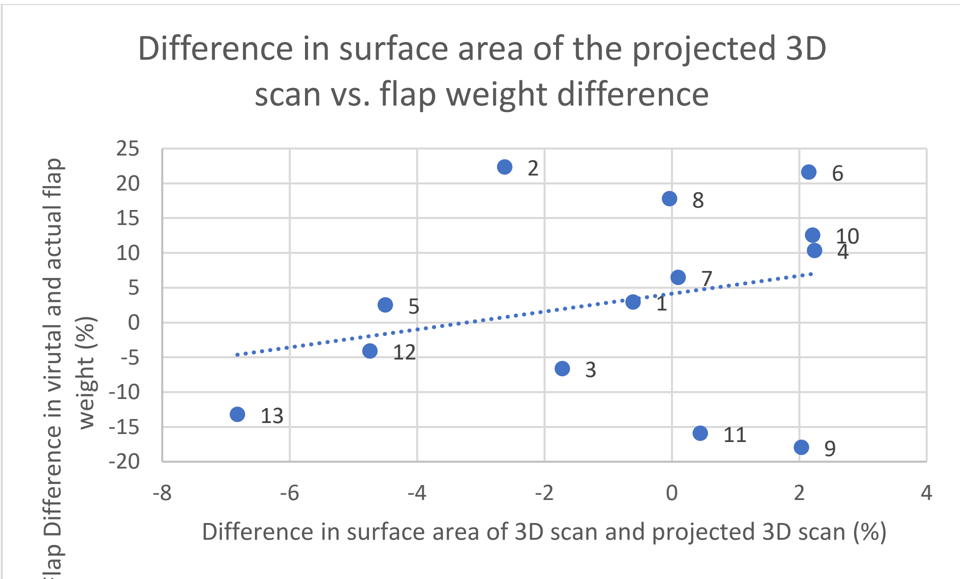

Figure 63. Scatterplot of the difference is surface area between the delineation of 3D scan and the delineation as projected on the cylinder versus the difference is flap weight of the harvested and virtual flap.

Appendix F. Additional images surgical planning

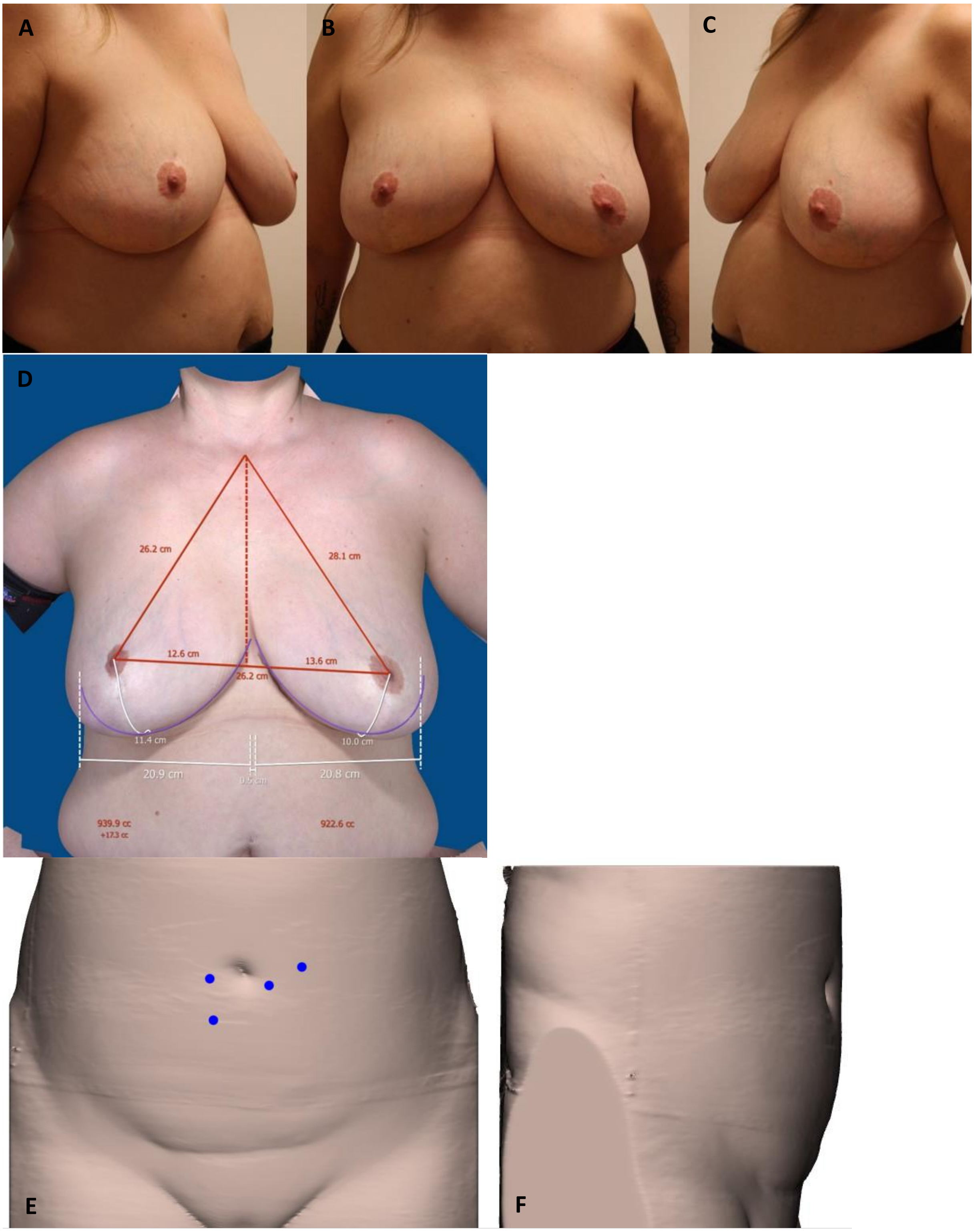

Figure 64. Overview of the data given to the plastic surgeon. A/B/C. 2D images of the breasts and abdomen of the patient. D. 3D photo of the breast with measurements. E. Front view of CTA model with perforators (blue dots). F. Lateral view of the CTA model.

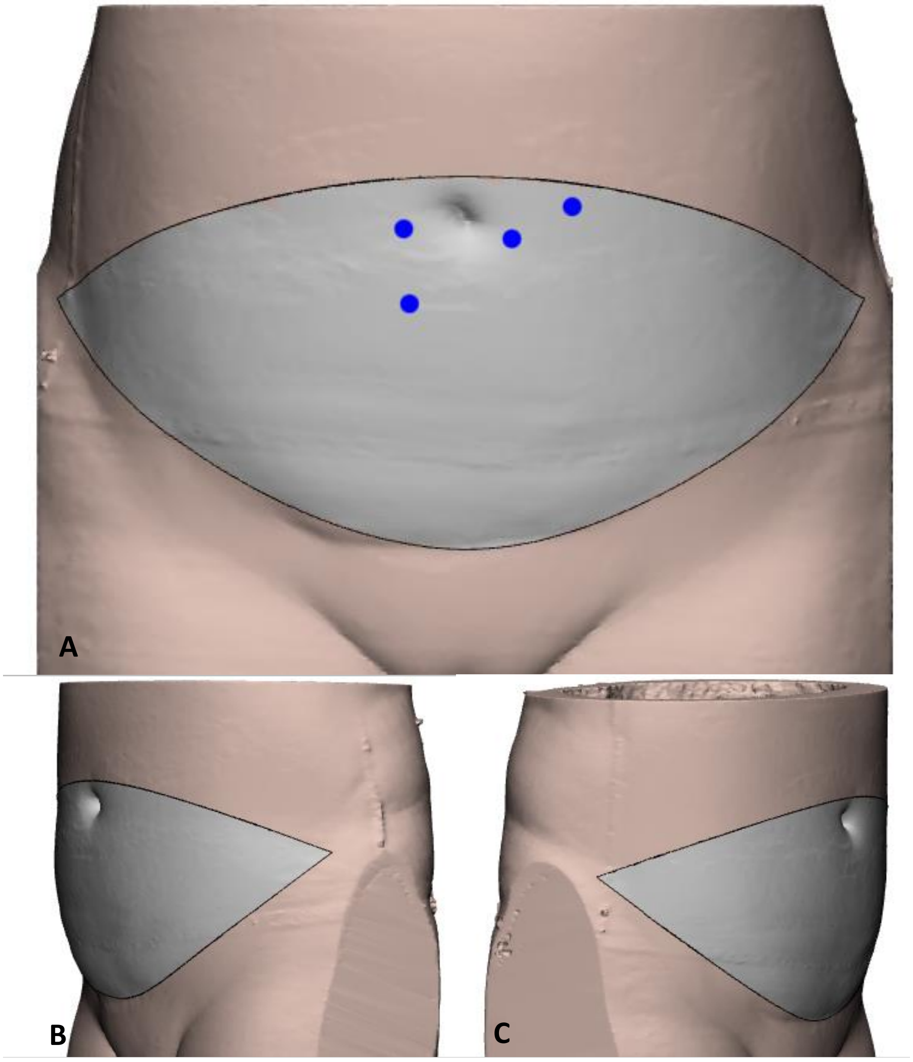

Figure 65. Visualization of the planning given for each planning. A. Frontal view with perforators (blue dots). B. Lateral left view. C. Lateral right view.

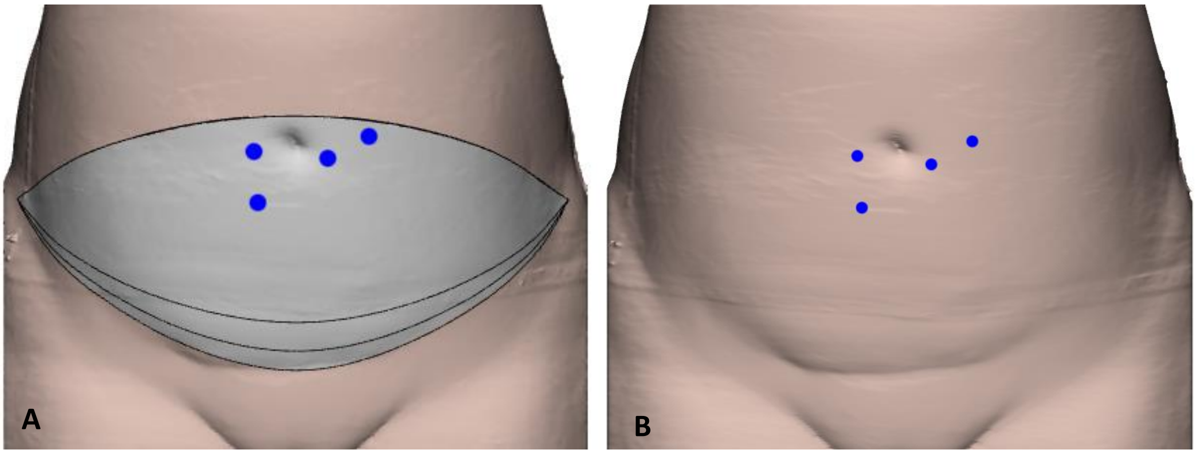

Figure 66. A. Summary of the plannings. CTA model with three plannings shown in grey with a black line surrounding it. The blue dots represent the perforators. B. The CTA model with perforators is presented next to it, as the grey areas can interfere with depth perception of the model.